ANL-6256

Argonne National Laboratory

THE EFFECT OF THE LIQUID VISCOSITY IN TWO-PHASE, TWO-COMPONENT FLOW

by

Melvin Jerome Fohrman

DISCLAIMER

Price $2.25 . *Available from the Office of Technical Services, Department of Commerce, Washington 25, D.C.*

ANL-6256
Physics
(TID-4500, 16th Ed.)
AEC Research and
Development Report

ARGONNE NATIONAL LABORATORY
9700 South Cass Avenue
Argonne, Illinois

THE EFFECT OF THE LIQUID VISCOSITY IN TWO-PHASE, TWO-COMPONENT FLOW

by

Melvin Jerome Fohrman

Based on a Thesis
Submitted to the Faculty
of
Illinois Institute of Technology
in Partial Fulfillment of the
Requirements for the Degree
of
Master of Science in Mechanical Engineering

November 1960

Operated by The University of Chicago
under
Contract W-31-109-eng-38

TABLE OF CONTENTS

TABLE OF CONTENTS

ACKNOWLEDGMENTS

The author wishes to express his gratitude to his advisor, Doctor S. P. Kezios, for his sincere encouragement and guidance throughout the experimental investigation, and to Ingersoll Milling Machine for their generous Fellowship and consent to proceed with the current investigation. He would also like to express his appreciation to the members of the Heat Engineering Section at Argonne National Laboratory for their assistance. The author is particularly indebted to J. F. Marchaterre for his guidance and helpful criticisms; to B. Brewer for greatly assisting in the construction and operation of the experimental apparatus and in the reduction of the data; to P. Zaleski for his assistance in the correlation of the data.

He is also indebted to the Graphic Arts Group for the reproduction of the thesis.

LIST OF TABLES

LIST OF ILLUSTRATIONS

LIST OF ILLUSTRATIONS (Continued)

LIST OF ILLUSTRATIONS (Continued)

LIST OF ILLUSTRATIONS (Continued)

LIST OF ILLUSTRATIONS (Continued)

NOMENCLATURE

Symbol	Quantity	Units
A	Area	ft^2
a	Constant in slip ratio correlation	
b	Viscometer constant	
C	Constant in Blasius Equation	
D	Diameter	ft
f	Fannings friction factor	
G	Mass flow rate	$lb_m/sec\ in.^2$
g	Acceleration of Gravity	ft/sec^2
K	Orifice coefficient	
L	Length	inches
m	Exponent in Blasius Equation	
n	Exponent in Blasius Equation	
N_{Re}	Reynolds number	
P	Total pressure	lb_f/ft^2
ΔP_{TP}	Two-phase pressure drop	lb_f/ft^2
ΔP_ℓ	Pressure drop due to liquid flowing at at a rate (1-x) times total flow rate	lb_f/ft^2
ΔP_g	Pressure drop due to gas flowing at a rate x times the total flow rate	lb_f/ft^2
p	Exponent in slip ratio correlation	
R_0	Perfect gas constant	$ft/^\circ R$
R_ℓ	Liquid volume fraction	
S.G.	Specific Gravity	
T	Temperature	°C
V	Velocity	ft/sec
W	Flow rate	lb_m/sec
x	Quality	
α	Void Volume fraction	
ρ	Density	lb_m/ft^3

NOMENCLATURE (Continued)

Symbol	Quantity	Units
σ	Slip ratio V_g/V_ℓ	
ϕ	$\left[\left(\frac{\Delta P}{\Delta \ell}\right)_{TP} \Big/ \left(\frac{\Delta P}{\Delta \ell}\right)_{SP}\right]^{\frac{1}{2}}$	
χ	$\left[\left(\frac{\Delta P}{\Delta \ell}\right)_{e} \Big/ \left(\frac{\Delta P}{\Delta \ell}\right)_{g}\right]^{\frac{1}{2}}$	

Subscripts

e	Equivalent
g	Gas phase
ℓ	Liquid
max	Maximum
S	Static
T	Total
tt	Liquid-turbulent; gas-turbulent
vt	Liquid-viscous; gas-turbulent

A number of special terms not included in this list are defined where they are used.

CHAPTER I
INTRODUCTION

The use of concurrent flow of liquid and gas mixtures in industrial components such as evaporators, gas pipelines, and heat exchangers has prompted a detailed investigation of the interaction of the variables associated with this phenomenon. Also, recent advances in the nuclear reactor field have made an accurate knowledge of the two-phase pressure drop and mixture density necessary for the proper design of boiling-water reactors.

Previous investigators have dealt with: (a) analytical studies based on physical models of idealized flow patterns, such as the theoretical treatment of the annular flow model by Levy;[1]* (b) experimental investigations concerning the relationships among the variables associated with two-phase flow, such as Richardson's[2] study on the effect of a sudden change in the flow area on the significant flow parameters for air-water mixtures; (c) combinations of theoretical and experimental investigations resulting in semi-empirical correlations, such as the studies of Martinelli et al.,[3,4,5] in which a macroscopic analysis of the flow phenomenon resulted in the prediction of the void volume fraction and the static two-phase pressure drop in single and two-phase, two-component flow.

Historical

Hoefer[6] was one of the first investigators to notice that bubbles in air-water mixtures move faster than the surrounding water during investigations on the rising main of an air-lift pump. Schmidt[7] Behringer,[8] and Schurig[9] recognized the importance of the relative motion of the gas to the liquid phase in their investigations of steam-water mixtures. Schmidt proposed a set of dimensionless groupings based on a Reynolds number concept, which were expressed on an $\alpha/(1-\alpha)$ basis, where α represents the void volume fraction. The need

*For all numbered references, see bibliography.

for experimental verification of the suggested parameters and further investigations of the effects of liquid viscosity and surface tension were stressed by Schmidt. Behringer conducted a series of tests in vertical columns containing steam-water mixtures at a pressure range from one to forty atmospheres. The specific gravity of the mixture was measured by a pressure-sensing device which moved along the length of the tube. The relative velocity (i.e., slip ratio) of the liquid to the gas phase appeared to decrease with the increasing pressure, and increase with a decreasing specific gravity of the mixture. The effect of the tube diameter on the slip ratio appeared to be less at the higher pressures. The results compared favorably with the theoretical predictions of Schmidt.

Schurig extended the experimental investigation to circulating mixtures at pressures up to forty atmospheres. He reported that the slip ratio and resistance to flow (i.e., pressure drop) in the circulating steam-water mixtures differed strongly with the results of Behringer and of Schmidt. This indicated that the addition of the circulation parameters changed the two-phase flow mechanism considerably.

In recent years, a number of studies have been performed on steam-water and air-water systems for pressure ranges from 14.7 to 2,000 psia in order to achieve a better understanding of the mechanism involved in two-phase flow. The slip ratio has been correlated to the inlet velocity, channel geometry, quality, void volume fraction, and other parameters in an attempt to obtain a generalized correlation. However, the void-volume fraction correlations of Martinelli remain as one of the few approaches that considers directly the effect of the liquid viscosity. Empirical correlations, based on theoretical flow models and experimental data have, for the most part, included the effect of viscosity of the liquid phase indirectly or have neglected it completely. Literature surveys by Cook,[10] Marchaterre,[11] and Galson,[12] initiated during the course of various investigations of the

subject, adequately cover the results of these studies. A recently completed study by Marchaterre and Petrick[13] from Argonne National Laboratory, deals with the use of the technique of gamma-ray attenuation for the measurement of void volume fractions in steam-water mixtures for pressures ranging from 150 to 2,000 psi. The results indicate that the slip ratio is primarily affected by the system pressure, mixture quality, circulation velocity and, to a smaller extent, by the channel geometry.

Martinelli et al. performed an extensive series of void volume fraction and pressure-drop investigations in two-phase, two-component flow using air and liquids such as benzene, kerosene, water, and SAE 40 oil (μ_{max} = 260 cp) at pressures ranging from 15 to 52 psia. The tests resulted in the prediction of the void volume fraction and the two-phase static pressure drop, where the following parameters were used to correlate the results:

$$\phi_\ell^2 = \left(\frac{\Delta P}{\Delta \ell}\right)_{TP} \Big/ \left(\frac{\Delta P}{\Delta \ell}\right)_\ell \tag{1.1}$$

$$\phi_g^2 = \left(\frac{\Delta P}{\Delta \ell}\right)_{TP} \Big/ \left(\frac{\Delta P}{\Delta \ell}\right)_g \tag{1.2}$$

$$\chi^2 = \frac{C_\ell \, (N_{Re_g})^m \, W_\ell^2 \, \rho_g}{C_g \, (N_{Re_\ell})^n \, W_g^2 \, \rho_\ell} \quad , \tag{1.3}$$

where the constants, C_ℓ, C_g, m and n depend on whether the liquid or the gas phase is flowing in a laminar or turbulent state. The development of the Martinelli analysis is shown in Appendix A.

Levy[1] verified the parameters used by Martinelli et al. in a theoretical analysis based on an annular flow model. The results of this analysis are compared to the predictions of Martinelli in figures 1.1 and 1.2. Deviations noted between the investigations of Martinelli and of Levy are due primarily to the idealized nature of the flow model used in Levy's theoretical analysis, wherein the assumptions of equal shear stress and steady conditions are made.

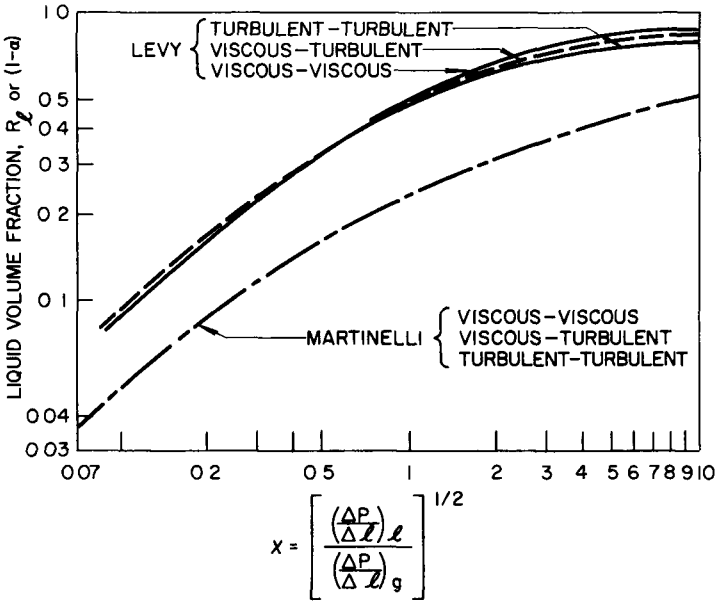

Figure 1.1 Comparison of the Liquid Volume Fraction - Empirical Correlation of Martinelli and Theory of Levy in Terms of the Parameter χ.

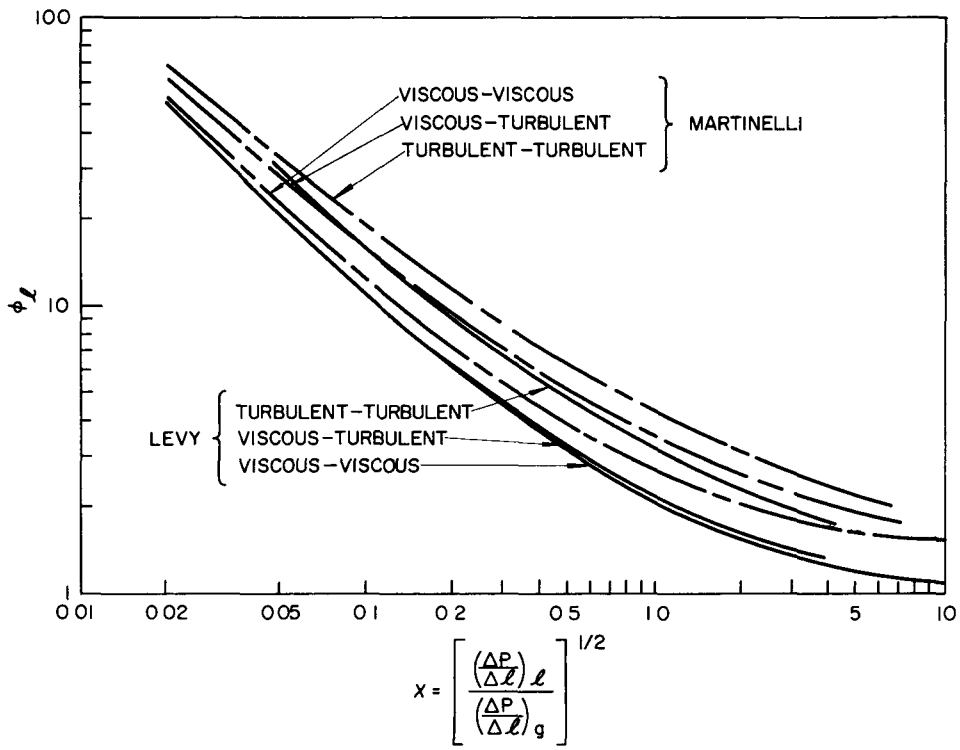

Figure 1.2 Comparison of the Two-phase Pressure Drop - Empirical Correlation of Martinelli and Theory of Levy in Terms of the Parameter χ.

The Martinelli parameters have been used by many investigators as a basis for the comparison of their void volume fraction results. A literature survey by Richardson[2] includes the results of these investigations and compares their experimental data to the void volume fraction correlation of Martinelli. The experimental data generally fall higher than predicted by the Martinelli correlation. Richardson has presented a correlation comparing the Martinelli predictions with his experimental results which were obtained for air-water mixtures (see figure 1.3). Richardson's experimental investigation also led to an empirical correlation of the slip ratio as a function of quality:

$$\sigma = 37\, x^{1/2} \quad , \tag{1.4}$$

where σ represents the slip ratio and x the quality; this equation correlates the data obtained from his experiments to within ± 30 percent. The correlation is for a quality range of 0.00073 to 0.054 and for a slip ratio range from 0.56 to 9.2.

Purpose and Scope

An experimental program was set up to evaluate the effect of the liquid phase viscosity on slip ratio. A forced circulation, two-phase, two-component system operating at atmospheric pressure and using air and glycerine-water (i.e., glycerol) mixtures was employed. The effect of the liquid phase viscosity on the pressure drop was observed, and the flow regimes were also identified and studied.

A combination of five qualities and five liquid flow rates were experimentally investigated at several values of liquid viscosities. The approximate range of the variables investigated in the experimental program were as follows:

Liquid Viscosity	0.75 to 500 cp
Quality	0.005 to 0.0184
Liquid Flow Rate	0.2 to 0.8 pound per second
Air Flow Rate	0.001 to 0.015 pound per second
Void Volume Fraction	0.34 to 0.78.

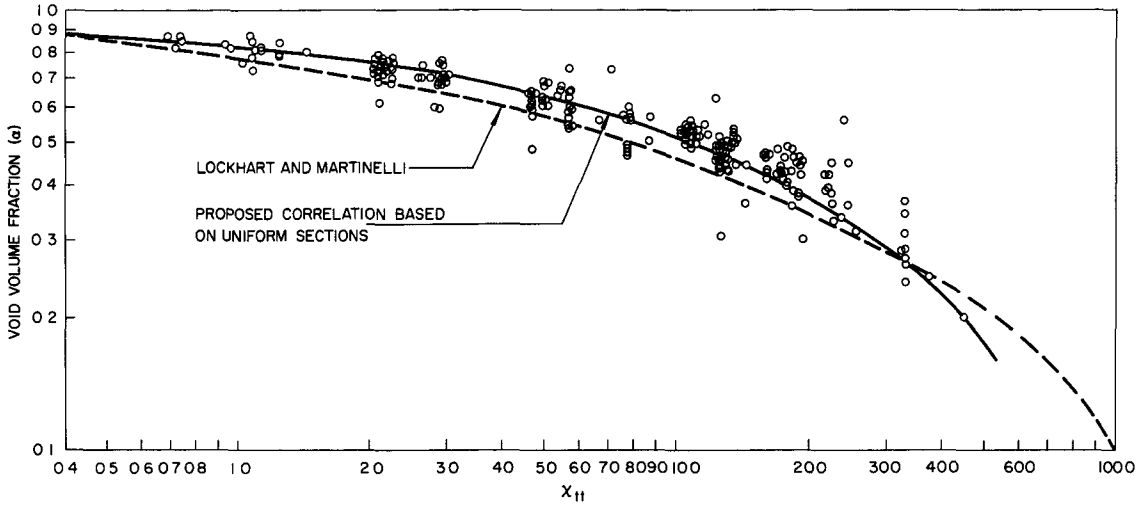

Figure 1.3 Proposed Void Fraction Correlation for Horizontal Flow from Richardson.

The void volume fraction and the approximate distribution of the two-phase mixture at a particular cross-sectional element of the test section was determined by the technique of gamma-ray attenuation. A set of five viscometers and a heat exchanger were used to measure and control the viscosity of the liquid phase.

CHAPTER II
A GAMMA RADIATION TECHNIQUE FOR VOID MEASUREMENT

The measurement of the void volume fraction in two-phase flow is necessary for the determination of the slip ratio and mixture density. Techniques based on mechanical means, such as trapping the mixture with the use of quick-acting valves, were employed by Thomsen,[14] by Taylor,[15] by Lockhart and Martinelli,[5] and by Johnson and Abou Sabe.[16] This method yields an average void volume fraction based on the length of the section between the two valves.

The need for an accurate local determination of the void volume fraction has led to the use of the radiation technique. One method of analysis uses the difference between the gamma-ray attenuation characteristics in systems which contain liquid only, gas only, and the two-phase mixture. The gamma radiation is emitted from a Tm^{170} source encased in a lead cylinder. The radiation passes through the test section and is detected by a scintillation crystal which is optically coupled to a photomultiplier tube. The signal is then amplified and transmitted to a recording device.

Historical

Cook[10] conducted experiments to determine the effectiveness of the gamma-ray attenuation method. He checked the validity of the exponential theory upon which the method was based, and noted the importance of correct alignment of the source, channel, and scintillation crystal. Results indicated the accuracy of the technique decreased for larger channel spacings and increased when the source was placed further from the channel. Filters were needed for low-energy scatter from the Tm^{170} source to maintain an exponential attenuation. Mockup studies were performed with Lucite blocks, as shown in figure 2.1. The Lucite mockups were designed to simulate preferential void distributions. Strong deviations from the actual void volume fractions were noted in the experimental analysis. However, radiographic studies

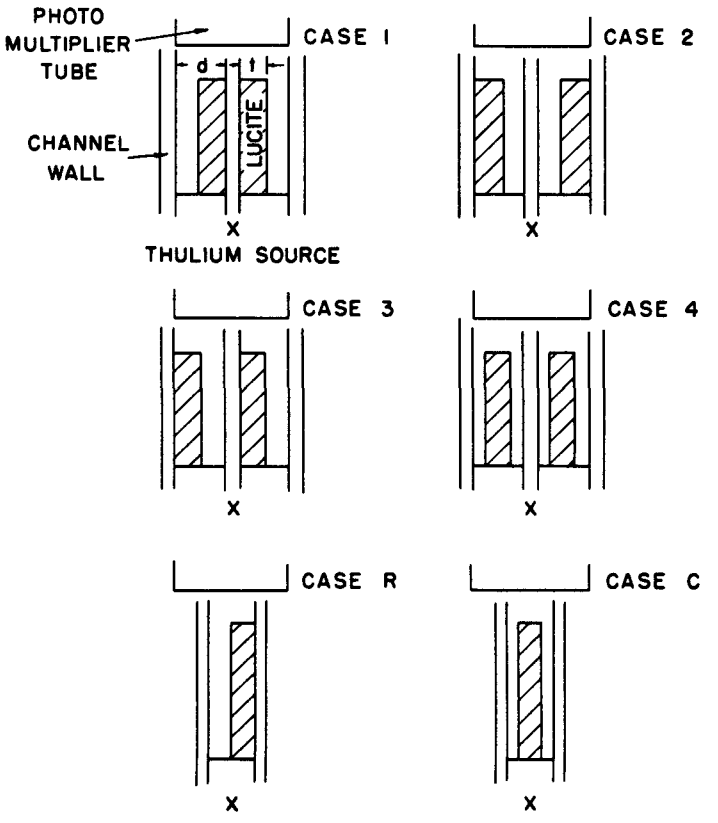

Figure 2.1 Configurations of Lucite Blocks (from Cook).

indicated that very little preferential void distribution occurred in the 600-psi steam-water mixture which was located in the channel under consideration. A maximum void volume fraction error of ± 3.5 percent was found during the calibration of the pressure vessel used in the investigation. This bore out the premise of negligible preferential void distribution in the test apparatus.

Egen, Dingee and Chastain[17] conducted an experimental program in a rectangular channel under boiling heat flux conditions at 2,000 psia. Void volume fractions, void distribution, and void formation were studied. Homogeneous and separated flow models were used to represent uniform and preferential void distributions. Agreement between experimental and theoretical results were good for the case of homogeneous flow. However, agreement was poor for the separated flow model. This substantiated the results obtained by Cook.

Hooker and Popper[18] performed an error analysis on the physical components involved in the use of the gamma-ray attenuation technique as based on theoretical and experimental considerations. They noted the magnitude of the errors caused by: (a) the electronics of the system; (b) the methods of void volume fraction measurement; and (c) the uniform and preferential void distributions. An absolute maximum error of approximately ± 3 percent was reported for uniform void distributions. The error increased as the void volume fraction decreased. Greater deviations for preferential void distributions were noted. Experimental investigations confirmed errors of ± 10 percent at a void volume fraction of 0.24. At the lower contents of voids, the errors increased rapidly. Based on these results, another technique for measuring void volume fractions was employed, whereby only a small increment of the test section was surveyed by the radiation apparatus at any particular time. The previous method attempted to survey the complete test section at one time. Preliminary tests using this refinement met with a considerable reduction in error.

The assumption of exponential attenuation in the theoretical analysis was verified experimentally by two tests in which layers of air and water, directed normal to the path of radiation, were employed. Improvements with regard to the finer regulation of the high-voltage supply of the photomultiplier tube, cooling of the scintillation crystal to reduce temperature variation, and the use of a more sensitive recorder were suggested by Hooker and Popper.

Recent studies in two-phase, two-component flow of air-water mixtures were performed by Petrick[19] and by Richardson.[2] Petrick investigated the two-phase flow phenomena in vertical rectangular channels. Richardson investigated the two-phase flow phenomena in horizontal rectangular channels. Two flow models were proposed by both investigators. A technique known as the "traversing method" was developed to provide greater accuracy in the measurement of preferential void volume fractions.

Using the corrective measures suggested by Hooker and Popper and by Cook, an exponential decay was assumed:

$$I = I_0 e^{-\mu x} \quad , \tag{2.1}$$

where

I = the intensity of the radiation at x (photons/cm^2 sec)

I_0 = the intensity of the beam at x = 0 (photons/cm^2 sec)

μ = the linear absorption coefficient (cm^{-1})

x = absorber thickness (cm) .

A flow model in which the vapor and the liquid phases are in parallel layers, perpendicular to the incoming radiation, is described by the following equation:

$$\alpha = \frac{\ln(I/I_\ell)}{\ln(I_V/I_\ell)} \quad , \tag{2.2}$$

where

I = radiation intensity for two-phase flow in the channel

I_ℓ = radiation intensity for all liquid flow in the channel

I_V = radiation intensity for all gas flow in the channel.

The second flow model consists of the vapor and liquid phases lying in parallel layers, parallel to the incoming radiation, and is described by the following equation:

$$\alpha = \frac{I - I_\ell}{I_v - I_\ell} \quad . \tag{2.3}$$

The derivations of equations (2.2) and (2.3) may be found in references 2 or 14. Equation (2.2) was used in the calculation of the void volume fraction because of the tendency for this configuration to be predominant in the two-phase flow investigation.

A technique employed by Cook was known as the "one-shot" method. In this method, the shield on the scintillation crystal contained an opening slightly larger than the test section, so that the incoming gamma rays from the Tm^{170} source covered the complete vertical width of the test section at one time. With the use of equation (2.2), three values taken when the channel was full of liquid, gas, and the two-phase mixture, served to determine the void volume fraction.

In an alternative method for measuring the void volume fraction, known as the "traversing technique," a shield is employed with a narrow slit cut on its face. Therefore only a small amount of the vertical width of the test section was surveyed at one time. In order to obtain a complete trace of the channel, a continuous trace was taken with the Tm^{170} source together with the scintillation crystal, moving normal to the test section for its entire width. Continuous traces were obtained when the channel was full of liquid, gas, and the two-phase mixture. Point determinations of the void volume fraction were made using equation (2.2), and the total void volume fraction was computed by a weighting technique using Simpsons' rule.

A comparison of the one-shot method and the traversing technique was initiated during the experimental studies of Petrick and of Richardson, with the use of void mockups. Lucite mockups, machined to simulate actual flow conditions, were used. Some typical mockups used in these investigations are shown in figure 2.2 through figure 2.4.

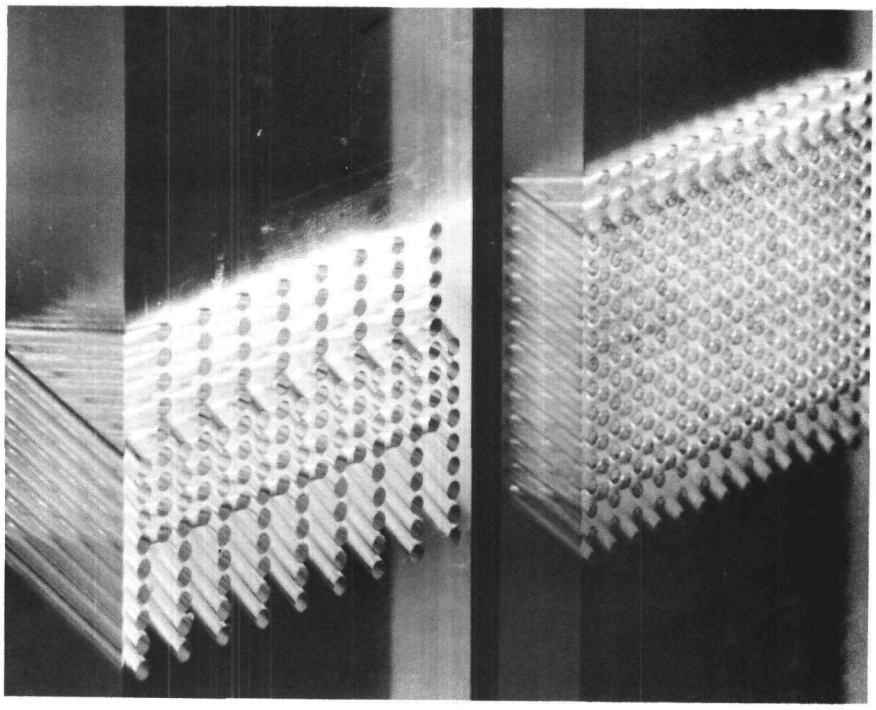

Figure 2.2 Closeup View of Churn (Homogeneous) Flow Model (from Petrick).

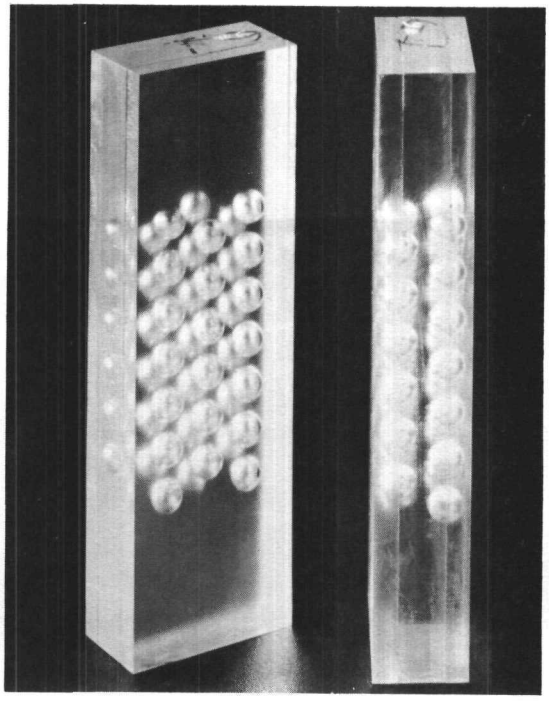

Figure 2.3 Double Annular Flow Model (from Petrick).

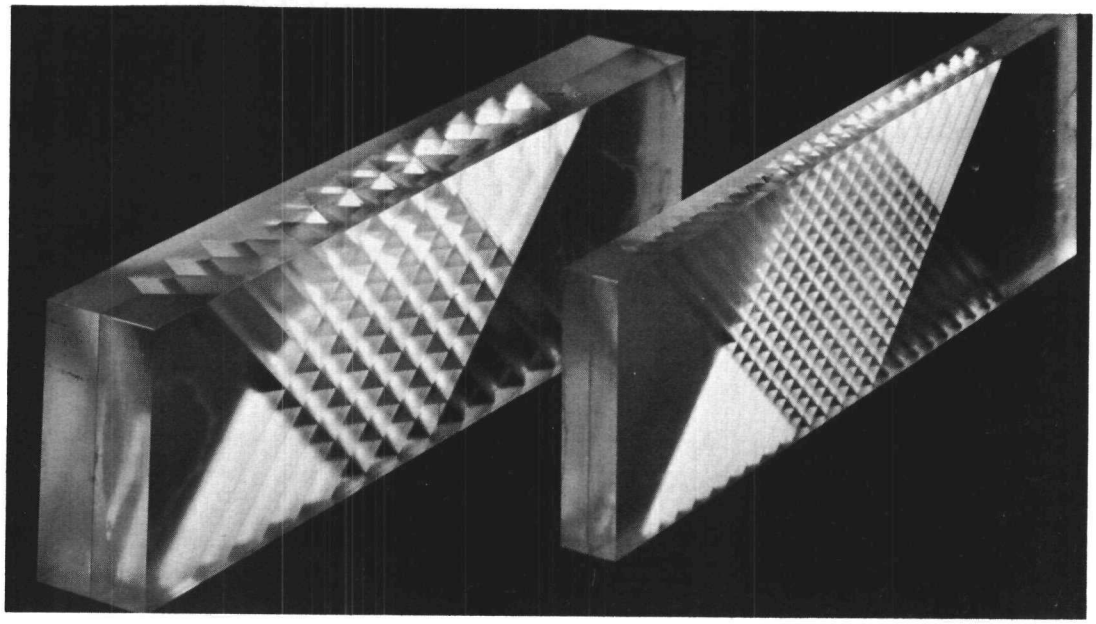

Figure 2.4 Local Boiling Flow Model (from Richardson).

Actual void volume fractions were determined by physical measurements and by weighing the Lucite blocks. The results obtained by Petrick and by Richardson are shown in table 2.1 and figure 2.5. The results indicate that: (a) the traversing technique is more accurate than the one-shot method, especially for preferential void distributions; (b) the errors in the void determinations increase for larger channel widths; and (c) the traversing technique provides the investigator with an approximate determination of the void distribution along the vertical width of the channel.

Table 2.1. Comparison of Void Fractions Obtained by Traversing and "One-shot" Techniques with Actual Void Fraction (from Petrick).

Simulated Phase Distribution in Mockup	Lucite Mockup Width, in.	Void Fraction		
		Traversing	"One-shot" Method	Actual
Local Boiling	1	0.406	0.143	0.364
Annular Flow	1	0.164	0.324	0.203
Double Annular	1	0.151	0.181	0.166
Parabolic	1	0.286	0.322	0.267
Parabolic	1/2	0.350	0.567	0.345
Annular Flow	1/2	0.589	0.741	0.606
Local Boiling	1/2	0.401	0.161	0.345
Churn Flow	1/2	0.420	0.419	0.415

Mockup Study

The void mockup blocks fabricated by Petrick and by Richardson were used in the present study for calibration purposes. The method of calibrating the void volume fraction was verified, and the errors due to the preferential void distributions were noted. The results of the mockup tests are tabulated in table 2.2. Greater deviations (as in Cases 3 and 4) were noted for the mockups that bore a closer physical similarity to the model described by equation 2.3 than by equation 2.2.

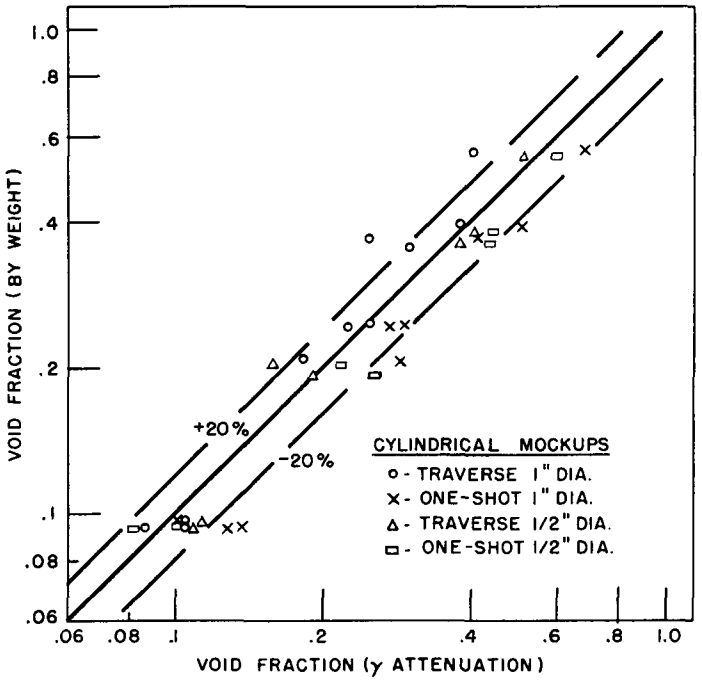

Figure 2.5 Comparison of Void Fraction by Weight and by Radiation Attenuation Techniques (from Richardson).

Table 2.2. Results of Mockup Study

Mockup Number	α Measured	α Actual	Percentage Error
1	0.373	0.394	- 5.23
	0.406	0.394	+ 3.15
2	0.178	0.188	- 5.1
	0.17	0.188	- 9.75
3	0.463	0.564	-17.9
	0.495	0.564	-12.2
4	0.305	0.345	-11.6
	0.318	0.345	- 7.82
5	0.410	0.415	- 1.2
	0.418	0.415	+ 0.722

CHAPTER III
EXPERIMENTAL EQUIPMENT AND MEASUREMENTS

The experimental investigation was designed to study the effect of the liquid-phase viscosity upon void volume fraction and flow regime for a fixed set of inlet flow conditions. The basic components of Richardson's experimental apparatus were utilized. Modifications in the equipment were made to permit operation at high values of liquid viscosity.

The experimental equipment is schematically illustrated in figure 3.1 and was basically operated in the following manner. Mixtures of glycerine and water were circulated by means of an internal gear pump. Air was obtained from the 100-psi laboratory supply line. The flows of the liquid and of the air were regulated by control valves and metered by a set of orifices. The two fluids were mixed together in a chamber located at the entrance to the test section. The two-phase mixture flowed through a horizontal Lucite test section and into the separator. During this time, the measurement of the void volume fraction was made by means of the penetration of beams of gamma radiation through the Lucite test section. The liquid then flowed into a storage tank and back to the pump, and the air was discharged to the atmosphere. The experimental equipment is shown in figure 3.2. In the lower portion of this figure, looking from right to left, are the storage tank, the internal gear pump connected to it, the control valves, gauges, and metering valves. Along the center portion of this figure, from left to right, are the mixing tee which connects to the test section, the traversing mechanism, and the discharge valve leading to the separator which is supported by the storage tank. The static pressure lines are located in the center of the figure above the test section.

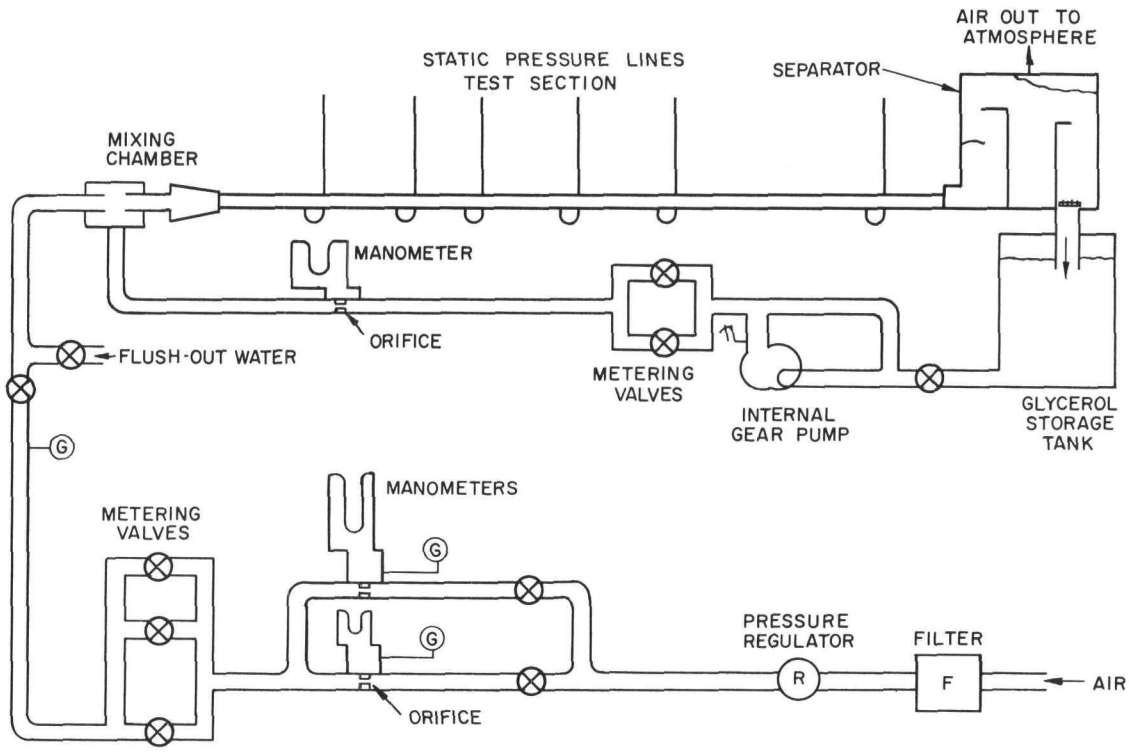

Figure 3.1 Experimental Loop - Schematic

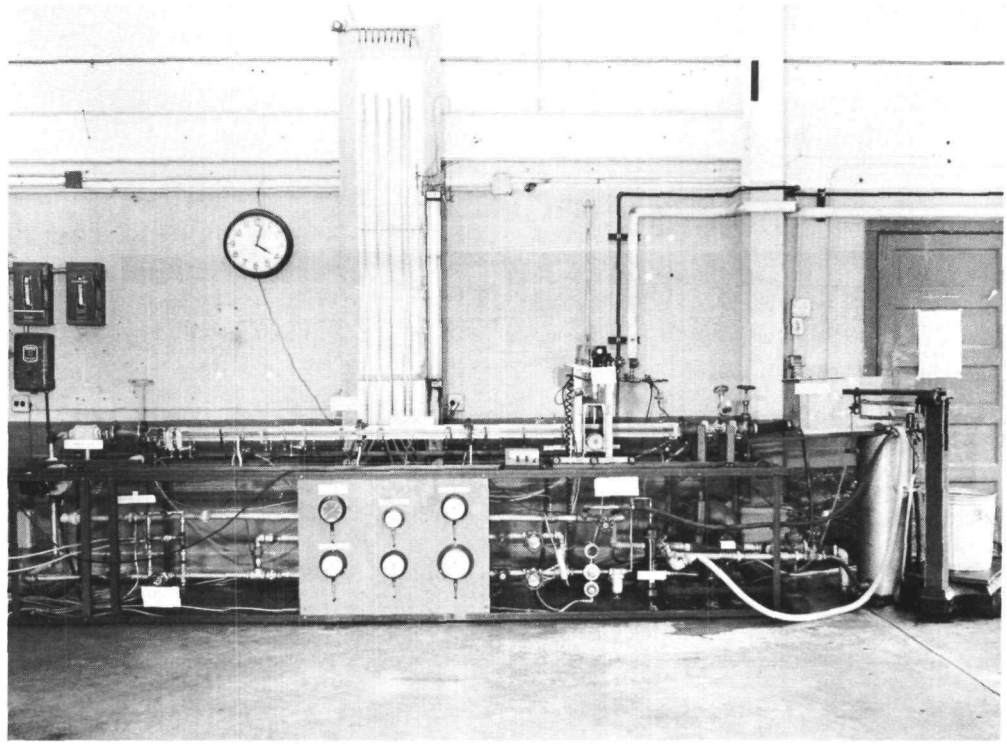

Figure 3.2 Experimental Loop, Traversing Mechanism and Auxiliary Equipment.

System Components

Liquid System

Viscosity. The viscosity of the glycerine-water mixtures depends on concentration and temperature. Highly concentrated glycerine was diluted with demineralized water to obtain the desired concentration. Cooling coils installed in the storage tank, served to control the temperature of the mixture.

A set of five Number 46460 Kimax Ostwald-type viscometers and a constant-temperature water bath were employed for the measurement of the viscosity of the glycerol. The constant-temperature water bath consisted of two 100-watt heaters, a thermostatic control circuit, and an agitator to maintain a constant bath temperature. The apparatus is illustrated in figure 3.3. No insulation was required on the glass container because the bath was held at room temperature, thus keeping the heat losses to a minimum.

The viscosity of a glycerol mixture was determined by measuring the amount of time it took for a measured quantity of the mixture to move through the capillary of the viscometer when it was immersed in the water bath. The method of determination is shown in Appendix C. The viscometers were calibrated according to the "step-down" procedure outlined in ASTM D445-53T.[20] A calibration fluid was used to determine the first viscometer constant. The remaining constants were determined by using a value for the liquid viscosity that had been evaluated by a viscometer with an overlapping viscosity range. Demineralized water was obtained from the laboratory, and secondary oils, number A-7, B-7, and C-8, were obtained from the Research Department of Standard Oil of Indiana for use for the calibration of the viscometers. During the experimental runs, the calibration constants were rechecked with the glycerol mixtures and were found to agree to within one percent of the originally determined constants. The range of the viscometers and the experimentally determined constants are

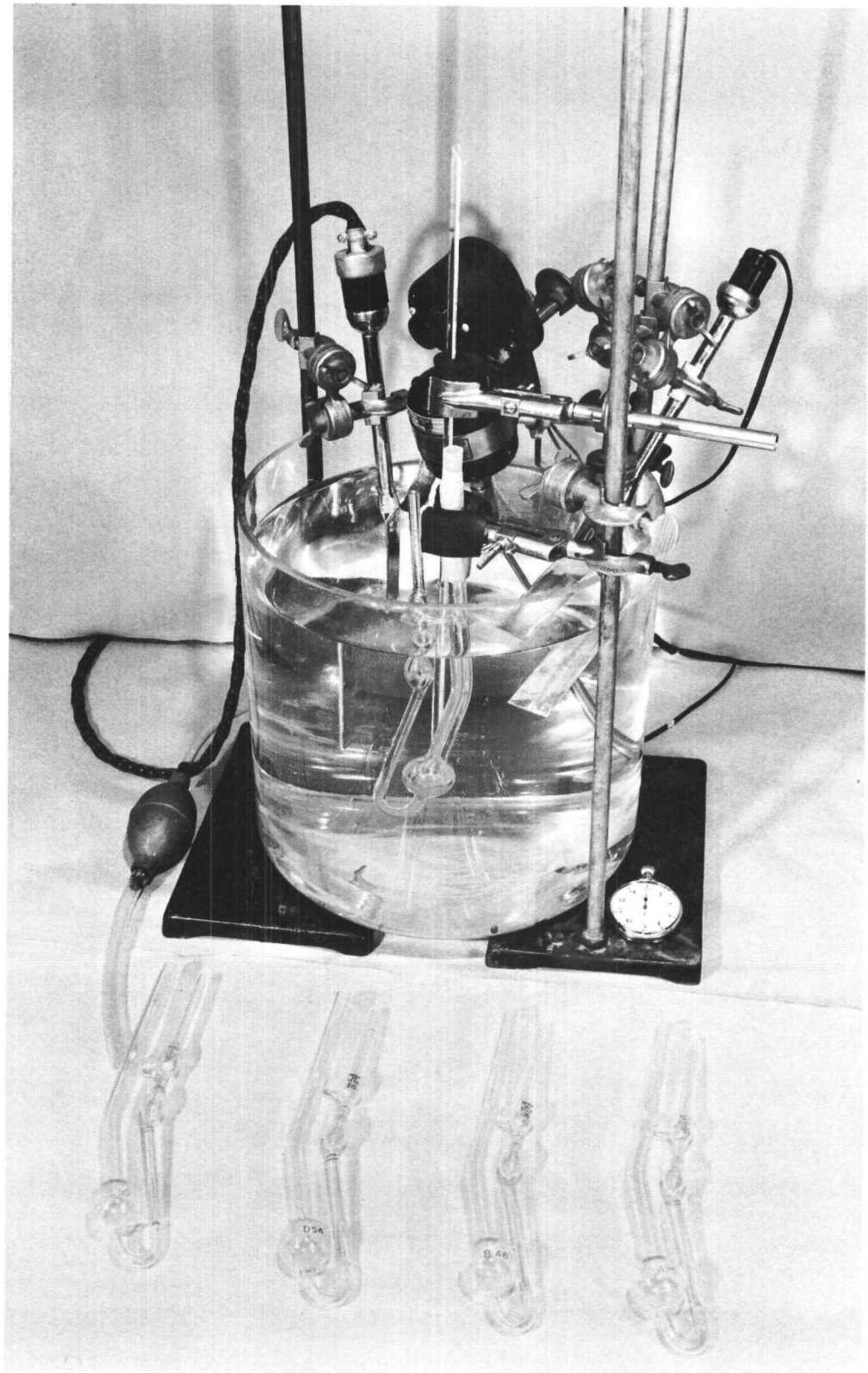

Figure 3.3 Ostwald Viscometers and Constant - Temperature Water Bath.

tabulated in table 3.1. The time was recorded with a stop watch calibrated to a tenth of a second.

Table 3.1. Viscometer Constants*

Viscometer number	Viscosity range (cp)	b
50	0.7 - 3.2	0.00276
100	3 - 22	0.0127
200	20 - 80	0.0988
300	50 - 200	0.248
400	240 - 960	1.110

*$\mu = b\ \rho\ t$,

where

μ = Viscosity. . . . . centipoises
b = Viscometer Constant
ρ = Density . . . . . lb_m/ft^3
t = Time . . . . . sec

A heat exchanger was installed in the liquid storage tank in order to control the temperature of the glycerine-water mixture. The liquid was controlled to within 0.2° Centigrade for the temperature range from 15° to 28° Centigrade. A thermocouple located near the inlet to the test section and a thermometer placed in the separator provided temperature measurements across the test section. Leeds and Northrup iron-constantan wire was calibrated in position and connected to a potentiometer to form the thermocouple circuit. The thermometer used was a Cenco centigrade type, number 500212, which was certified to maintain a tolerance of $\pm$0.1° Centigrade by the National Bureau of Standards for the range of temperatures investigated. This arrangement provided for control of the temperature through the test section, which in turn provided for a means of regulating the viscosity of the liquid phase. Thermocouple connections are shown in figure 3.4.

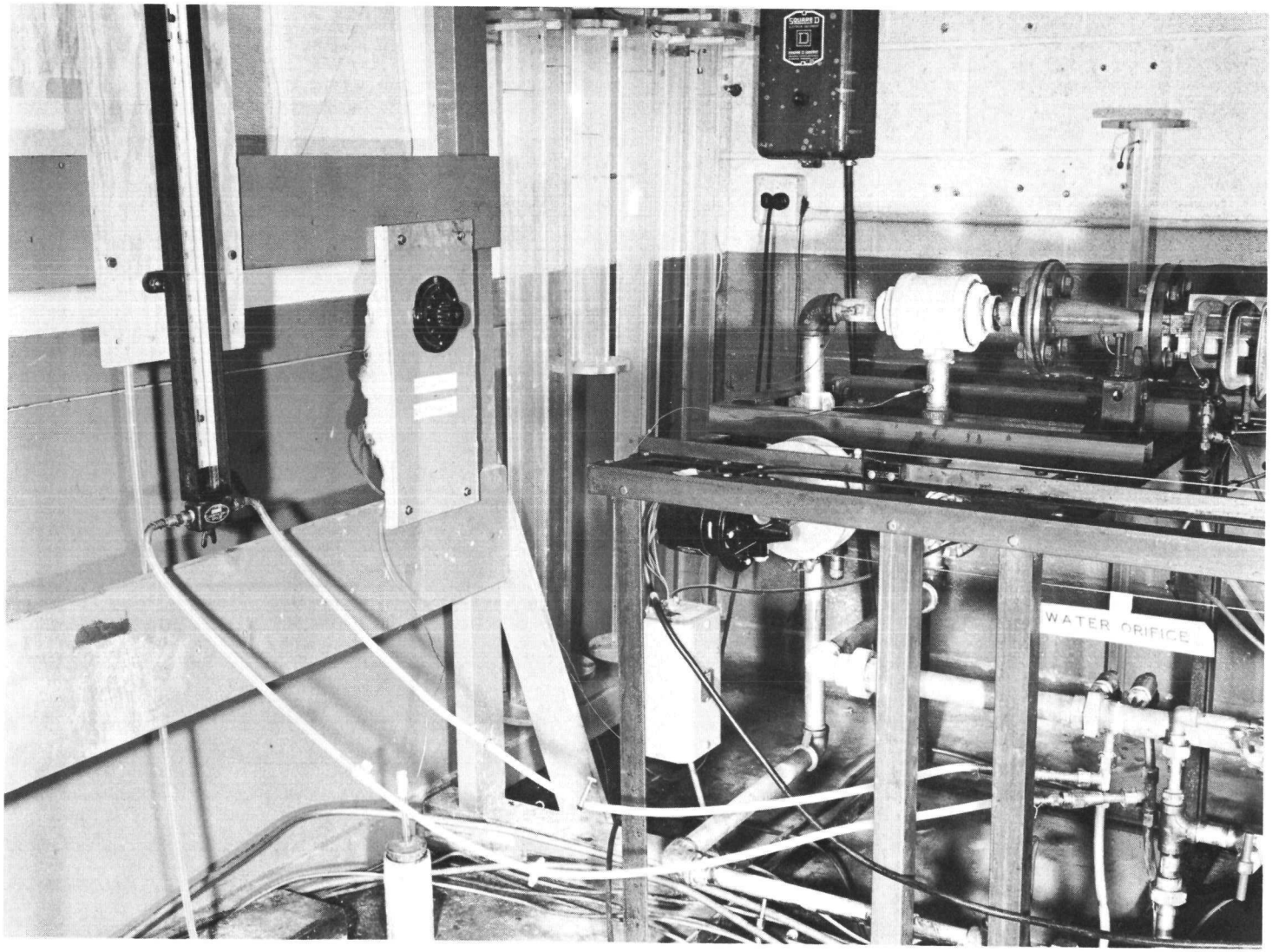

Figure 3.4 Thermocouple and Water Orifice Connections

Flow Rates. The glycerol mixture was controlled by a set of valves in parallel, and metered by a 0.5215-inch orifice and two U-tube manometers in series, as schematically shown in figure 3.1. The orifice coefficient "K" was experimentally determined for a Reynolds number range from 10 to 80,000 by means of a large number of calibration runs. These runs were made for a large range in concentration of the glycerol mixtures in order to obtain the required Reynolds number range. A series of runs were made at a particular concentration range and the best weighted curve was drawn through the data. The final curve, shown in figure 3.5, represents a synthesis of these curves over the required Reynolds number range.

The results of another investigation by Tuve and Sprenkle,[21] which contains a summary of the results of a number of investigators, are also presented in figure 3.5 for the same range of Reynolds numbers. The viscosity of the water and glycerol mixtures was determined by Sheely[22] to within ± 0.02 percent for the range of concentrations and temperatures corresponding to the present investigation, as shown in figure C.1 (in Appendix C). Experimental investigations of the densities of water and glycerol mixtures over a wide range of concentrations and temperatures has been determined by a number of investigators, and the results of these investigations are summarized in figure C.2 (see Appendix C). The results of these studies served to determine the liquid flow rates for various concentrations and temperatures, so that the running conditions could be predicted, as shown in Appendix C.

In the viscosity range from that of water (i.e., 1 cp) to approximately 100 cp, a conventional U-tube manometer with indicating fluids of 1.95 and 13.65 specific gravity were used. In the higher viscosity range, from 100 cp to 500 cp, errors in the flow rate measurement due to bubble entrainment and sluggish fluid movement in the Tygon lines were noted. To eliminate these errors in the measurement of the flow rates, the following steps were taken. Clear Tygon tubing was connected in series to the orifice taps to visually detect bubble

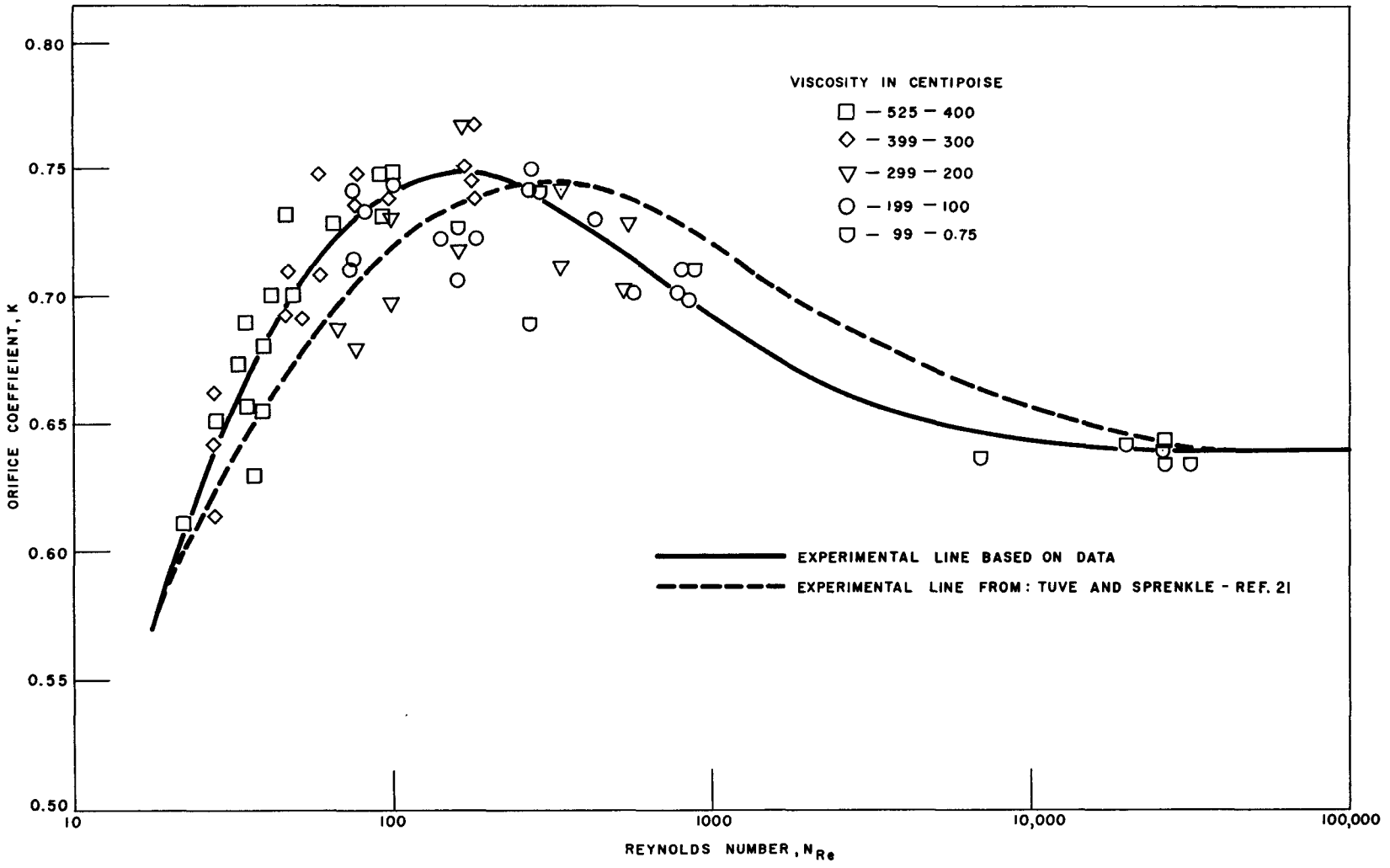

Figure 3.5 The Effect of the Reynolds Number on the Orifice Coefficient for the Liquid Component

entrainment. Static pressure readings were taken with the glycerin-water solution acting as the indicating fluid to reduce the sluggishness on the part of the fluid. Equal air pressure was maintained on the static lines to control the height of the fluid within them. This procedure allowed for the accurate metering of the flow rate, since it depended on the pressure difference and not on the total head. The manometer system is shown in figure 3.4 and 3.6.

An independent method of measuring flow rates was employed at the separator. It consisted of weighing the separated liquid stream before its return to the storage tank. This system determined the flow rates during the run and was used to check the flow rates measured by the orifice. The apparatus is shown in figure 3.2.

Air System

The air passed from the 100-psi laboratory supply line into a set of filters which removed impurities. The two orifices with diameters of 0.961 and 0.2705 inch metered the flow and were installed according to the method described by Grace and Lapple.[23] A constant pressure of 75 psig was maintained at the orifices by means of a Norgren air regulator. Two manometers containing fluids with specific gravities of 1.25 and 13.65, respectively, together with three regulating valves, both connected in parallel, provided for the range and control in the measurement of the air flow rates. The system is also shown in the schematic figure 3.1.

Flush-out System

Daily void traverses were taken of the channel when it contained air in order to minimize the errors due to the drift in the recorder and the decay of the radioactive source. After an experimental run was completed, the glycerol mixture which remained on the inner walls of the test section was rinsed out with water, and the channel was completely dried with air. During the flushing operation, the test section was isolated from the rest of the system by means of valves located

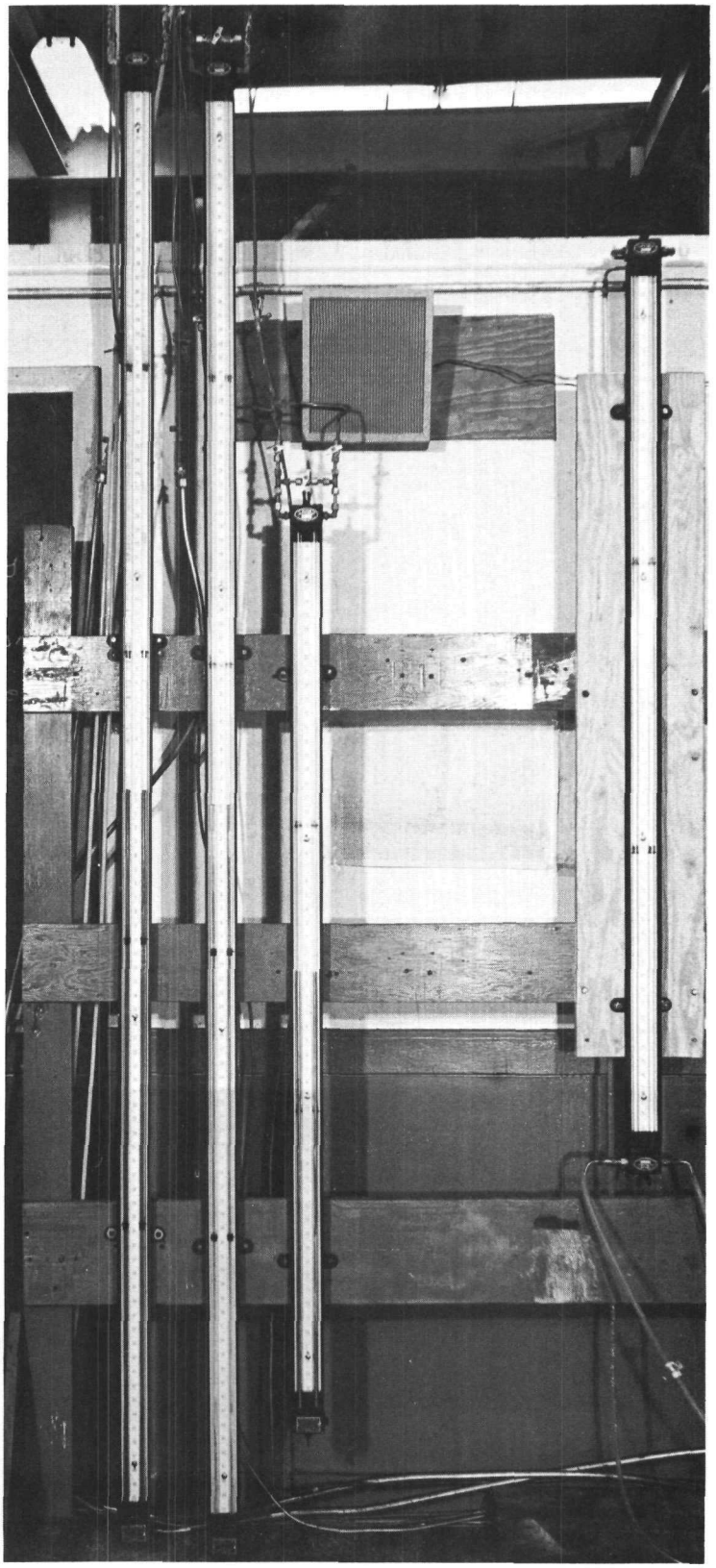

Figure 3.6 Manometer System for the Measurement of the Gas and Liquid Flow Rates.

at the entrance and exit. This prevented the water from contaminating the glycerol mixture. A set of valves provided for the introduction of water to the isolated channel at the entrance, while another set of valves provided for drainage at the exit. Drainage valves were also installed on the Tygon lines leading to the pressure board. After the test section and the Tygon lines were rinsed out, the channel was dried out with air. The concentrations of the glycerol mixtures were measured before and after the test section was flushed out; no significant variations were apparent. The flush-out system is schematically shown in figure 3.7 through figure 3.9.

Test Section

A rectangular Lucite channel, ten feet long, with an outside cross section of 1 x 2.5 inches and a wall thickness of 0.25 inch was selected for the investigation. Metal flanges were clamped to the outside of the test section to serve as a reinforcement during the experimental runs at the high liquid viscosities and flow rates. The location of the pressure taps on the Lucite channel are shown in the schematic figure 3.10.

Pressure System

The pressure system provided an adequate means of measuring the total pressure and the pressure drop between the taps in the test section. It was composed of strips of clear Tygon tubing fastened to a ten-foot board in a vertical direction, level with the test section, and connected to the bottom of the test section at various points along its length. A mercury U-tube manometer was connected to both the top of the Tygon tubes by means of a manifold and pieces of Tygon tubing, and to the 100-psi air supply line by means of a valve. The system is illustrated in figure 3.1 and schematically shown in figure 3.10.

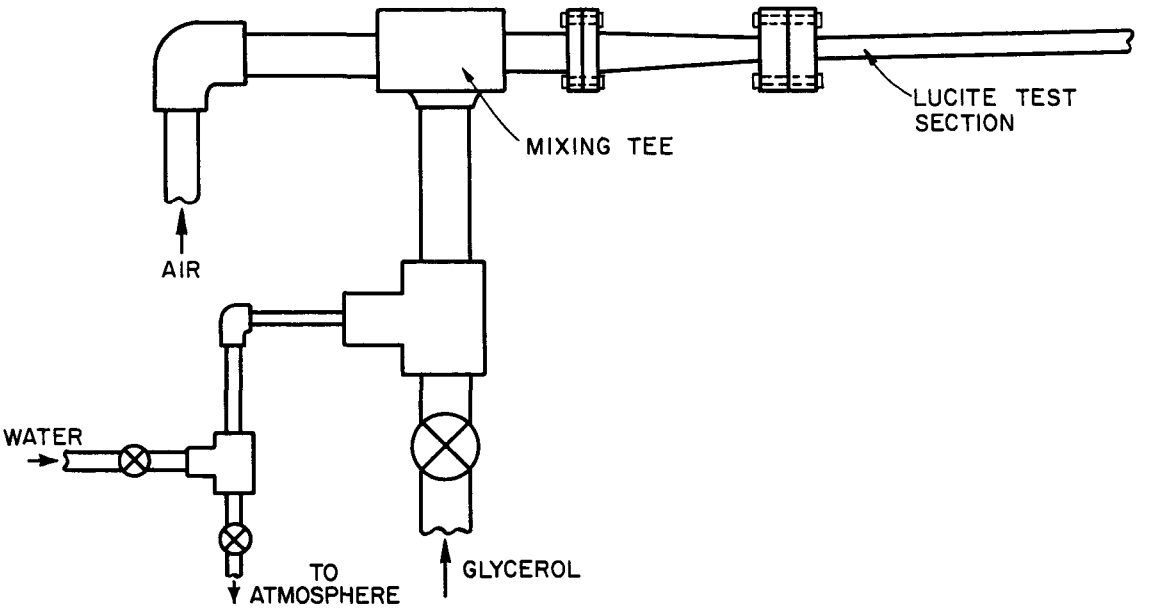

Figure 3.7 Test Section Entrance

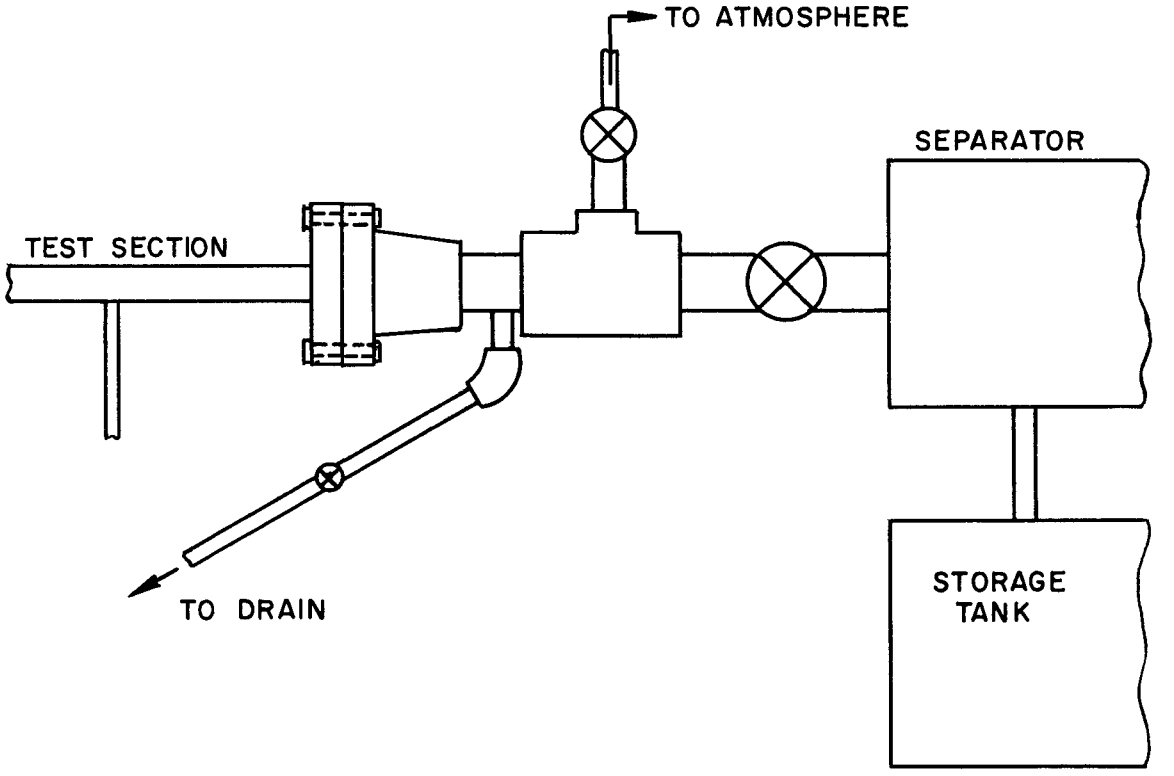

Figure 3.8 Test Section Exit

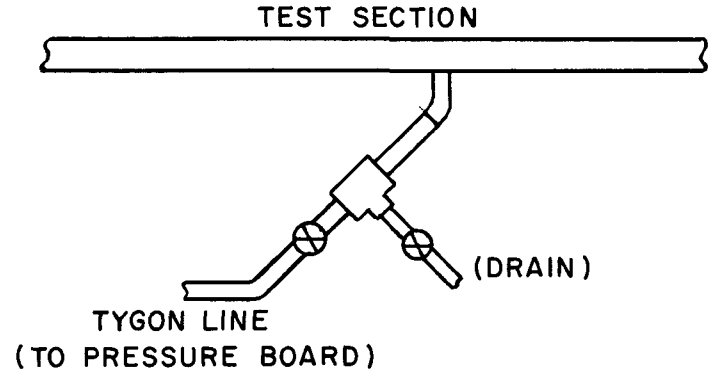

Figure 3.9 Drainage on Tygon Pressure Line

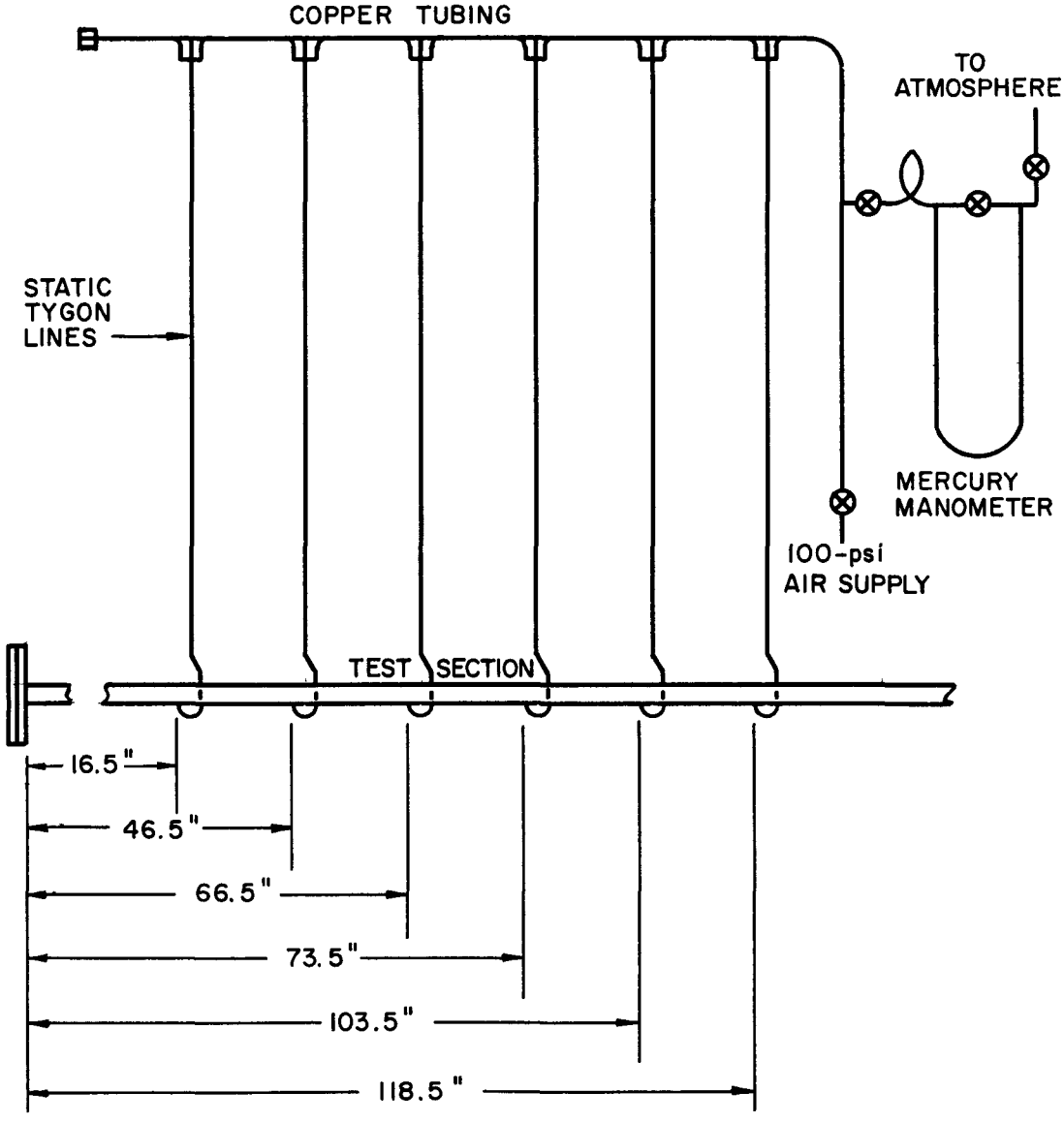

Figure 3.10 Pressure System - Schematic

The height of the glycerol mixture in the Tygon tubing indicated the magnitude of the static pressure in the test section. As the static pressure in the test section increased, the height of the glycerol column rose in the Tygon line proportionately. For large values of static pressure, enough back pressure was maintained on the top of the glycerol columns, by adjusting the valve connected to the air-supply lines, to keep their heights at a reasonable level. The mercury manometer measured the magnitude of the back pressure on the columns of glycerol. The difference in the heights of the columns of glycerol in the Tygon lines determined the pressure drop in the test section. The total pressure exerted by the fluids in the test section was determined by combining the readings from the mercury manometer with the height of the glycerol column in the static line at the particular pressure tap desired. This method indicated the total pressure in the test section at each pressure tap. The calculations in Appendix C indicate how the pressure measurements were used in the reduction of the data.

Capillary tubes were inserted in the Tygon lines, at the lower liquid viscosities, to reduce fluctuations due to pressure variations during the experimental runs. The capillary tubes were removed for experimental determinations at the higher liquid viscosities (i.e., 100 to 500 cp), because the fluctuations were damped out by the viscous action of the fluid.

Void-measuring Equipment

Richardson's traversing equipment was employed for the measurement of the void volume fractions. The equipment consisted of a source and a detector, rigidly held together in a U-shaped frame, which was raised or lowered by a system of pulleys and cables, allowing for a traverse to be taken of the test section. The equipment was supported on four grooved fibre wheels which rolled on rails and allowed for the measurement of void volume fractions at any spot along the ten-foot channel. The system is shown in figure 3.11.

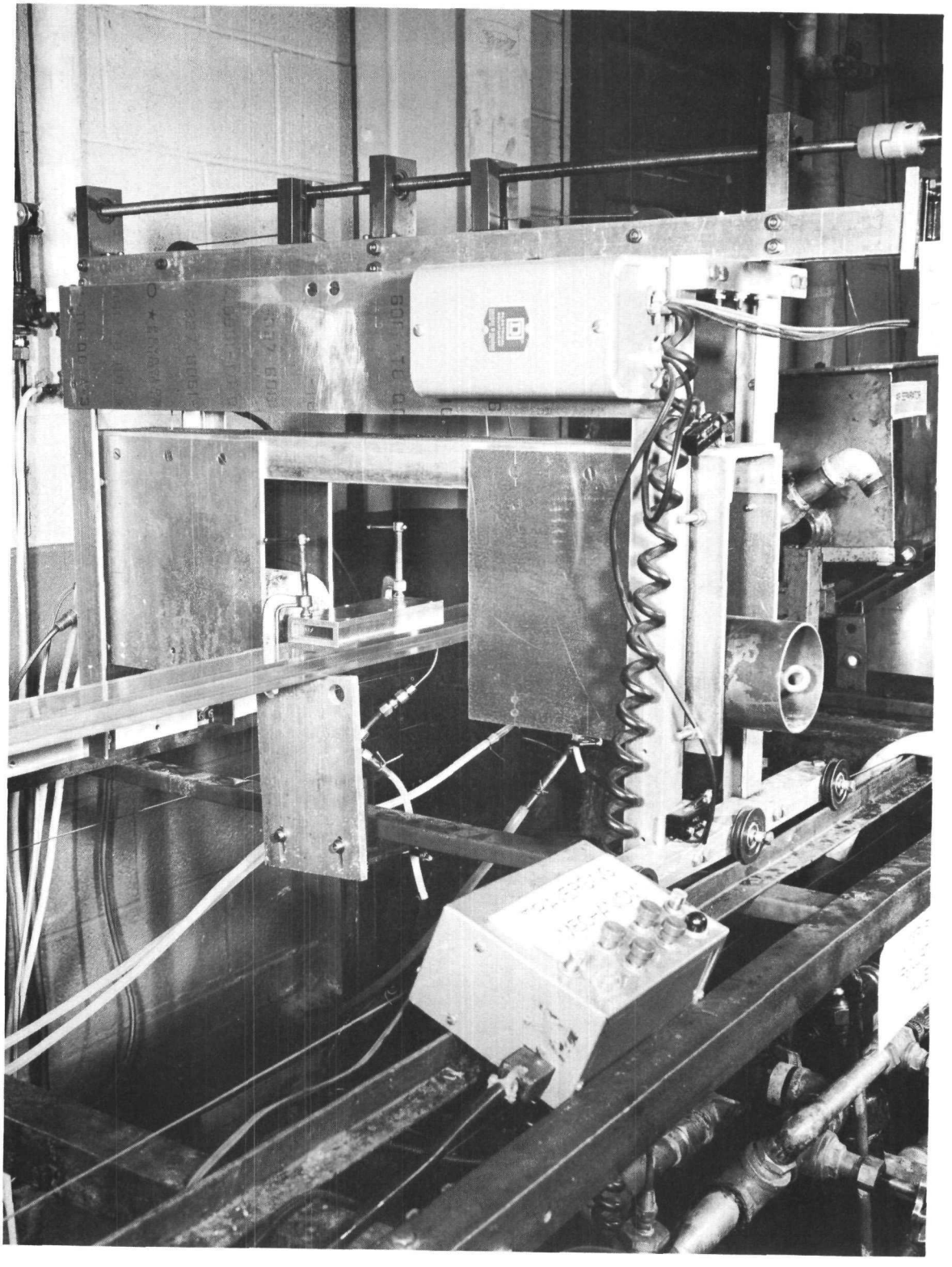

Figure 3.11 Void Mockup Setup and Traversing Mechanism.

The source, which is shown enclosed in the circular shell which is supported by the U-shaped frame in figure 3.11, was a Tm^{170} pellet. This pellet provided the required gamma-ray emission for the measurement of the void volume fraction. Tm^{170} has a half-life of 129 days with energy peaks at 0.053 and 0.084 Mev. The decay and energy schemes are depicted in figure 3.12. The pellet was encased in a 3.5-inch diameter cylinder, 6 inches in length which is shown in figure 3.13. A 0.25-inch lead filter was placed over the end of the cylinder to eliminate most of the radiation of lower energy, so that the desired exponential radiation could be emitted.

A scintillation crystal optically coupled to a photomultiplier tube and encased in an aluminum shield provided for the detection of the gamma radiation passing through the test section. The system is shown in figure 3.14. To protect the scintillation crystal from picking up extraneous radiation, a lead shield was placed around the system. A rectangular slot was cut on the face of the shield to provide for the emission of the gamma radiation. A high-voltage supply was connected to the detection system and coupled to a linear current amplifier for the monitoring of the signals produced by the incoming radiation.

A Brown Recording Potentiomenter (Model S-153X-16-X-156) was used to record the signals from the detection system. The amplifier, power supply, and recorder are shown in figure 3.15.

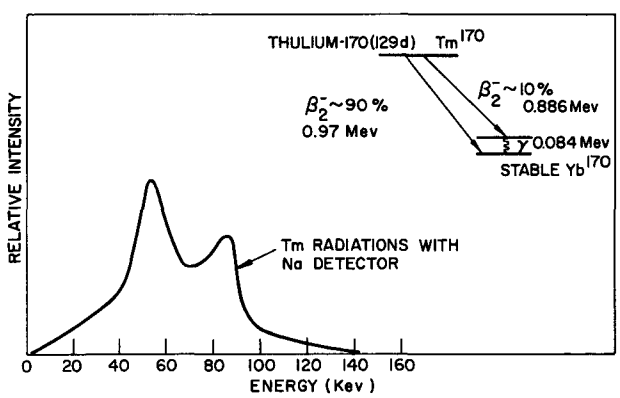

Figure 3.12 Energy Spectrum and Decay Scheme for Thulium-170.

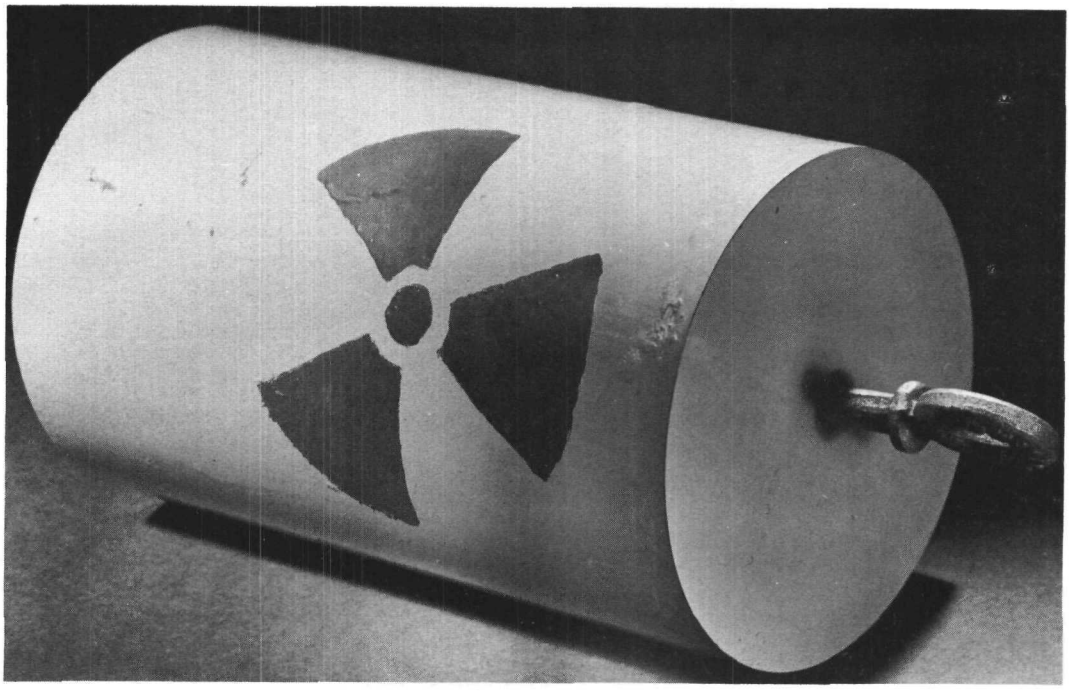

Figure 3.13 Thulium-170 Source in Lead Cylinder.

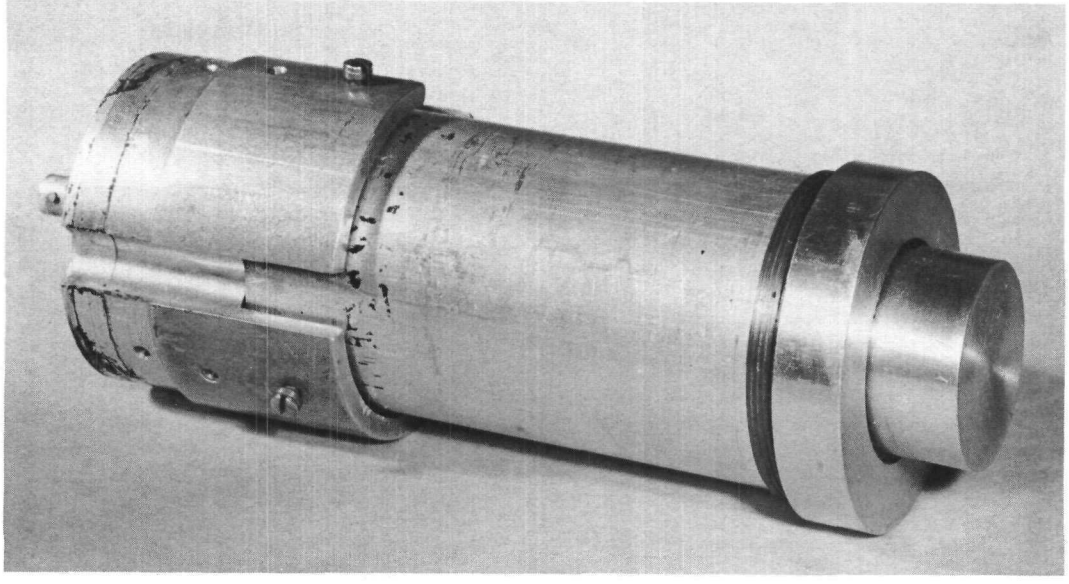

Figure 3.14 Scintillation Crystal Photomultiplier Tube Assembly.

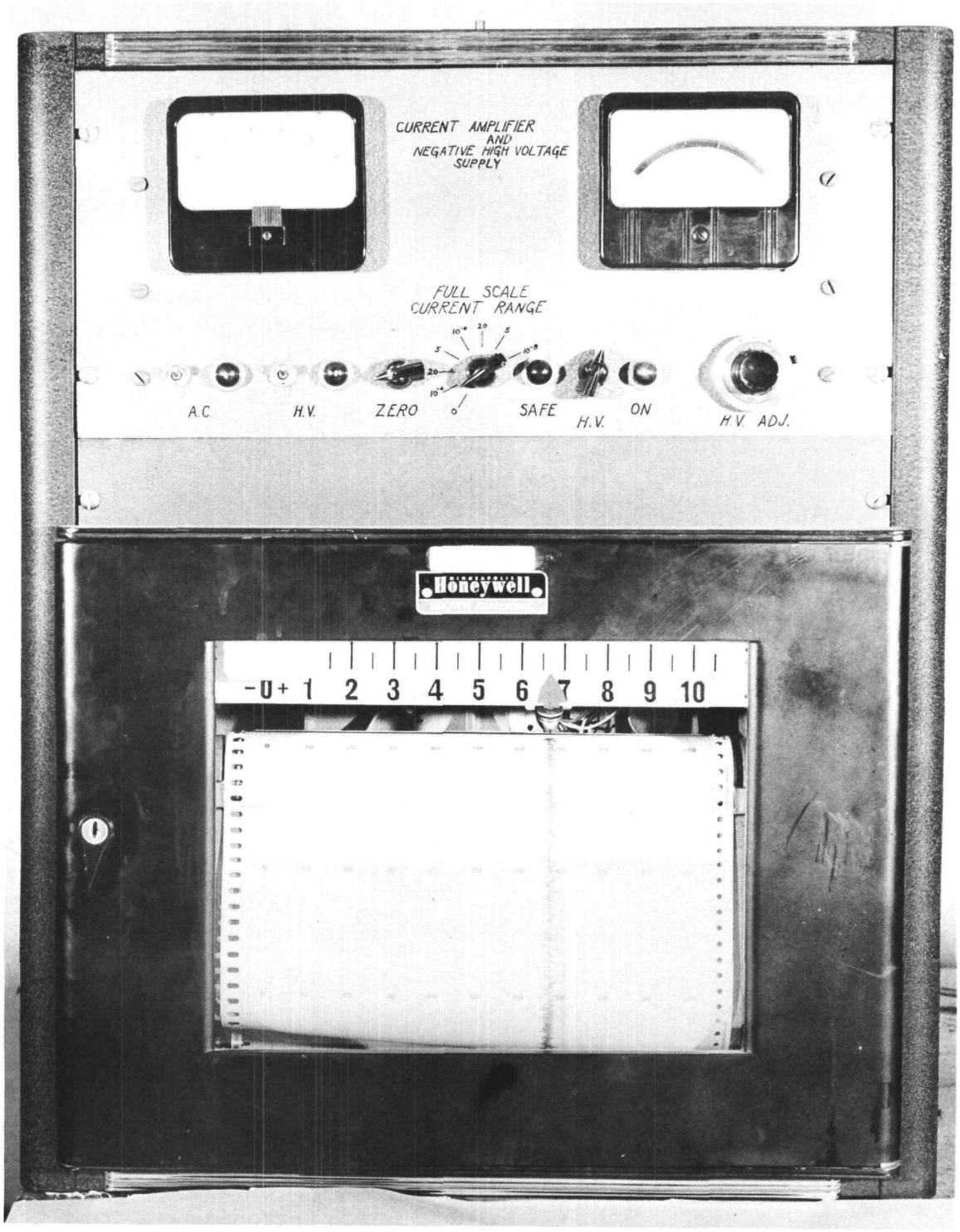

Figure 3.15 Amplifier, Power Supply and Recorder.

CHAPTER IV
EXPERIMENTAL PROCEDURE

Certain techniques were followed during the course of the experimental program to maintain uniform operating conditions. The following description of a typical test run illustrates the method used throughout the experimental program.

Typical Test Run

The recorder was adjusted to the required voltage and current settings for the day's operations, and set at the zero position. After each traverse, the positioning was rechecked to reduce drift. The alignment of the test section was checked with a hand level. The agitator was turned on to circulate the water in the bath. The traversing equipment was moved to the desired position along the length of the test section. A traverse in both vertical directions was taken of the test section containing air only. This traverse was denoted as the "empty" and the traverse taken when the test section was completely filled with the liquid component was denoted as the "full" traverse. Empty and full traverses were taken in both directions so that the test run traverse could be compared to them for the same direction so as to eliminate any errors due to the misalignment of the traversing mechanism. A barometer reading was also taken, and the concentration of the glycerol mixture was determined by measuring the viscosity, in the constant-temperature water bath, of a sample taken from the storage tank.

The glycerol mixture was circulated through the test section while the full traverse was taken. During this time, the manometer corresponding to the desired flow rate was selected, bled to remove any air entrained in the lines, and set for the desired flow rate. The flow rate was determined by the procedure described in Appendix C. After equilibrium conditions were attained, a gravitational flow rate determination was made and compared to the flow rate determined

from the manometer readings. The viscosity of the liquid mixture was regulated by controlling the temperature of the circulating glycerol mixture. The desired temperature was determined from the concentration measurements, and the control valves on the heat exchanger were adjusted accordingly. The temperature and pressure-drop readings were recorded when the system became stable.

The valves regulating the air supply were opened at this time. Adjustments were made to maintain the desired 75-psig back pressure on the orifice at the desired flow rate of air. A soap-bubble check was made to detect any leaks in the air-manometer system. The temperature and liquid flow rates were readjusted and a gravitational flow rate determination was made after the system was allowed to stabilize. After all the desired conditions were established, the test run traverse was made. During this time, readings of the thermocouples at the inlet to the test section, the thermometer in the separator tank, the gas and liquid flow rates, and the pressure-drop readings for the test section were recorded.

After the test runs were completed for the day, the test section was closed off and flushed out with water. The horizontal alignment of the test section was checked while still partly filled with water. The test section was then thoroughly flushed out and dried with air. The heaters in the water bath, the high-voltage supply, and the current amplifier were left on to insure steady-state conditions in these components for operations the next day.

CHAPTER V
FLOW PATTERNS AND PHASE DISTRIBUTION

Analytical and semi-empirical predictions connected with two-phase flow are based on idealized flow models. It has been generally accepted that the slippage between the gas and liquid phases varies with the flow regime. Investigations by Baker[24] and by Bergelin and Gazely[25,26] have been made to correlate the pressure drop associated with two-phase flow for particular types of flow patterns. The current investigation is concerned with the effect of the liquid viscosity on the flow pattern and phase distribution. This, in turn, serves as an aid in determining the slip ratio and the pressure drop in the two-phase mixture.

Historical

The flow of liquid and gas mixtures in horizontal channels has been separated into the following categories by Alves.[27] They are reported in their order of transition for a constant liquid flow rate and an increasing gas flow rate. They are:

1. Bubble Flow. The gas phase consists of bubbles which move slowly along the upper portion of the liquid phase.
2. Plug Flow. The bubbles combine to form gas pockets which flow along the surface in long segments at slightly greater velocities.
3. Stratified Flow. The gas pockets or plugs combine to form a smooth interface between the two phases. Gas remains on top due to its bouyancy.
4. Wavy Flow. The interface between the two phases becomes irregular, resulting in a wavy interface between the gas and the liquid phase.
5. Slug Flow. The amplitude of the waves increases resulting in sealing of the tube so that slugs of gas intermittently race down the channel.

6. Annular Flow. The gas phase becomes concentrated in a rapid stream down the center of the channel with the liquid phase surrounding it. Small bubbles of gas are usually entrained in the liquid phase.
7. Spray Flow. The gas envelops the outer liquid perimeter and carries it along as dispersed droplets.

Bernert[28] has suggested that several of the reported flow patterns may be considered as metastable regimes because the phase velocities and void volume fractions are not allowed to reach steady-state conditions. It is highly probable that the most stable flow patterns are represented by the annular and stratified flow regimes.

Martinelli et al.[3] presented a semi-empirical correlation for the two-phase pressure drop based on an annular flow model. Visual studies were made of the flow patterns, although the effect of the variation of the flow pattern was not considered in their correlation. However, the analysis was based on whether the individual liquid and gas phases were in a laminar or turbulent state. The results of the flow pattern survey indicated a general agreement with the observations of Alves.

Bergelin and Gazely conducted visual flow studies and performed an experimental investigation primarily concerned with the stratified flow patterns. The results of their visual survey are shown in figure 5.1. A semi-theoretical analysis based on an idealized stratified flow model served to adequately predict their experimental pressure drop data.

Investigators have reported the results of their visual flow studies in a variety of ways. Richardson's report includes a survey of the various investigations in the field and their methods of correlation.

At the present time there is no general correlation available in the literature that can adequately predict flow patterns for a wide variety of conditions. Investigators are in disagreement as to the boundaries of the various flow regimes and the types of flow patterns. The

lack of agreement is mainly due to the following factors: (a) the variation in the geometry of the mixing tee and the test sections that were used in the various investigations; (b) the hysteresis effect which occurs during the transition between flow patterns; (c) the thin film on the surface of the test sections which tend to obscure the flow configuration during the visual surveys; and (d) the gradual change of the flow regime from one type to another. Although the transition of the flow patterns are depicted as lines by the investigators such as shown in figure 5.1, the transitions are actually gradual changes.

Experimental Scope

The effect of the viscosity of the liquid phase on flow configurations was investigated experimentally by means of photographs, a visual flow regime study, and a phase distribution study.

Photographs were taken of the representative flow patterns at a liquid viscosity of 500 cp. These pictures were compared with Richardson's photographs of air-water mixtures. A visual flow regime study was conducted in the 1 x 2.5-inch Lucite test section at liquid viscosities of 1, 20, 150, 250, and 500 cp. Constant liquid flow rates were maintained as the gas flow rate was increased. The gamma-ray attenuation system produced a continuous trace of the void volume fraction for any desired location along the length of the test section. Void volume fractions taken during the experimental investigation provided an approximate distribution of the gas and liquid phases along the vertical width of the test section. Experimental conditions were selected so that the effects of liquid viscosity, quality, and liquid flow rate on the phase distribution could be adequately evaluated.

Results

Visual Analysis-Photographs. Photographs of representative flow patterns at a liquid viscosity of 500 cp are shown in figure 5.2 through figure 5.11. They are presented in the order of transition for a constant liquid flow rate and an increasing rate of gas flow. The flow

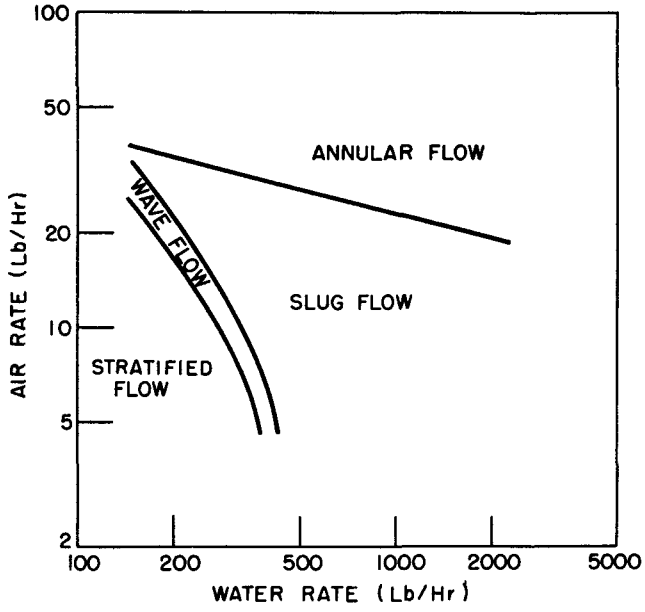

Figure 5.1 Areas of Flow Patterns for the Flow of Two-phase Air-Water Mixtures (from Bergelin and Gazely).

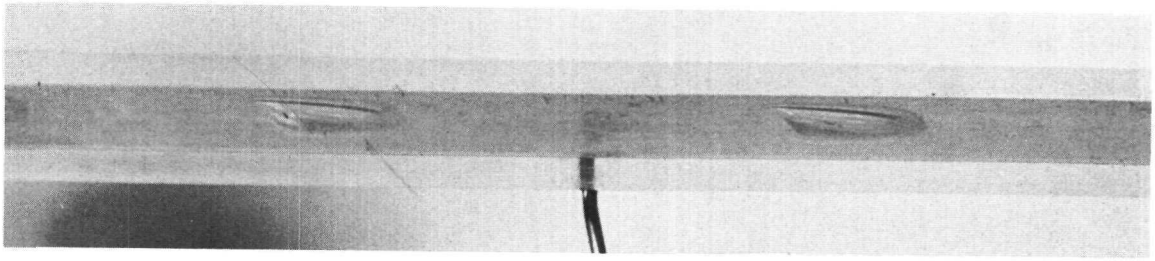

Figure 5.2 Bubble Flow. (Viscosity 500 cp)

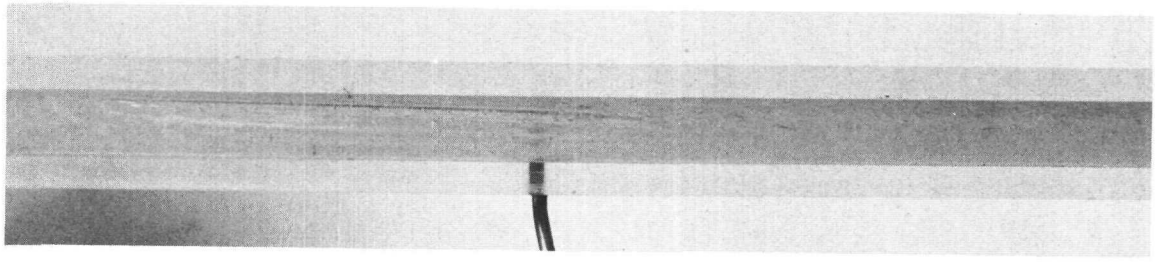

Figure 5.3 Transition from Bubble to Plug Flow. (Viscosity 500 cp)

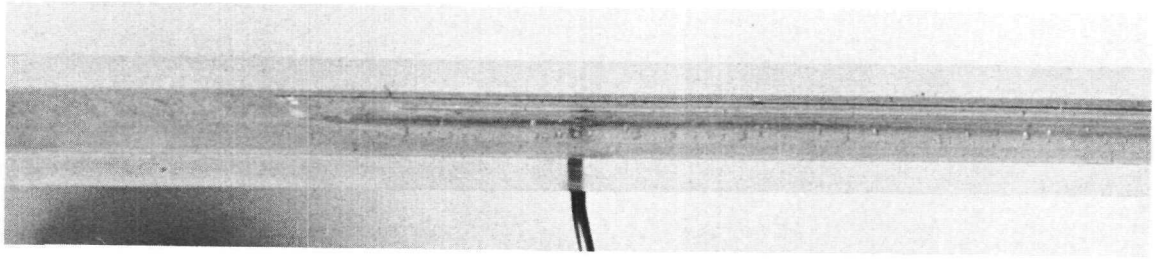

Figure 5.4 Plug Flow. (Viscosity 500 cp)

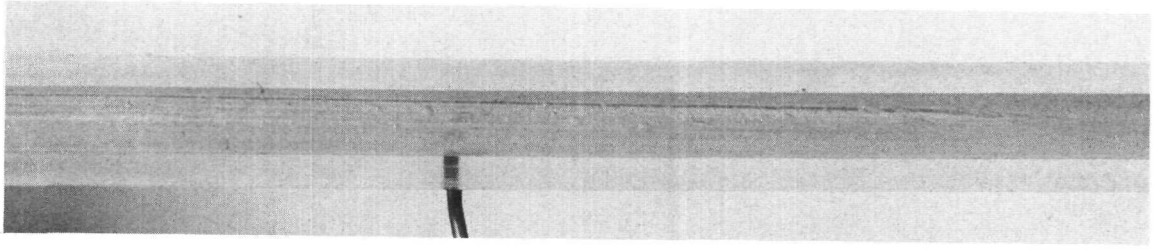

Figure 5.5 Transition from Plug to Stratified Flow. (Viscosity 500 cp)

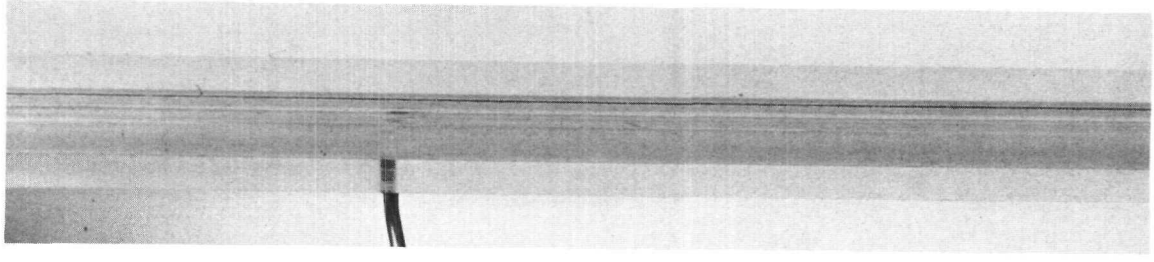

Figure 5.6 Stratified Flow. (Viscosity 500 cp)

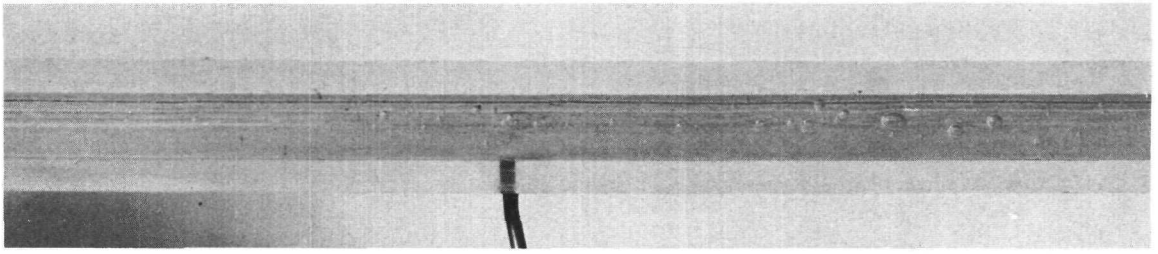

Figure 5.7 Wave Flow. (Viscosity 500 cp)

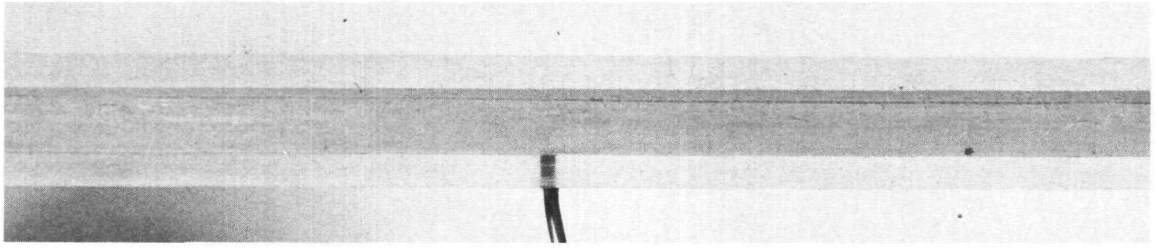

Figure 5.8 Transition from Wave to Slug Flow. (Viscosity 500 cp)

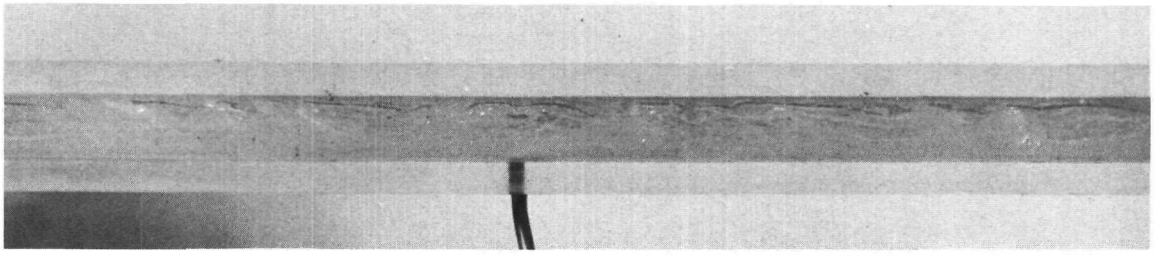

Figure 5.9 Slug Flow. (Viscosity 500 cp)

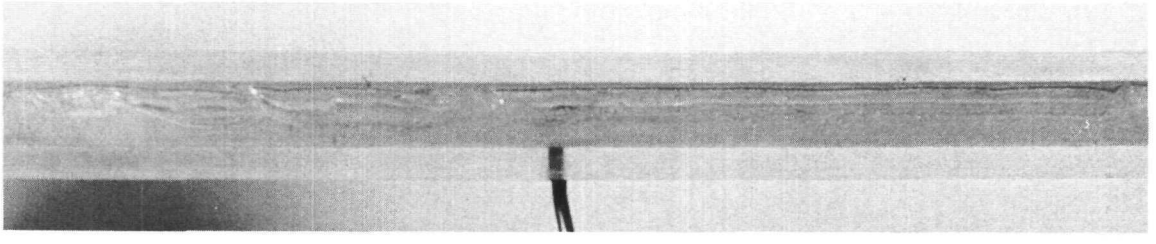

Figure 5.10 Transition from Slug to Stratified Annular Froth Flow. (Viscosity 500 cp).

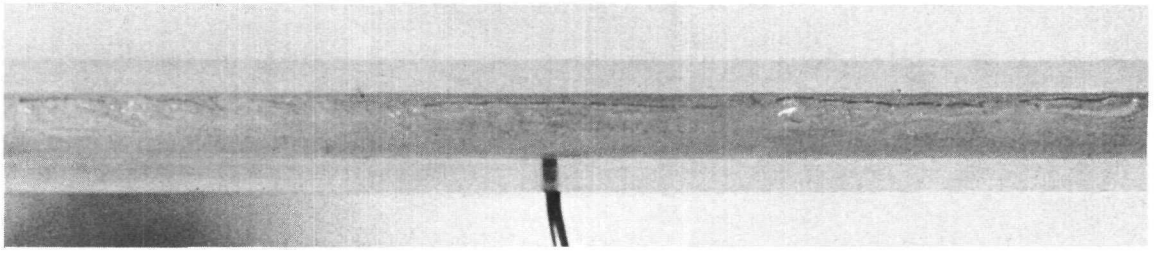

Figure 5.11 Stratified Annular Froth Flow. (Viscosity 500 cp)

patterns for the lower rates of gas flow are similar to those reported by Alves. However, the annular and spray flow patterns are not present at the higher flow rates. Instead, a flow pattern designated as "Stratified Annular Froth" is present. It consists of a highly turbulent stream of gaseous slugs of varying sizes. The liquid stream surrounding the slugs appears to be a froth at the very high rates of gas flow. The gaseous slugs move in a random, jerky motion down the length of the channel. This effect was evident for a majority of the flow configurations encountered in the present investigation. It increased in frequency and intensity as the gas flow rate and/or liquid viscosity increased.

The effect of the liquid viscosity on the flow pattern can be seen from a comparison of the pictures taken at 500 cp in the current study and the pictures taken by Richardson for air-water mixtures. They are shown in figure 5.12 thru figure 5.15. A smoother interface is noted for most of the flow configurations at the higher liquid viscosities. The air-water mixtures exhibited a greater amount of froth for the high air and liquid flow rates as compared with the air-glycerol mixtures. The smoother interface between the two phases and the reduction in frothing at the higher liquid viscosities can be attributed to the laminar condition of the liquid phase in this viscosity region.

Flow-Regime Study. The results of the flow regime study are presented in figure 5.16 through figure 5.20. It can be seen from these figures that, as the liquid viscosity increases, the transition from one flow pattern to another occurs more rapidly, and at higher gas flow rates. However, the transition period between fully established flow patterns takes longer at the higher liquid viscosities. Therefore the bands between flow patterns, which are denoted by lines in the figures, widen as the liquid viscosity increases.

The flow regime investigation covered the range of flow rates encountered in the current investigation of slip ratio. Richardson's

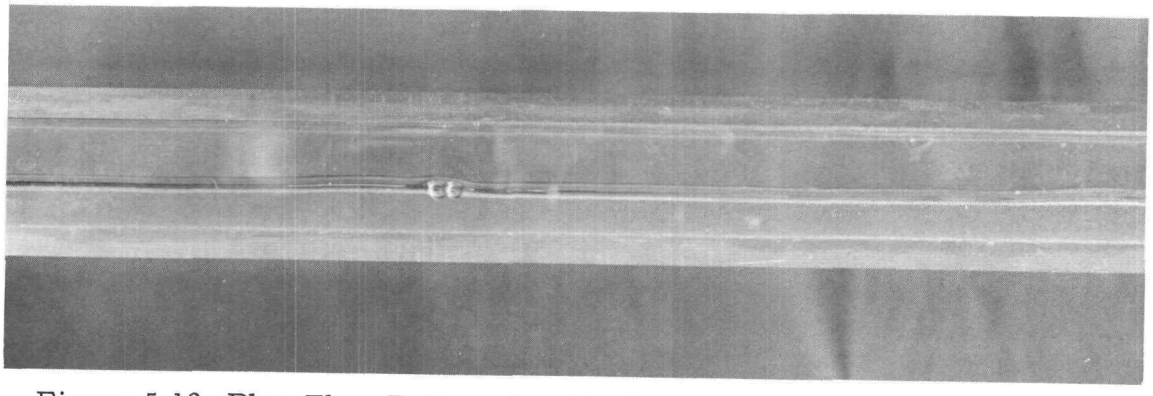

Figure 5.12 Plug Flow Pattern for Air-Water Mixtures from Richardson.

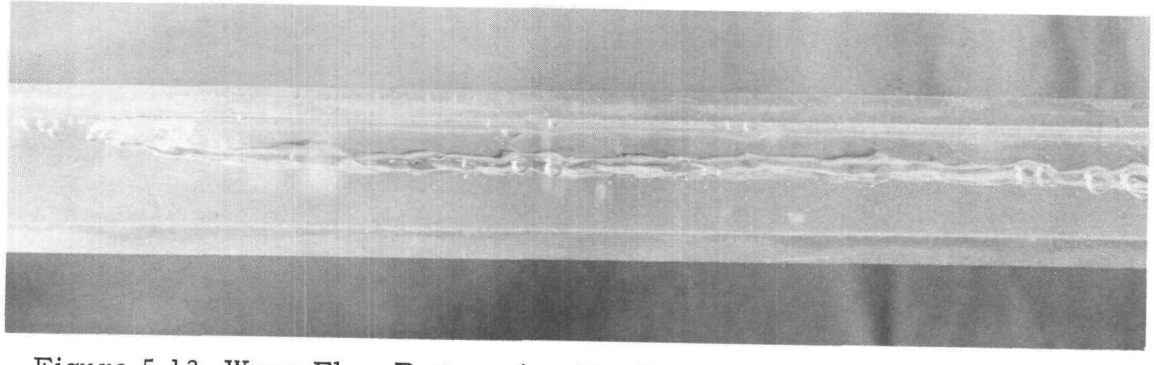

Figure 5.13 Wave Flow Pattern for Air-Water Mixtures from Richardson.

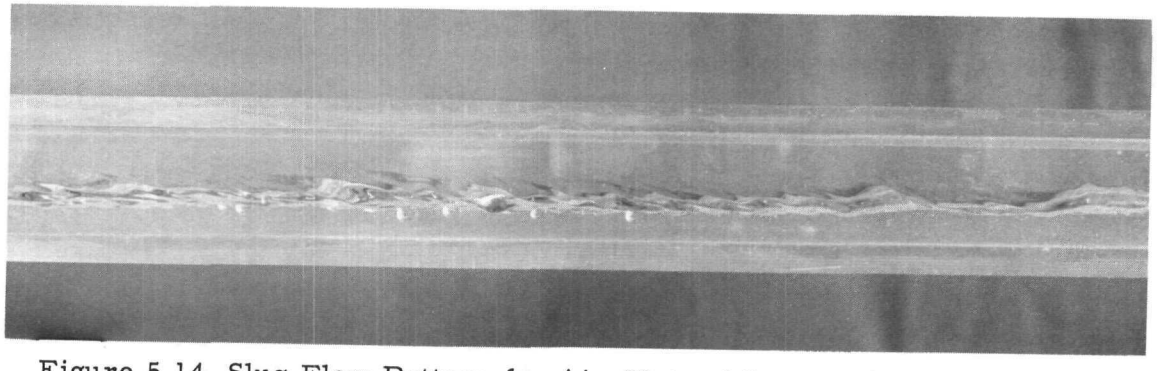

Figure 5.14 Slug Flow Pattern for Air-Water Mixtures from Richardson.

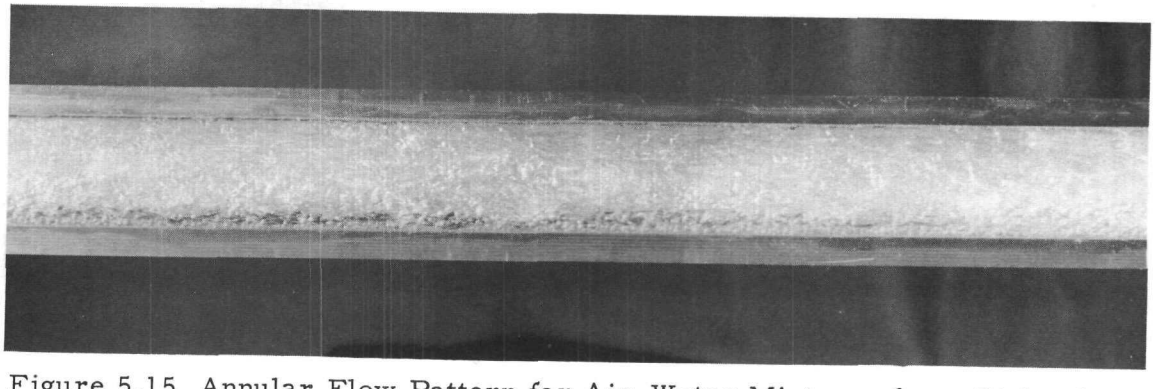

Figure 5.15 Annular Flow Pattern for Air-Water Mixtures from Richardson.

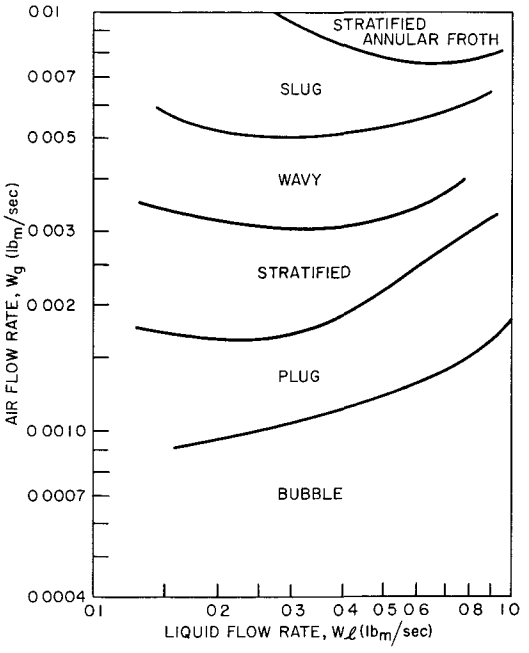

Figure 5.16 Flow Pattern Boundaries for a Liquid Viscosity of 500 cp.

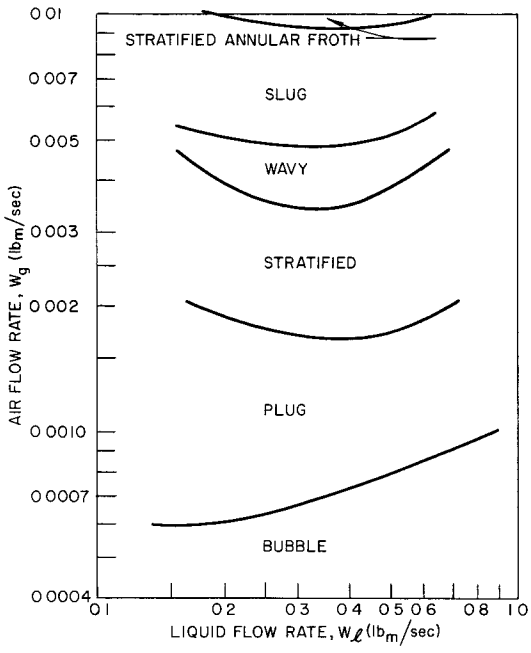

Figure 5.17 Flow Pattern Boundaries for a Liquid Viscosity of 250 cp.

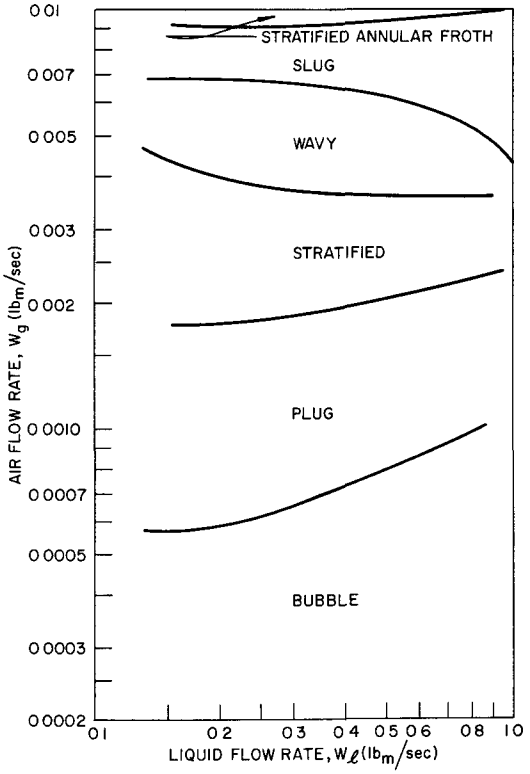

Figure 5.18 Flow Pattern Boundaries for a Liquid Viscosity of 150 cp.

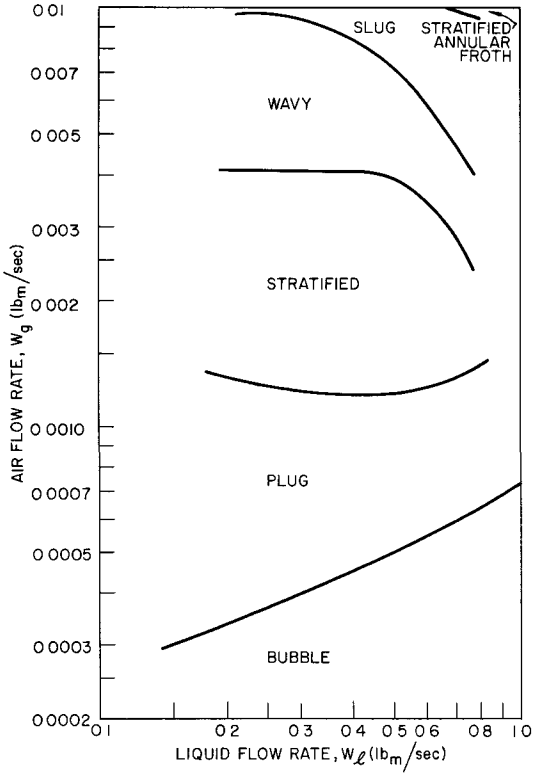

Figure 5.19 Flow Pattern Boundaries for a Liquid Viscosity of 20 cp.

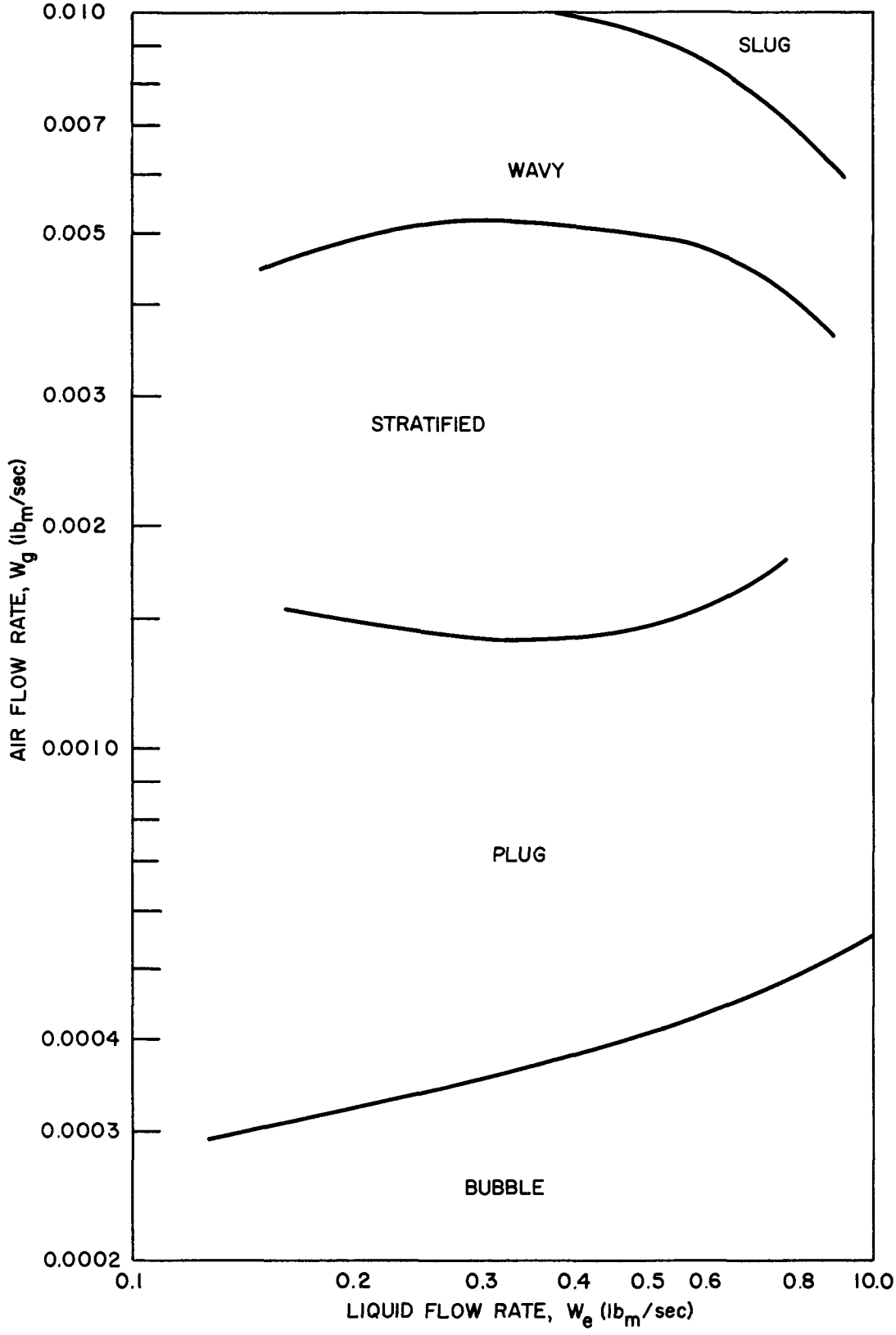

Figure 5.20 Flow Pattern Boundaries for a Liquid Viscosity of 11 cp. (Water)

flow pattern study for the same test section was conducted for the same range of air flow rates but for higher water flow rates. It is shown in figure 5.21. A comparison of figure 5.20 and figure 5.21 reveals that the stratified and wavy flow regimes gradually disappear as the liquid flow rate is increased for the particular channel geometry and dimensions used in the current investigation.

Phase Distribution Study. The effect of the liquid viscosity, quality, and liquid flow rate on the phase distribution is quantitatively described by plots of the void volume fraction versus channel width. The width is denoted as the vertical distance from the lower to the upper surface of the inner portion of the test section. The experimental values for the flow conditions are depicted as various "Run Numbers" and are tabulated in table C.1.

The effect of the liquid viscosity on the phase distribution is shown in figure 5.22 through figure 5.27. Eleven equally spaced point values of the void volume fraction are plotted along the vertical width of the test section in these figures. It can be seen from these figures that: (a) as the liquid viscosity is decreased from 500 cp to 1 cp, the void volume fraction tends to envelop a greater cross-sectional area of the channel; (b) as the gas and liquid flow rates are increased (from Run 11 to Run 55), the void volume fraction appears to "round out" to an approximate semicircular distribution along the width of the channel.

The effect of the quality of the two-phase mixture on the total void volume fraction and phase distribution is shown in figure 5.28 through figure 5.32. It can be seen from these figures that, for constant liquid flow rates and increasing qualities and air flow rates (i.e., Runs 11, 15 and Runs 51, 55): (a) the total void volume fraction at the higher liquid viscosities tends to increase; and (b) the gas phase becomes more concentrated in the center of the test section. As the liquid viscosity decreases, the intensity of the effects noted at the higher viscosities decreases somewhat.

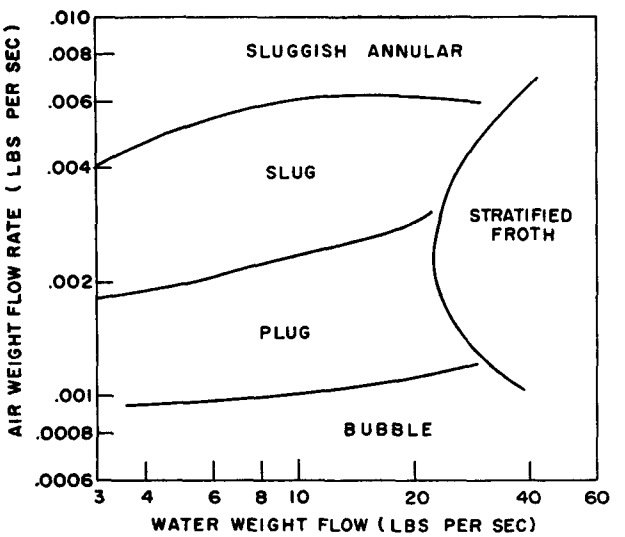

Figure 5.21 Flow Pattern Boundaries for Air-Water Mixtures (from Richardson).

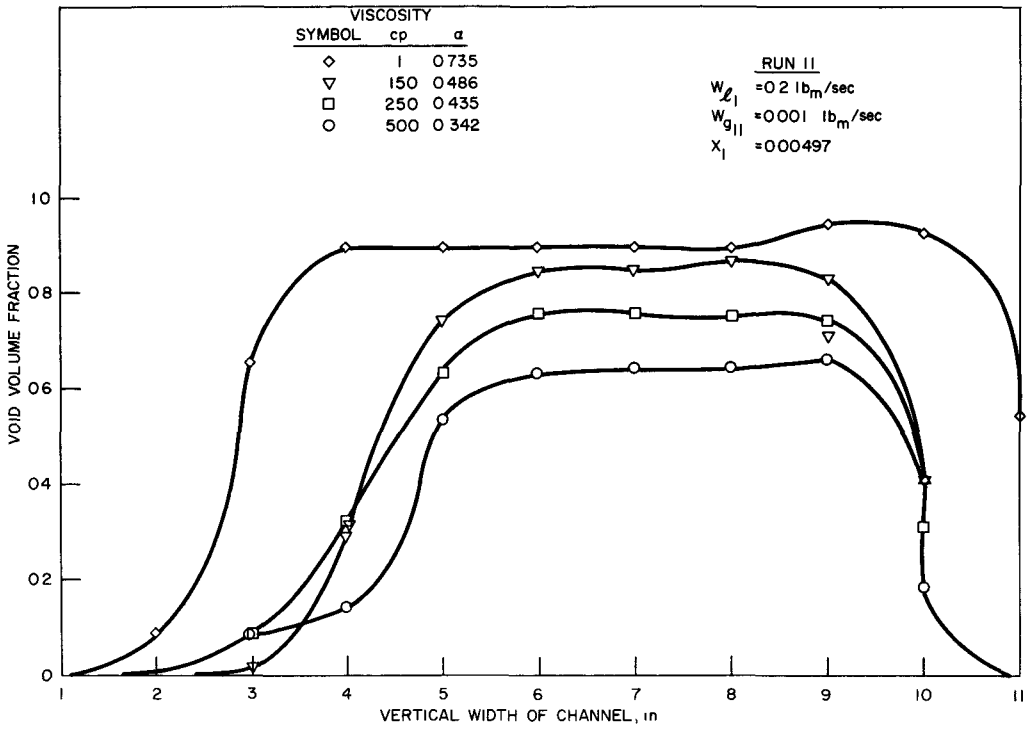

Figure 5.22 Cross-sectional Distribution of Void Volume Fraction for Run 11 and Various Liquid Viscosities.

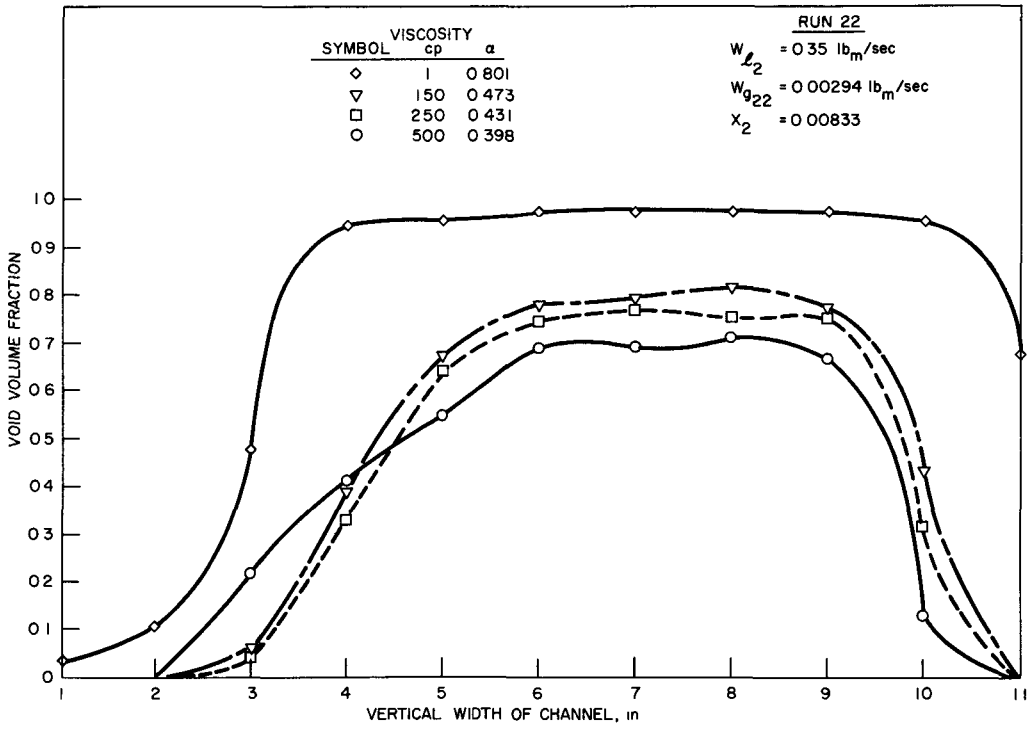

Figure 5.23 Cross-sectional Distribution of Void Volume Fraction for Run 22 and Various Liquid Viscosities.

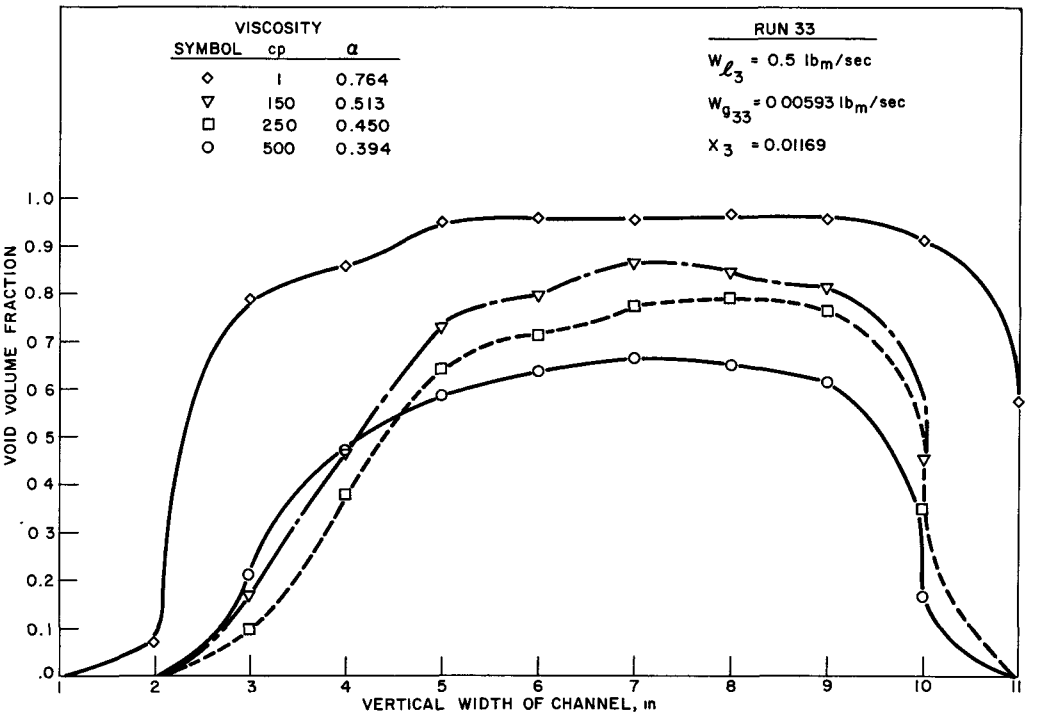

Figure 5.24 Cross-sectional Distribution of Void Volume Fraction for Run 33 and Various Liquid Viscosities.

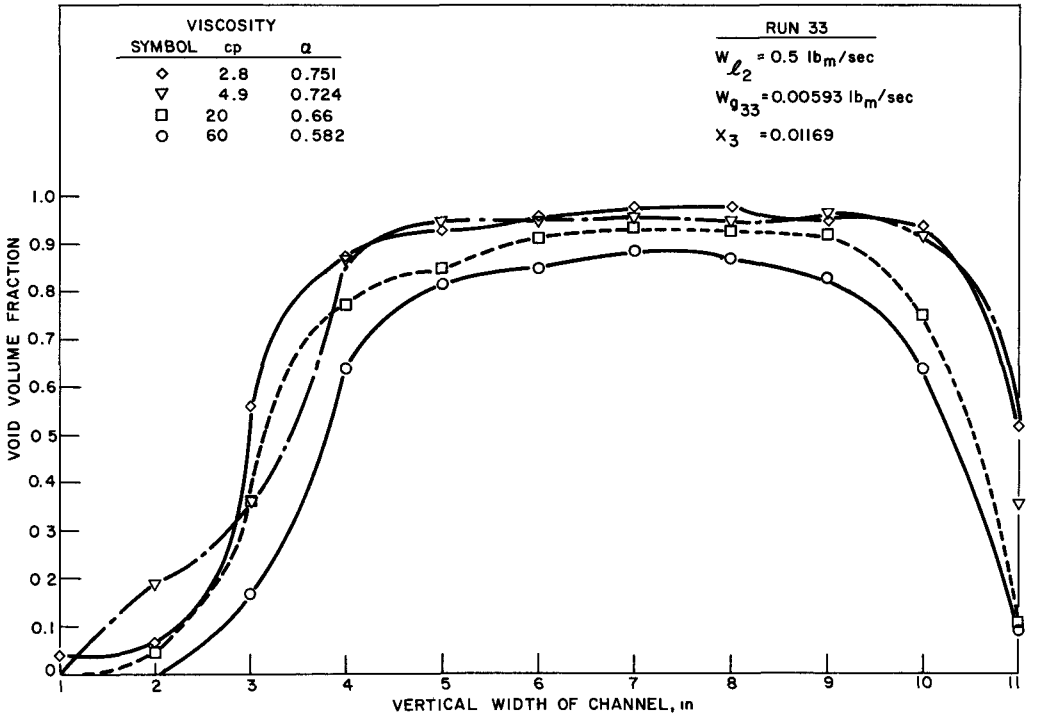

Figure 5.25 Cross-sectional Distribution of Void Volume Fraction for Run 33 and Various Liquid Viscosities.

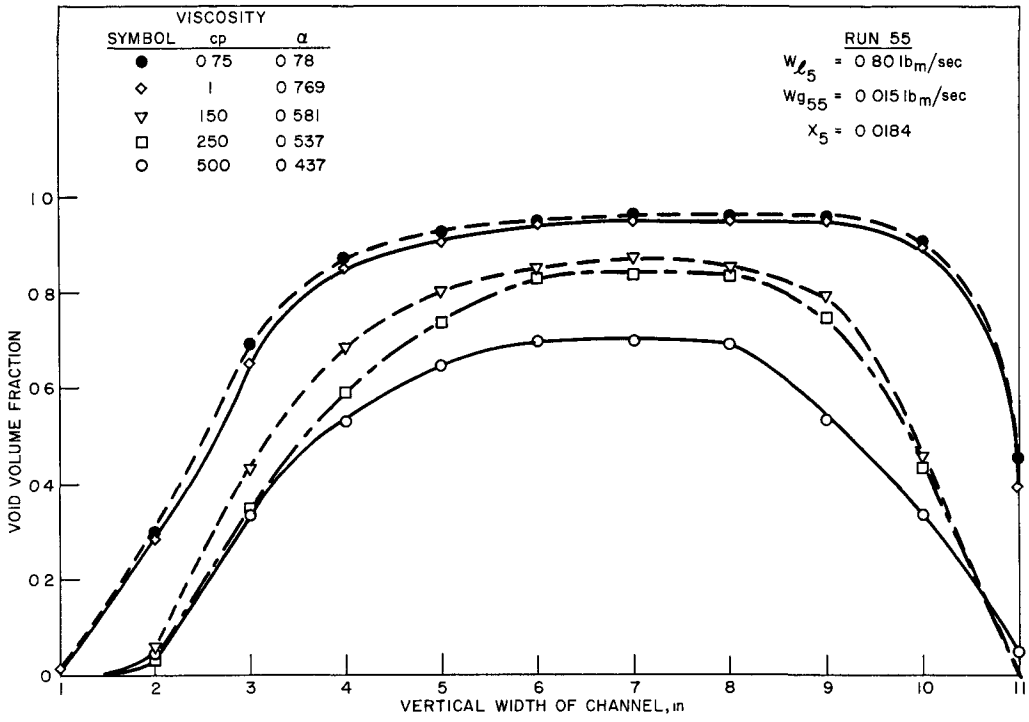

Figure 5.26 Cross-sectional Distribution of Void Volume Fraction for Run 44 and Various Liquid Viscosities.

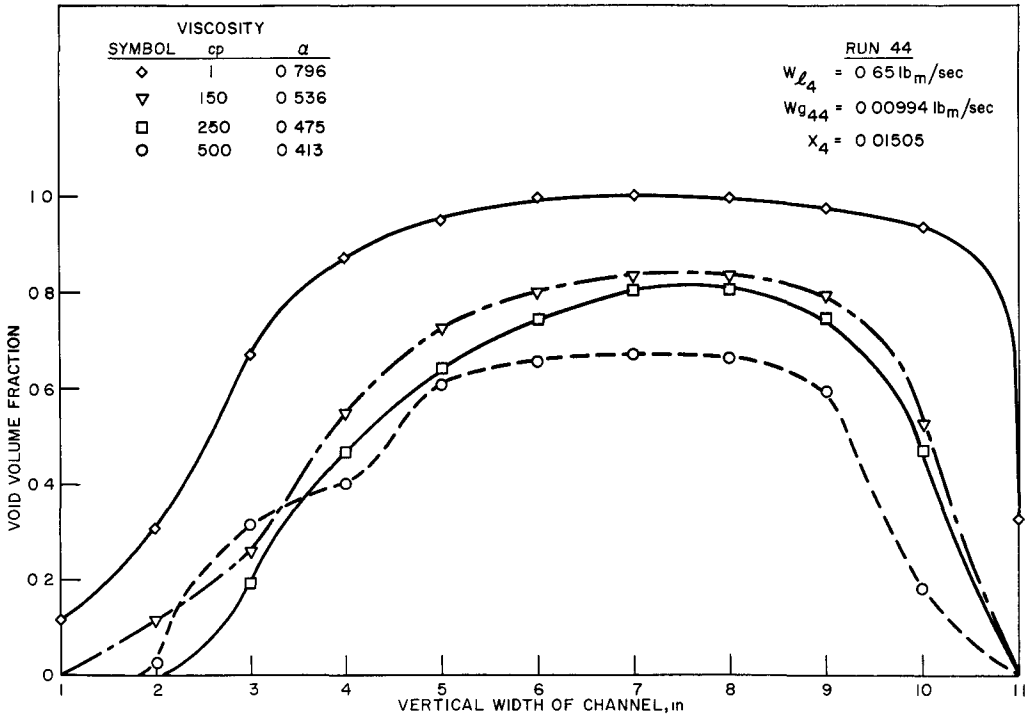

Figure 5.27 Cross-sectional Distribution of Void Volume Fraction for Run 55 and Various Liquid Viscosities.

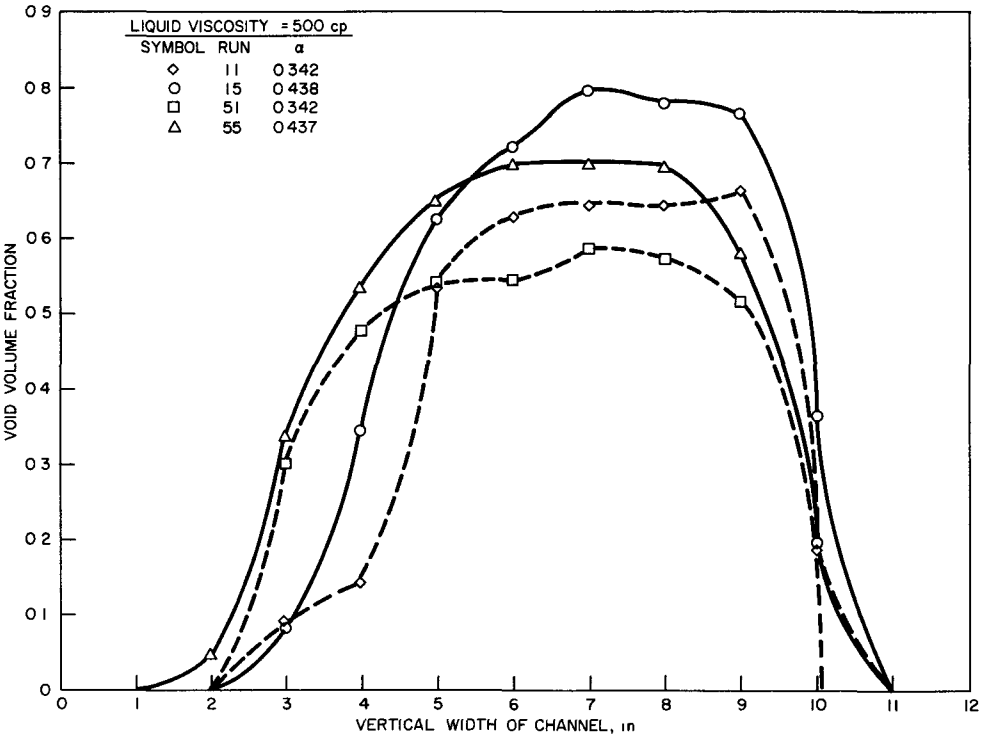

Figure 5.28 Cross-sectional Distribution of Void Volume Fraction for a Liquid Viscosity of 500 cp and Run 11, 15, 51, 55.

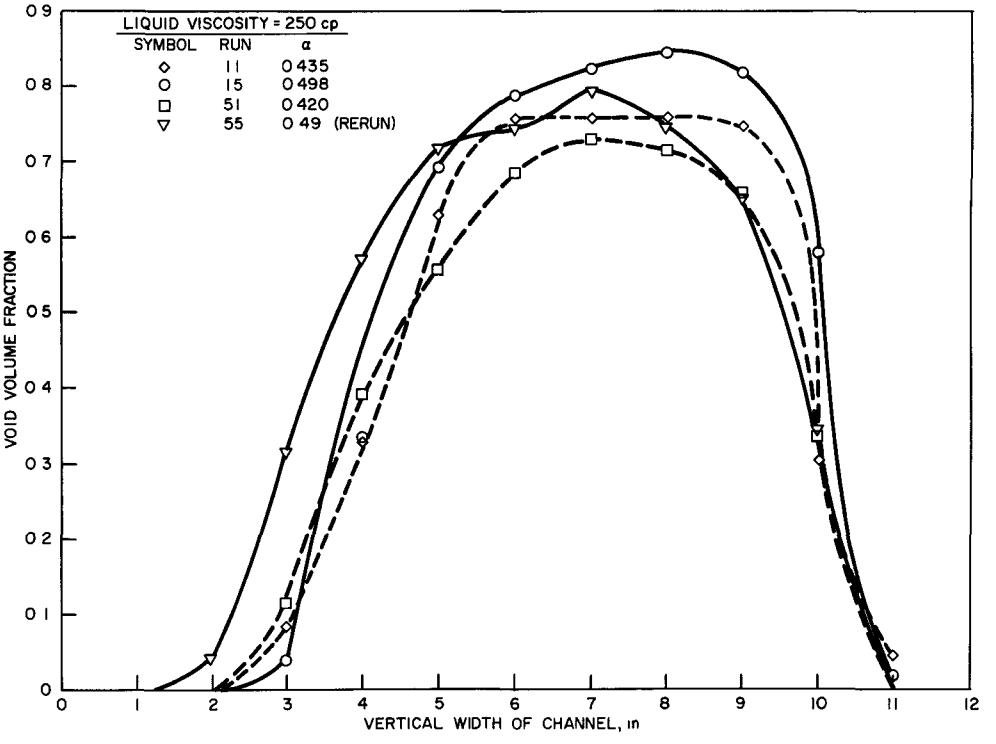

Figure 5.29 Cross-sectional Distribution of Void Volume Fraction for a Liquid Viscosity of 250 cp and Run 11, 15, 51, 55.

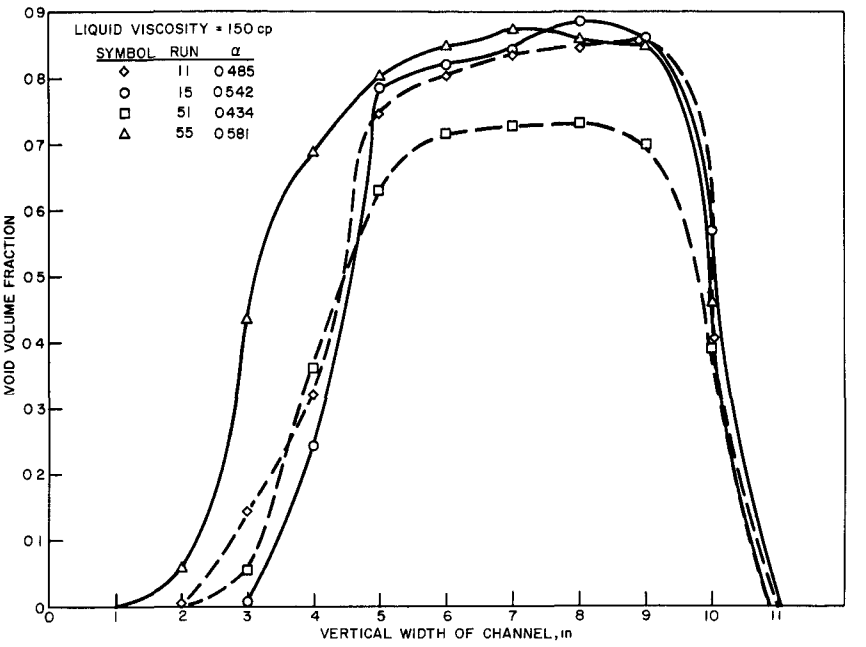

Figure 5.30 Cross-sectional Distribution of Void Volume Fraction for a Liquid Viscosity of 150 cp and Run 11, 15, 51, 55.

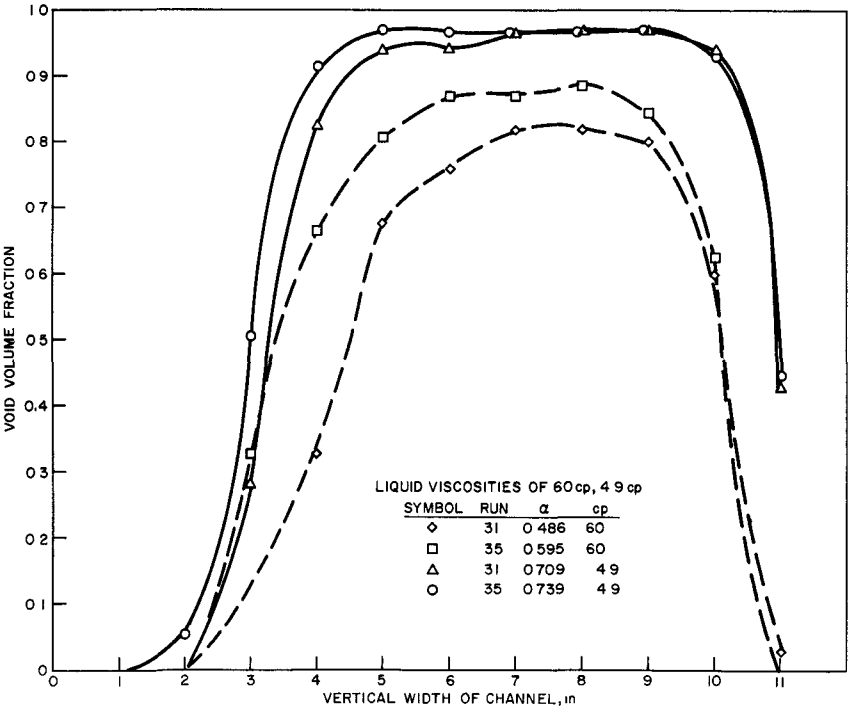

Figure 5.31 Cross-sectional Distribution of Void Volume Fraction for a Liquid Viscosity of 60 cp and 4.9 cp and Run 31, 35.

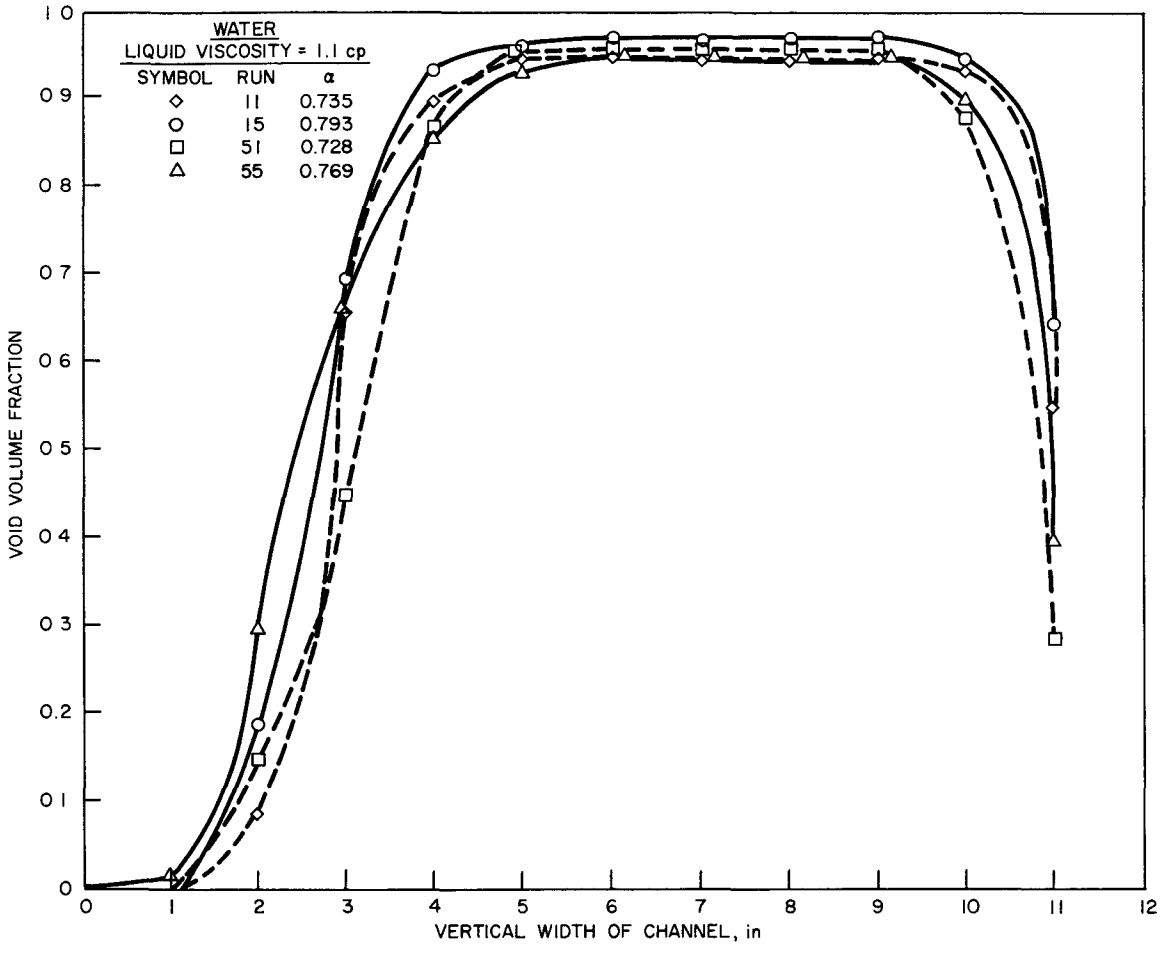

Figure 5.32 Cross-sectional Distribution of Void Volume Fraction for Water and Run 11, 15, 51, 55.

The effect of the liquid flow rates on the total void volume fraction and phase distribution is also shown in figure 5.28 through figure 5.32. It can be seen in these figures that, for constant qualities and increasing gas and liquid flow rates (i.e., Runs 11, 51, and 15, 55), (a) the total void volume fraction at the higher liquid viscosities tends to remain the same; and (b) the major portion of the gas phase shifts from the upper portion of the test section to the center and flattens out slightly. These effects also tend to diminish as the viscosity of the liquid phase decreases.

CHAPTER VI
SLIP RATIO AND VOID VOLUME FRACTION ANALYSIS

Introduction

The slip ratio may be expressed by a mass balance of the liquid and gas phases for an adiabatic system by the following equation:

$$\sigma = \left(\frac{x}{1-x}\right)\left(\frac{1-\alpha}{\alpha}\right)\left(\frac{\rho_\ell}{\rho_g}\right) \quad , \tag{6.1}$$

where

σ = the slip ratio

α = void volume fraction

x = quality

$$\frac{\rho_\ell}{\rho_g} = \frac{\text{density of the liquid component}}{\text{density of the gas component}} \quad .$$

The derivation of equation 6.1 is shown in Appendix B.

Equation 6.1 suggests a strong dependence of slip ratio upon the void volume fraction for a particular set of inlet flow conditions (i.e., quality). The void volume fraction, in turn, is dependent on: the flow pattern; the shear stress between the two components and between the walls of the channel; the viscosities of the liquid and gas phases; and the system pressure and temperature. The interaction of these components within the two-phase system is complex. Therefore the void volume fraction is difficult to correlate for a wide range of flow patterns and physical conditions. Martinelli has noted that the void volume fraction appears to be markedly affected by the viscosity of the liquid phase. However, no significant analysis of an experimental nature is currently available in the literature directly concerning the effect of viscosity of the liquid phase on the slip ratio in two-phase flow. Therefore, the current study has been initiated to investigate this problem. Flow rates and qualities are selected so that the effect of the liquid flow rate on the slip ratio for various liquid viscosities can also be experimentally evaluated.

The effect of the liquid viscosity on the slip ratio is presented in terms of an empirical correlation and a comparison with the Martinelli void volume fraction predictions.

Test Program

The object of the program was to determine the effects of the liquid viscosity, liquid flow rates, and quality on the slip ratio of two-phase, two-component mixtures. The viscosity of the liquid phase was varied for a set of predetermined flow conditions. Twenty-five liquid and gas flow rates, consisting of five values of qualities and five values of liquid flow rates, were selected for the investigation, and they are tabulated in table C.1. The maximum gas and liquid flow rates were determined by the highest pressure that the Lucite test section could withstand. The minimum air and liquid flow rate settings were determined by the lowest air and liquid flow rate settings that could be accurately measured.

The viscosity of the liquid phase was varied in steps from 0.75 cp to 500 cp. A total of 145 experimental runs was made. Four sets of twenty-five runs (see table C.1) were made at liquid viscosities of 1.1, 150, 250, and 500 cp. Four sets of five runs were made at a liquid flow rate of 0.5 lb_m/sec (i.e., Runs 31-35) and at liquid viscosities of 2.8, 4.9, and 60 cp. An additional twenty-five runs, randomly selected over the range of liquid viscosities, served as a check on the previous runs. Measurements taken of the static and total pressure, temperature, flow rate, and void volume fraction served as a basis for calculating the slip ratio, as shown in Appendix C. All the experimental determinations were made at isothermal conditions at pressures ranging from 14.8 to 18 psia.

Results

Slip Ratio Correlation. The results of the experimental investigation indicated that the liquid viscosity had a noticeable effect on the slip ratio. At a liquid viscosity of 1.1 cp, the slip ratio varied from

1.5 to 4.5. For the same inlet flow rate conditions and at a liquid viscosity of 500 cp, the slip ratio varied from 8.5 to 24.9.

The data were plotted on the basis of the slip ratio versus the inlet flow conditions (i.e., quality) which suggested an equation of the following form:

$$\sigma = a\mu^m x^n \quad , \tag{6.2}$$

where a, m, and n represent empirically determined constants.

Two methods were applied to the data to determine the constants. One method consisted of obtaining the best curve that fit the data at each particular viscosity satisfying the equation

$$\sigma = b x^n \quad . \tag{6.3}$$

A value of n = 0.77 was obtained by averaging the values of n obtained at each viscosity value. This value of n = 0.77 was then substituted into equation 6.3 and the values of b were determined by obtaining the best fit of this equation at each viscosity. The values of b were then plotted against viscosity, as shown in figure 6.1. The following equation resulted in an adequate correlation.

$$b = 80\ \mu^{0.3} \quad . \tag{6.4}$$

Equation 6.4 was then substituted into equation 6.3, giving the following equation:

$$= 80\,\mu^{0.30}\, x^{0.77} \quad . \tag{6.5}$$

The data obtained in the experimental investigation were compared with equation 6.5 in figure 6.2. An error analysis is presented in figure 6.3, which indicates that over seventy five percent of the data can be predicted to within ±10 percent by equation 6.5.

Applying the method of least squares to the data obtained from the 145 experimental runs, there resulted a second method for evaluating the constants in equation 6.2. The results are indicated by the following equation.

$$= 79\,\mu^{0.288}\, x^{0.753} \quad . \tag{6.6}$$

The data obtained in the experimental investigation were compared with predictions from equation 6.3, as shown in figure 6.4. An error

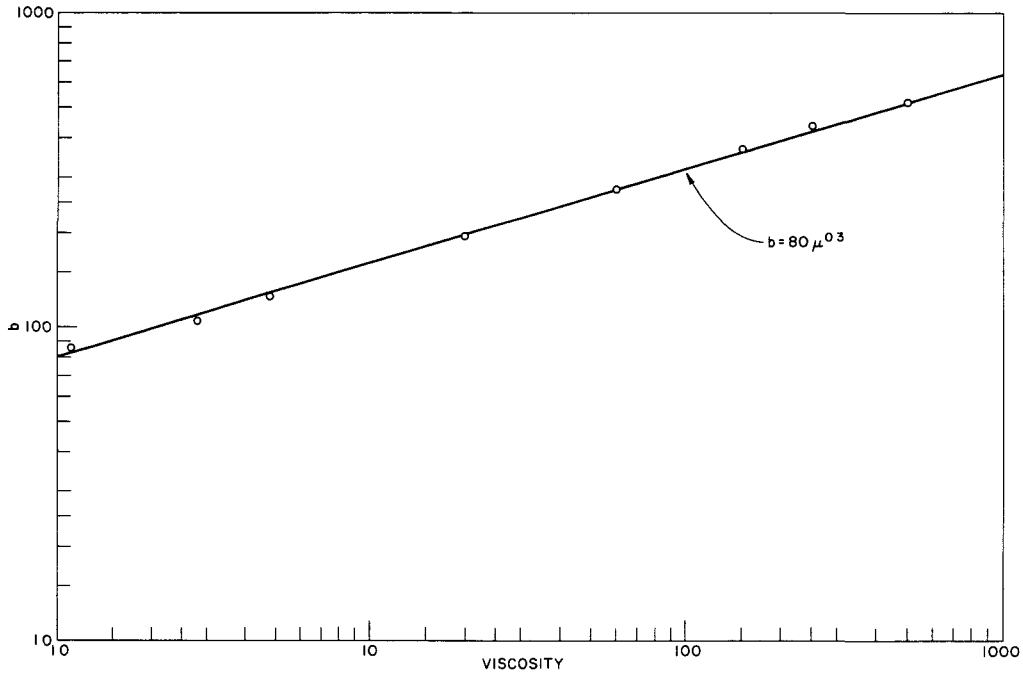

Figure 6.1 Determination of Viscosity Term for Slip Ratio Correlation, $\sigma = bx^{0.77}$

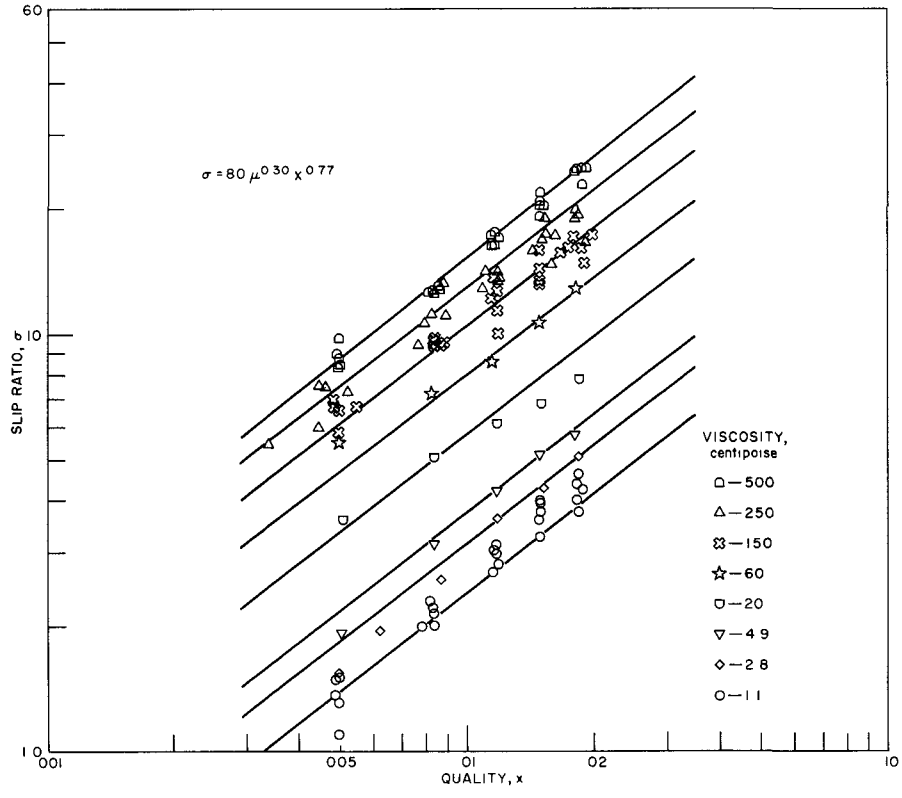

Figure 6.2 Proposed Slip Ratio Correlation as a Function of the Liquid Viscosity and the Quality of the Two-phase Mixture, $\sigma = 80\ \mu^{0.30}\ x^{0.77}$.

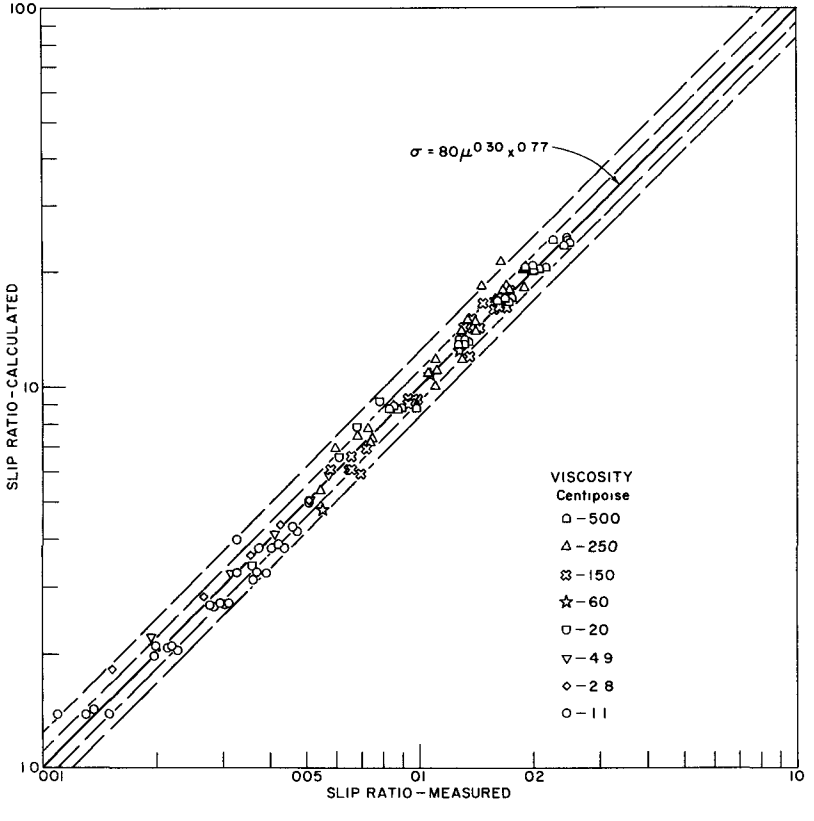

Figure 6.3 Comparison of Measured and Predicted Slip Ratio, $\sigma = 80\ \mu^{0.30}\ x^{0.77}$.

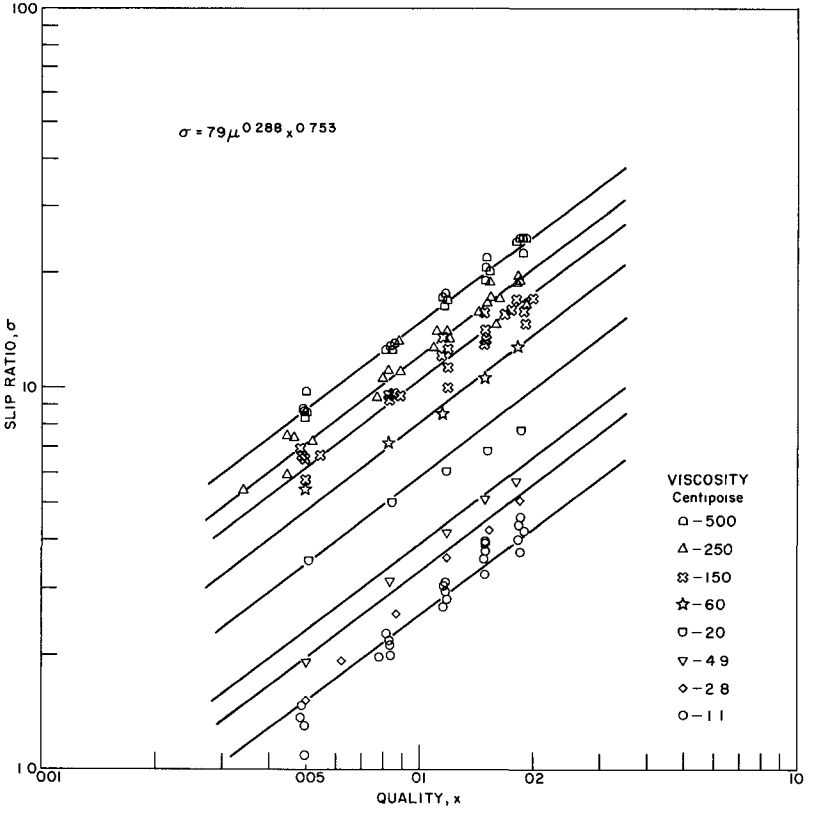

Figure 6.4 Proposed Slip Ratio Correlation as a Function of the Liquid Viscosity and the Quality of the Two-phase Mixture, $\sigma = 79\ \mu^{0.288}\ x^{0.753}$.

analysis is presented in figure 6.5, which indicates about the same accuracy as obtained by equation 6.5. A comparison between figure 6.2 and figure 6.4 indicates that equation 6.5 correlates the viscosity parameter better and therefore will be used in the following analysis.

It was noted in the preceding chapter that, throughout the liquid viscosity range investigated, when the quality was held constant and the liquid flow rates were varied, the cross-sectional distribution of the gas phase changed significantly while the total void volume fraction remained fairly constant. This indicated that there was no significant mass-flow rate effect in the region investigated. The results of the slip ratio investigation do not reveal any mass-flow rate effect either.

Richardson's slip-ratio correlation, $\sigma = 37\ x^{1/2}$, predicts values of slip ratio for air-water mixtures which lie in the same region as the present correlation predicts for air-water mixtures. However, there is a difference in the exponent of the quality term of the two correlations. The difference is primarily due to a combination of the following: (a) the omission of the liquid viscosity effect in Richardson's correlation; (b) the large amount of scatter in the lower liquid viscosity regions in the current study and in Richardson's data (approximately ±30 percent) which served as a basis for the correlations; and (c) the limited range of qualities investigated in the current study.

Martinelli Void Correlation. The effect of the liquid viscosity is evident when the results of the current experimental investigation are compared with the Martinelli void correlations, as shown in figure 6.6 through figure 6.11. In the region of lower liquid viscosity for air-water mixtures, as shown in figure 6.6 and on the left side of figure 6.11, the data are slightly higher than would be predicted by the Martinelli correlation. This trend was noted by many other investigators, as has been mentioned earler in Chapter I. However, as the viscosity of the liquid phase increases, the deviations noted between the Martinelli void correlation and the current experimental data increase, as shown in figure 6.6 through figure 6.11. The experimental

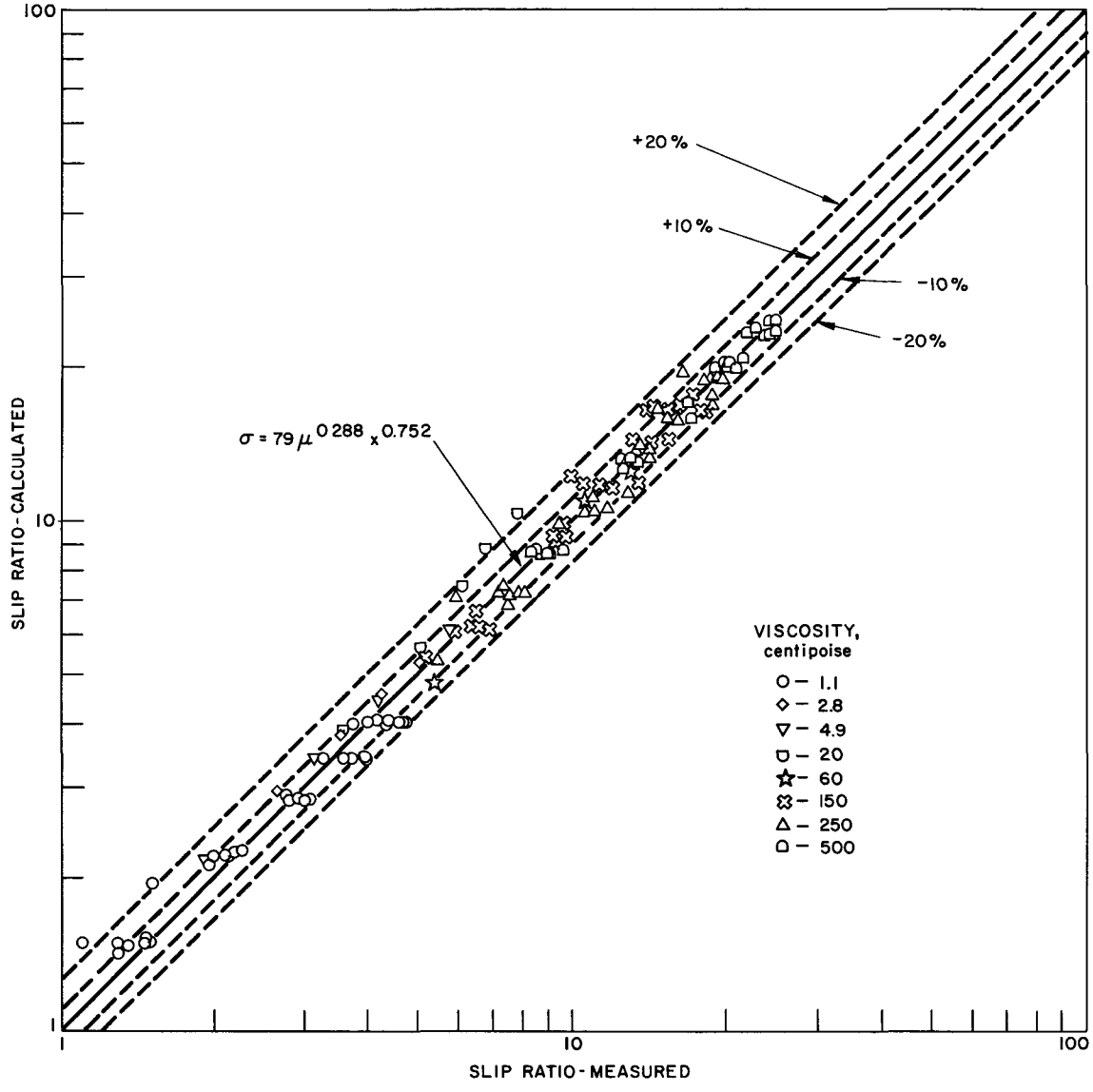

Figure 6.5 Comparison of Measured and Predicted Slip Ratio, $\sigma = 79\,\mu^{0.288}\,x^{0.753}$.

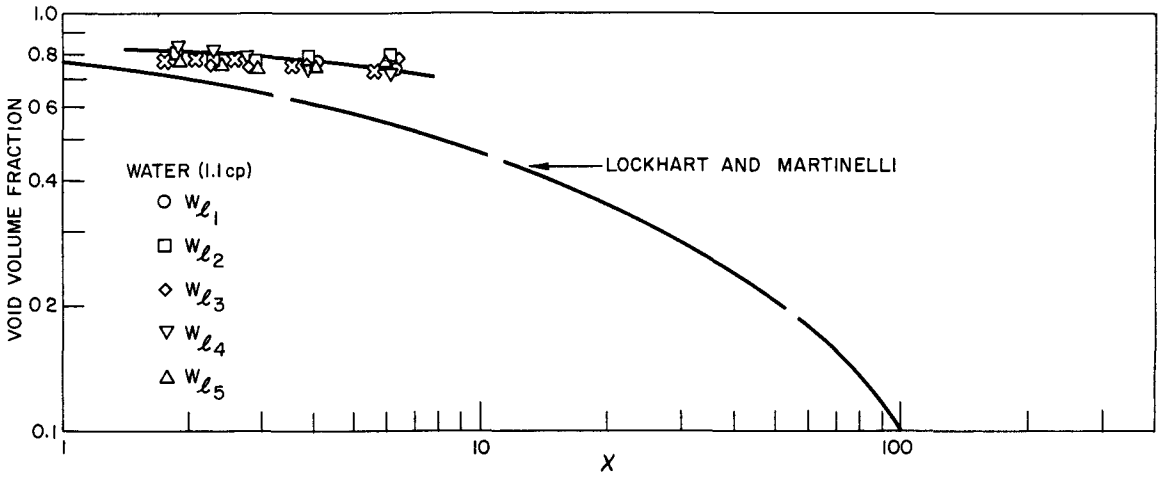

Figure 6.6 Proposed Void Volume Fraction Correlation for a Liquid Viscosity at 1.1 cp. (Water)

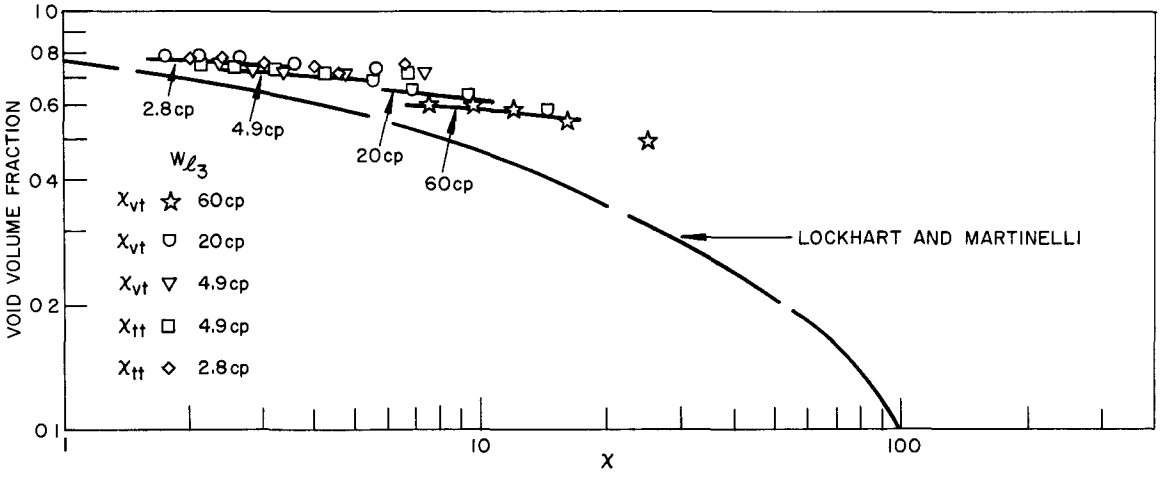

Figure 6.7 Proposed Void Volume Fraction Correlation for a Liquid Viscosity of 60 cp, 20 cp, 4.9 cp and 2.8 cp.

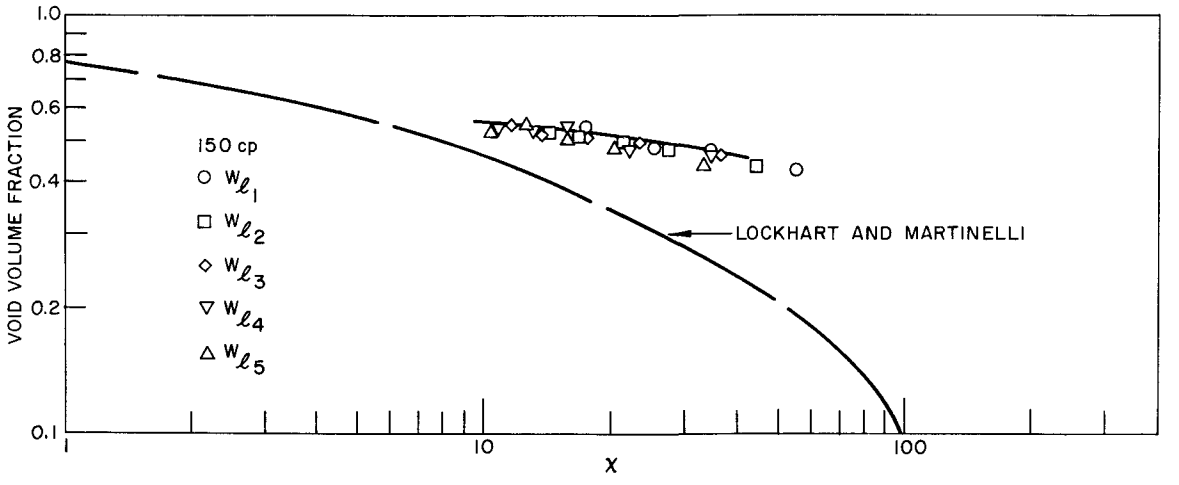

Figure 6.8 Proposed Void Volume Fraction Correlation for a Liquid Viscosity of 150 cp.

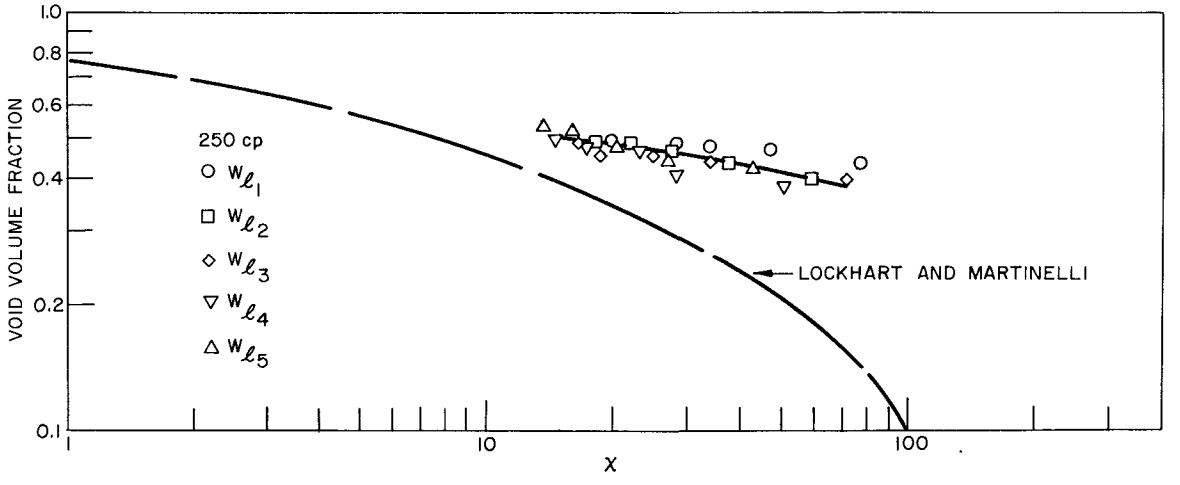

Figure 6.9 Proposed Void Volume Correlation for a Liquid Viscosity of 250 cp.

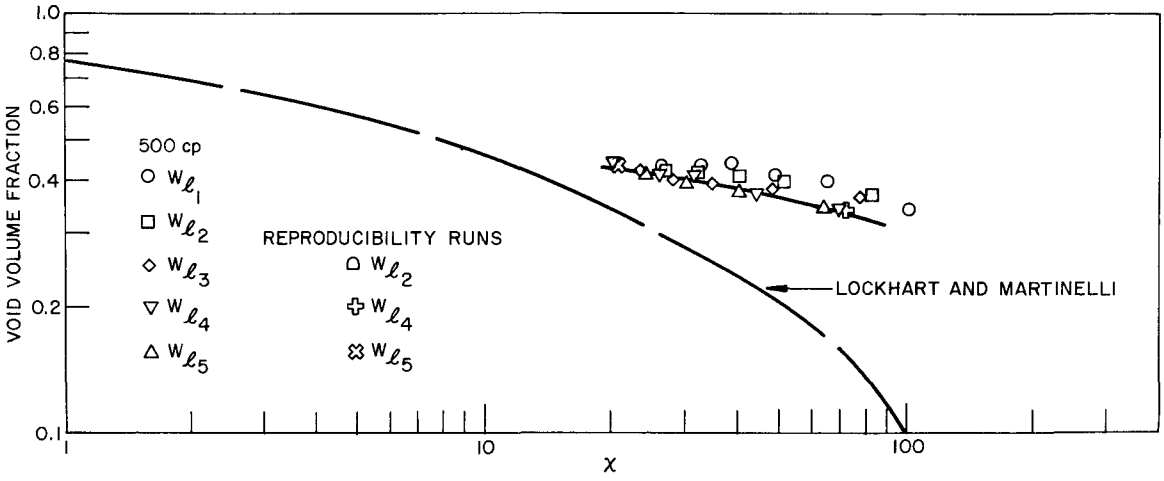

Figure 6.10 Proposed Void Volume Fraction Correlation for a Liquid Viscosity of 500 cp.

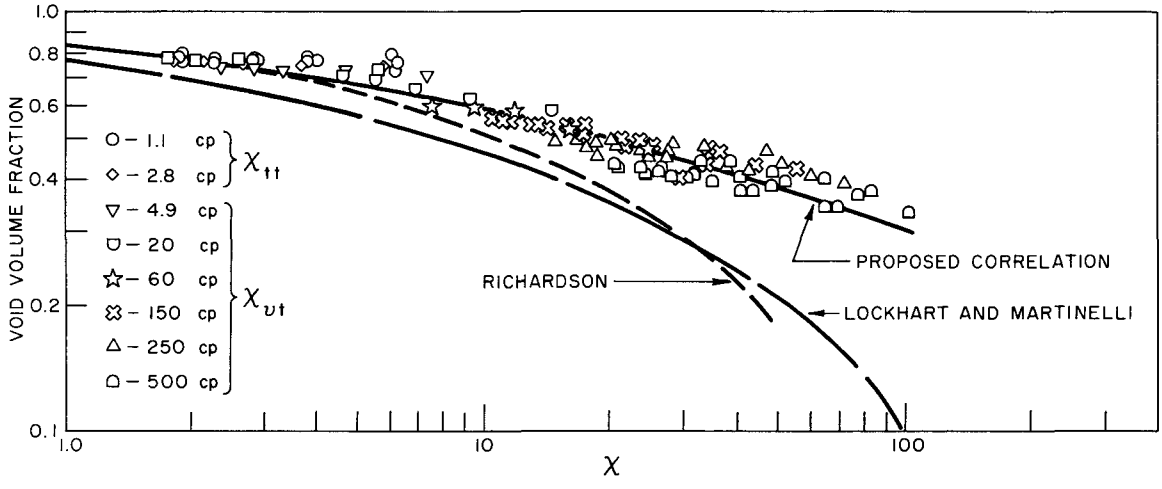

Figure 6.11 Proposed Void Volume Fraction Correlation for Liquid Viscosities from 1.1 cp to 500 cp.

program was originally set up for a fixed set of qualities and liquid flow rates, which were to be varied over a large range of liquid viscosities. Therefore, the deviations noted presently are primarily due to the increase in the viscosity of the liquid phase. These void deviations are noted to occur in the region where the slip ratio increases considerably.

The results of the experimental program can be correlated in terms of the Martinelli void parameters by a single curve drawn through the data points, as shown in figure 6.11. However, a closer investigation indicates that the slip ratio correlation $\sigma = 80\ \mu^{0.30} x^{0.77}$ can represent the data more accurately at each viscosity level, as shown by the solid lines in figure 6.6 through figure 6.11 which do not interconnect, as shown in figure 6.12. The slip ratio can also be determined at any desired liquid viscosity level from the void correlation presented in figure 6.12 by using it together with equation 6.1 and a given set of flow conditions for the liquid and gas components.

The results of the present void study indicate that the Martinelli void correlation is limited to the region of lower liquid viscosity. However, further investigation is required at a higher quality range and for values of liquid viscosities similiar to the current study in order to confirm the deviations noted in the present investigation.

Discussion of Results. A noticeable effect of the liquid viscosity on the slip ratio is evident from the data, although the reasons for this effect are not readily apparent. However, it can be seen from equation 6.1, that the void volume fraction is an important parameter in the determination of the slip ratio. The present study indicates that this parameter is strongly affected by a change in the viscosity of the liquid phase. Therefore, a closer examination of the void volume fraction reveals a possible explanation of the mechanism responsible for the effect of liquid viscosity on the slip ratio.

It has been noted from the void distribution graphs in Chapter V, that, as the liquid viscosity increased for a fixed set of flow conditions,

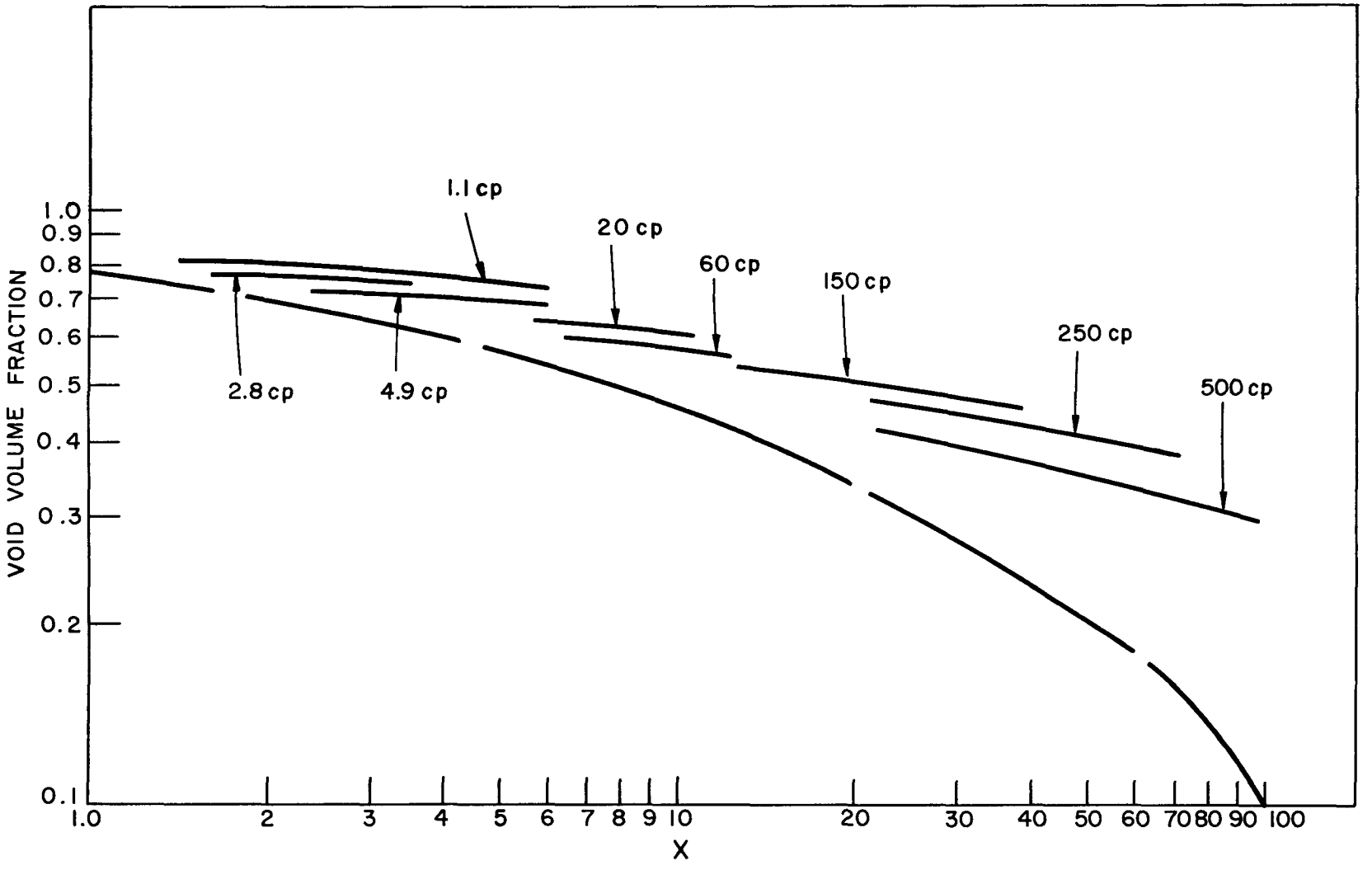

Figure 6.12 Proposed Void Volume Correlation on the Basis of the Slip Ratio Correlation, $\sigma = 80\,\mu^{0.30}\,x^{0.77}$

the gas phase tended to concentrate in the center of the test section while the major portion of the liquid phase remained along the side walls of the test section. This trend is depicted in figure 5.22 through figure 5.27. The shear stress between the walls of the test section and the glycerol mixture increased as the viscosity of the liquid phase was increased from 1.1 cp to 500 cp. This served to retard the flow of the liquid phase. Since the amount of liquid entering the test section per unit time remained the same, the cross-sectional area that the glycerol mixture occupied increased, as noted from a consideration of the continuity equation $W = VA\rho$, where W is the flow rate, V is the velocity, A is the area, and ρ is the density of the incompressible liquid phase. The compressible gas phase was then forced into a smaller area, which served to increase the velocity considerably. The net result was a large increase in the ratio of the velocity of the gas phase to that of the liquid phase, i.e., of the slip ratio.

CHAPTER VII
TWO-PHASE PRESSURE DROP STUDY

Introduction

The effect of the viscosity of the liquid phase on the pressure drop was determined for air-glycerol mixtures flowing together. The data were correlated in terms of the Martinelli parameters and then compared to the results of Lockhart and Martinelli,[5] and of Richardson.[2] The current investigation was conducted in conjunction with the study of slip ratio in order to provide a more complete experimental picture of the effect of the viscosity of the liquid phase in two-phase, two-component flow.

Historical

Lockhart and Martinelli presented a correlation for two-phase pressure drop using the assumptions and equations outlined in Appendix A, together with equation 1.1 and equation 1.2. The tests were conducted in horizontal channels at atmospheric pressure and room temperature, using air and a variety of hydrocarbons and water. Levy's theoretical analysis also verified the parameters selected by Martinelli, as shown in figure 1.1.

Subsequent studies have for the most part modified and extended the Martinelli correlations so as to include a wider range of pressures (i.e., other than atmospheric) and flow patterns, for both single and two-component flow. Other "Friction-Factor" methods have been presented by Bergelin and Gazely[25] for stratified flow patterns, and by Schneider et al.,[29] for steady flows (i.e., excluding slug and stratified flow regimes). These investigations and others in this area have been summarized and evaluated in literature surveys by Isben,[30] by Masnovi,[31] and by Bennett.[32]

Richardson conducted a pressure-drop study during his investigation of air-water mixtures in horizontal channels. His data were presented in terms of the Martinelli pressure-drop parameters and

were compared with the results of the correlation of Lockhart and Martinelli, as shown in figure 7.1. The results covered a quality range from 0.000246 to 0.0552 and a liquid flow rate range from 0.302 pound per second to 2.65 pounds per second. Richardson's data agreed fairly well with the Lockhart and Martinelli correlation, as noted from figure 7.1, although the data appeared to be slightly higher than the correlation.

Experimental Investigation and Results

Two-phase pressure-drop measurements were taken for the same range of liquid viscosities and flow rates as considered in the study of slip ratio. Single-phase liquid pressure-drop measurements were also taken, resulting in the friction-factor plots for the laminar and turbulent region, as shown in figure 7.2 and figure 7.3. Values of C_g, C_l, m, and n were determined from the friction-factor plots. These values were used for the calculation of the Martinelli parameter constants in χ_{vt}, and χ_{tt}, which are shown in Appendix A. The resulting equations were

$$\chi_{vt}^2 = 290 \left(N_{Re_g}\right)^{-0.75} \left(\frac{W_\ell}{W_g}\right)\left(\frac{\mu_\ell}{\mu_g}\right) \left(\frac{\rho_g}{\rho_\ell}\right) \tag{7.1}$$

and

$$\chi_{tt}^2 = \left(\frac{W_\ell}{W_g}\right)^{1.75} \left(\frac{\mu_\ell}{\mu_g}\right)^{0.25} \left(\frac{\rho_g}{\rho_\ell}\right) \tag{7.2}$$

The data obtained from the experimental study have been calculated by means of equations 1.1, 1.2, 7.1, and 7.2, and the results are tabulated in Appendix D. The results are also shown in graphical form in figure 7.4 through 7.9.

Based on the Martinelli laminar-turbulent flow boundaries as outlined in Appendix A, the liquid-phase component of the two-phase mixture with liquid viscosities of 2.8 cp and 4.9 cp lie in the transition region. All the flow rates with liquid viscosities greater than these values lie in the laminar region, whereas all the flow rates with liquid

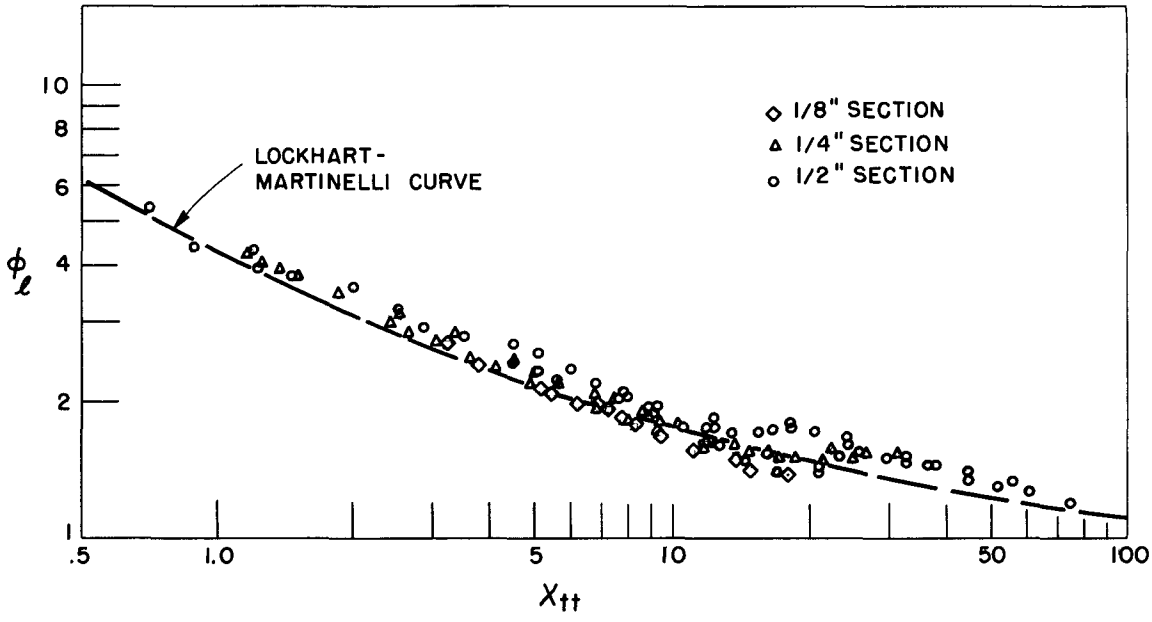

Figure 7.1 Comparison of Pressure-drop Data with Lockhart-Martinelli Correlation (from Richardson).

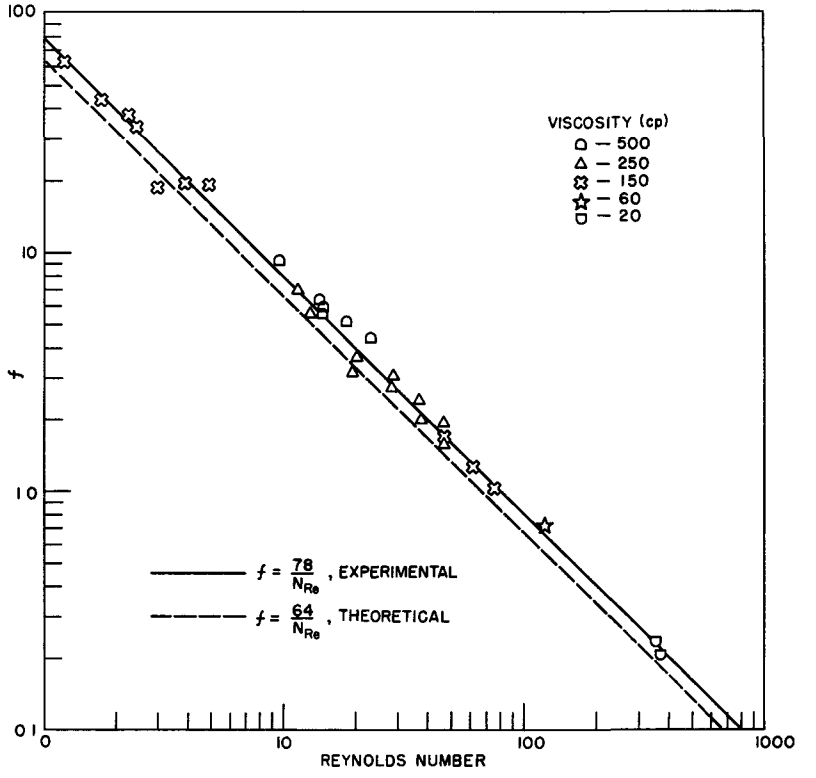

Figure 7.2 Friction Factor vs Reynold's Number in Lucite Test Sections for Laminar Region.

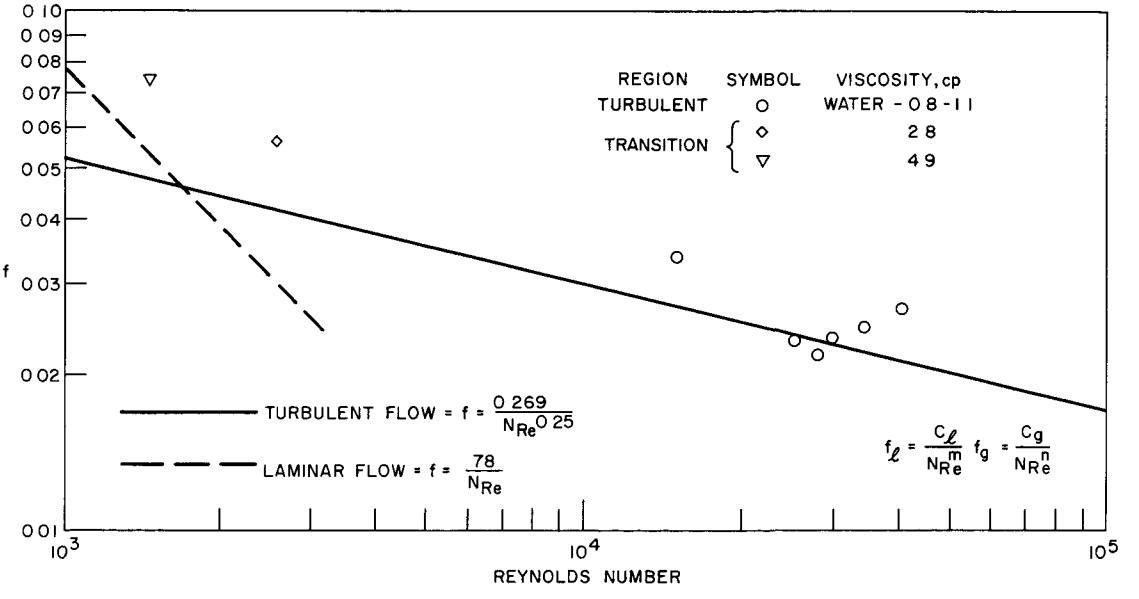

Figure 7.3 Friction Factor vs Reynold's Number in Lucite Test Sections for Turbulent Region.

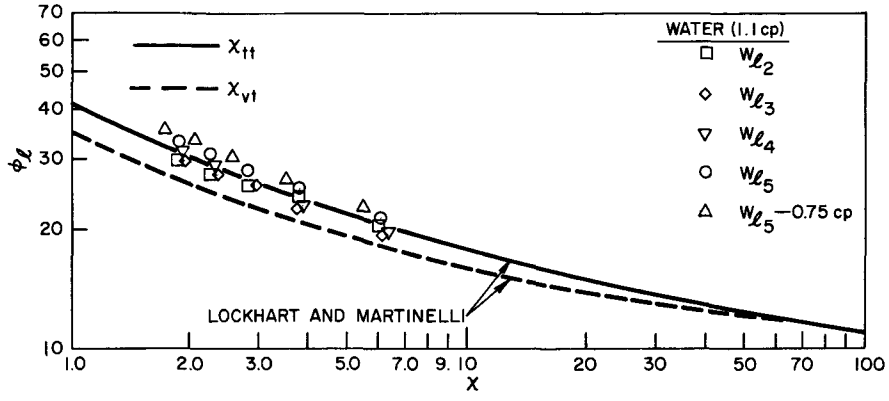

Figure 7.4 Comparison of Pressure Drop Data with Lockhart-Martinelli Correlation for Liquid Viscosity of 1.1 cp and 0.75 cp (Water).

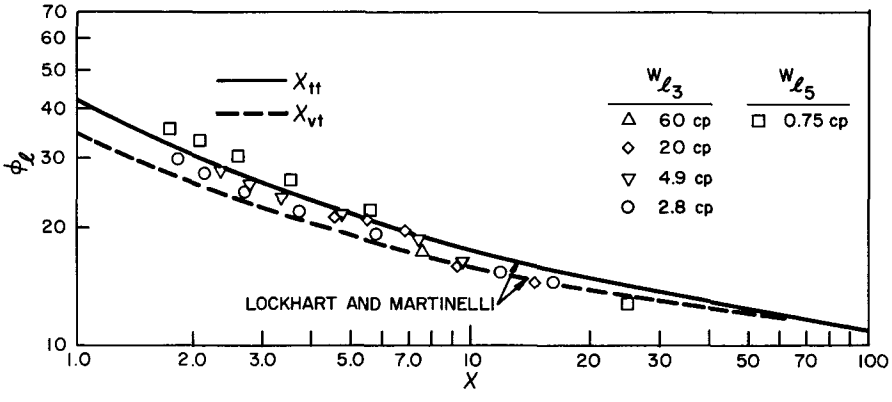

Figure 7.5 Comparison of Pressure Drop Data with Lockhart-Martinelli Correlation for Liquid Viscosities of 60 cp, 20 cp, 4.9 cp, 2.8 cp and 0.75 cp.

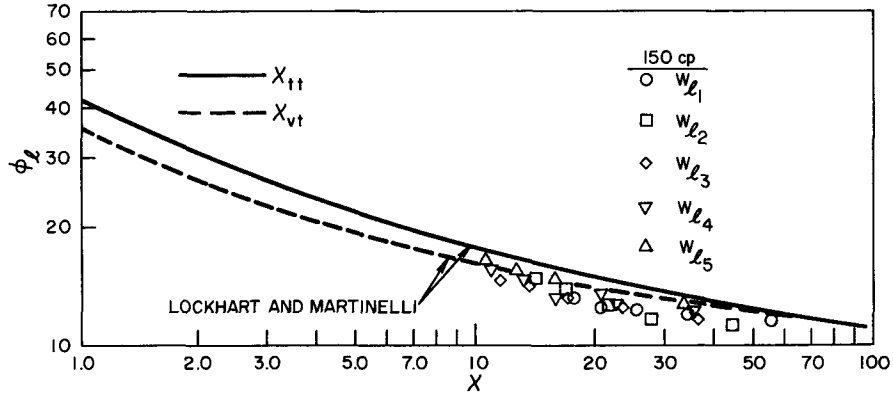

Figure 7.6 Comparison of Pressure Drop Data with Lockhart-Martinelli Correlation for Liquid Viscosity of 150 cp.

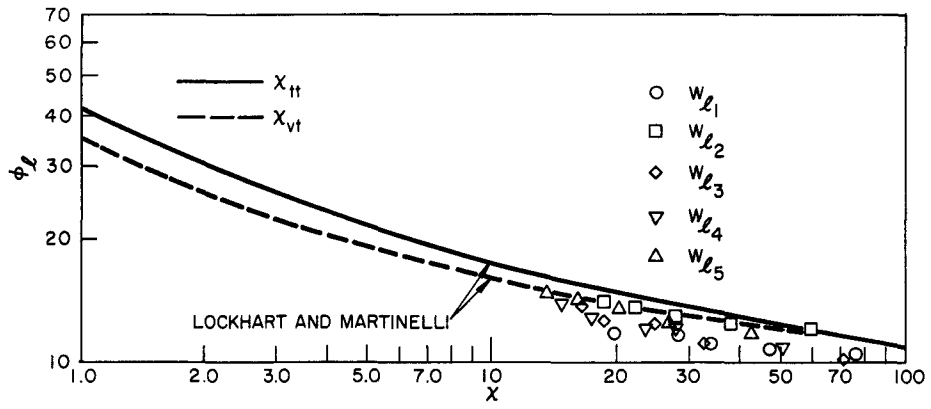

Figure 7.7 Comparison of Pressure Drop Data with Lockhart-Martinelli Correlation for a Liquid Viscosity of 250 cp.

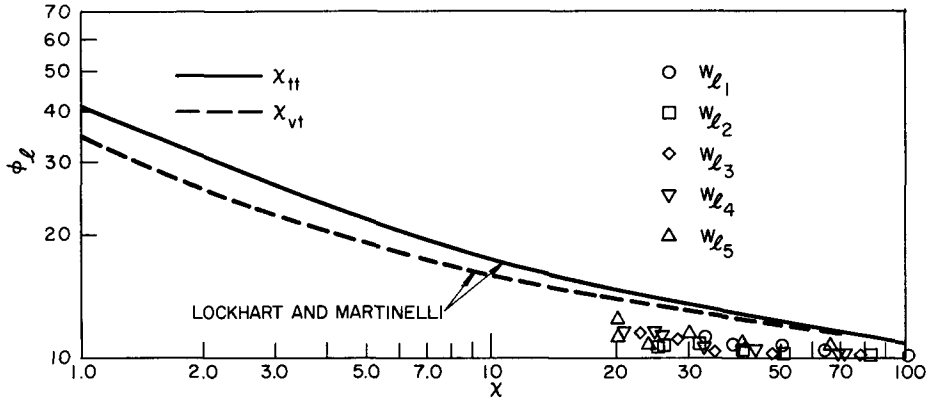

Figure 7.8 Comparison of Pressure Drop Data with Lockhart-Martinelli Correlation for a Liquid Viscosity of 500 cp.

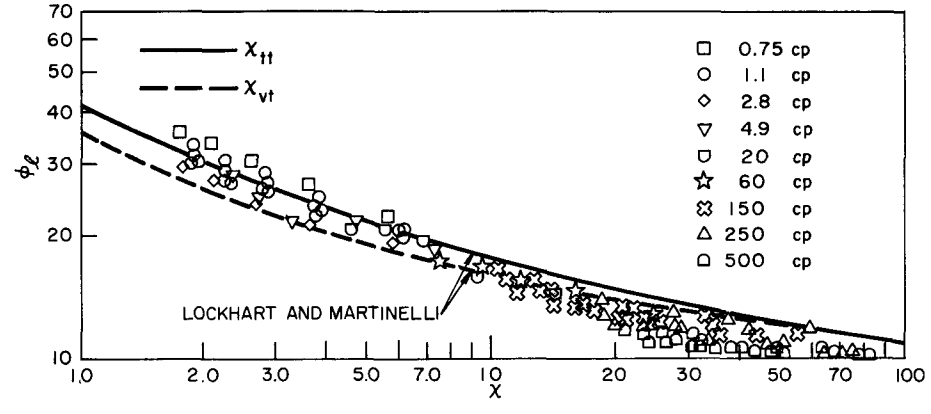

Figure 7.9 Comparison of Pressure Drop Data with Lockhart-Martinelli Correlation for Liquid Viscosities from 0.75 cp to 500 cp.

viscosities lower than these values lie in the turbulent region. In figure 7.4 through figure 7.9, the solid line denotes the region where the χ_{tt} parameter applies and the dotted line denotes the region where the χ_{vt} parameter applies. In the region of lower liquid viscosity, the two phases are both in a turbulent state (i.e., for μ = 1.1 cp and 0.75 cp) and the Martinelli prediction correlates the data of the current investigation reasonably well. As the liquid viscosity is increased, the liquid phase moves into the transition region between the turbulent and the laminar states, and the data fall midway between the solid and dotted lines. Therefore, the data in this region also agree reasonably well with the Martinelli prediction. However, in the regions of higher liquid viscosity, (i.e., μ = 150 cp to 500 cp), the data fall approximately 15 percent lower than predicted by the Martinelli correlation. This deviation can either be attributed to the higher liquid viscosity or to the geometry of the test section. Since the test section is rectangular, the "hydraulic radius" concept was used to evaluate the diameter in the parameter χ_{vt} when the liquid was in a laminar state. Vennard[33] notes that errors may be introduced by using the hydraulic radius method for the determination of the equivalent diameter in the laminar region. He points out that the friction forces act throughout the fluid in laminar flow, as opposed to turbulent flow, where these friction forces act primarily in the region close to the boundaries of the fluid and the container. The magnitude of this error cannot be accurately determined from the present investigation. Further studies in circular channels at liquid viscosities of 500 cp are needed to determine the effect of the use of the hydraulic radius concept for the calculation of the diameter on the Martinelli correlation.

No significant effect of flow rate was noted in the region where the gas was in a turbulent state and the liquid was in a laminar state, as shown in figure 7.6 through figure 7.8. However, a slight effect of liquid flow rate was noted in the region where the gas and liquid were

both in a turbulent state, as shown in figure 7.4. Nonetheless, no positive conclusions could be reached because of the small amount of data taken in this region.

CHAPTER VIII
RESULTS AND CONCLUSIONS

The effect of the liquid viscosity on the slip ratio, flow regime, flow distribution, and pressure drop on two-phase, two-component mixtures has been experimentally investigated. The following is a brief summary of the results obtained from this study and the conclusions that were derived from the results.

Results

Flow Patterns and Phase Distribution

Visual Analysis Photographs. A comparison of the photographs taken for two-phase gas-liquid mixtures at a liquid viscosity of 500 cp and of 1 cp revealed that the interfaces between the two phases and the test section walls tended to smooth out considerably as the viscosity of the liquid phase was increased. This was due mainly to the change of liquid phase from a turbulent to a laminar state.

Flow Regime Study. The occurrence of the various types of flow patterns was graphically depicted by plotting the gas flow rate versus the liquid flow rate for a liquid viscosity range from 1 cp to 500 cp. The results of these plots followed the general trend of the results obtained by Richardson for air-water mixtures at higher rates of liquid flow. As the liquid viscosity increased, the transition from one flow pattern to another occurred more rapidly, and at higher rates of gas flow.

Phase Distribution Study. The change in the void volume fraction for the two-phase mixture was graphically presented for varying liquid viscosities, liquid flow rates, and qualities. The results indicated that the total void volume fraction: (1) increased as the liquid viscosity decreased; (2) remained the same for varying gas and liquid flow rates at constant qualities; and (3) increased for increasing qualities and gas flow rates at constant liquid flow rates. The gas phase tended to concentrate more towards the center of the channel as the gas and liquid flow rates were increased.

Slip Ratio and Void Volume Fraction Analysis

Slip Ratio Correlation. A correlation was determined from the data of the experimental study. The resulting equation, $\sigma = 80\mu^{0.30}x^{0.77}$, correlated seventy-five percent of the data to within ± 10 percent. No flow pattern or mass flow rate effects were evident in the data obtained from the experimental study.

Martinelli Void Correlation. The experimental data indicated that slightly higher values of void volume fractions were obtained than were predicted by the Martinelli void correlation in the region of lower liquid viscosity (i.e., water). The deviation increased as the liquid viscosity was raised to 500 cp, which indicated a large effect due to liquid viscosity in this region. No mass flow or flow pattern effect was apparent over the entire range of the experimental study. The results of the experimental program could be correlated by a single line drawn through the data. However, a more accurate correlation involved individual curves drawn through the data in each liquid viscosity range, which corresponded to the empirical slip-ratio correlation $\sigma = 80\mu^{0.30}x^{0.77}$.

Two-phase Pressure Drop Study. The Lockhart and Martinelli pressure-drop correlation agreed reasonably well with the data obtained from air-water mixtures at liquid viscosities of 0.75 cp and 1.1 cp, and for the transition region where the liquid phase changed from a turbulent to a laminar state, at liquid viscosities of 2.8 cp and 4.9 cp. However, as the liquid viscosity increased to 500 cp, the data from the current study fell to about 15 percent below the predicted curve of Lockhart and Martinelli. A slight effect of liquid flow rate was noted in the data for air-water mixtures. No flow pattern effect was noted throughout the range of the experimental study.

Conclusions

The following conclusions can be drawn from the results of the experimental investigation:

(1) The viscosity of the liquid phase is an important parameter in the determination of the slip ratio or the void-volume fraction in two-phase, two-component flow.

(2) Richardson's revision of the Martinelli void correlation is valid for air-water mixtures only. Deviations from this correlation may be expected to increase as the liquid viscosity is raised above this level. The Lockhart and Martinelli pressure-drop correlation is adequate for a liquid viscosity range from water (i.e., 1.1 cp) to at least 150 cp.

(3) The use of the traversing technique with the gamma-ray attenuation system provides a valuable means of obtaining the magnitude of the void volume fraction and the distribution of the two phases at any desired cross section along the length of the test section.

(4) The slip-ratio and pressure-drop results do not indicate any considerable variation due to changes in flow pattern or liquid flow rates for the range of flow conditions and liquid viscosities encountered in the present investigation.

A further study of the current problem for the same liquid viscosity range in circular channels at higher pressures and liquid flow rates would be useful in providing a more comprehensive evaluation of the effect of the liquid-phase viscosity in two-phase flow. It is hoped that the current investigation will act as a guide for the formulation of physical flow models for use in future theoretical investigations.

APPENDIX A
MARTINELLI CORRELATIONS

Martinelli et al.,[3,5] proposed a set of empirical correlations which were based on the following postulates for two-phase, two-component systems: (a) the static pressure drop per unit length of the liquid phase is equal to the static two-phase pressure drop per unit length of the gas phase when they are flowing concurrently in the channel; (b) the volume of the gas phase plus the volume of the liquid phase at any instant is equal to the total volume of the channel.

Although the second postulate limited the analysis to annular flow, the correlations have been applied to a variety of flow patterns with a reasonable degree of success.

Void volume fraction and pressure drop were correlated on the basis of a parameter which is defined as follows:

$$\chi^2 = \left(\frac{\Delta P}{\Delta \ell}\right)_\ell \Bigg/ \left(\frac{\Delta P}{\Delta \ell}\right)_g \quad . \tag{A.1}$$

Using the Fanning equation for the liquid and gas phases,

$$\left(\frac{\Delta P}{\Delta \ell}\right)_\ell = \frac{f_\ell \rho_\ell V_\ell^2}{2 g De} = \frac{f_\ell W_\ell^2}{2g De \rho_\ell A_T^2} \tag{A.2}$$

and

$$\left(\frac{\Delta P}{\Delta \ell}\right)_g = \frac{f_g \rho_g V_g^2}{2 g De} = \frac{f_g W_g^2}{2 g De \rho_g A_T^2} \tag{A.3}$$

are obtained, in which the friction factors defined by the Blasius equation are

$$f_\ell = \frac{C_\ell}{N_{Re_\ell}^n} \tag{A.4}$$

and

$$f_g = \frac{C_g}{N_{Re_g}^m} \quad . \tag{A.5}$$

The constants C_ℓ, C_g, m, and n depend on whether the liquid or gas phase flowing concurrently in the channel is in a turbulent or laminar

state. The transition region is arbitrarily defined at a Reynold's number between 1000 and 2000 and is determined by assuming each fluid to flow separately in the channel.

Therefore, the generalized form of the parameter χ is

$$\chi^2 = \frac{C_\ell \left(N_{Re_g}\right)^m (W\ell)^2 \rho_g}{C_g \left(N_{Re_\ell}\right)^n (W_g)^2 \rho_\ell} \quad . \tag{A.6}$$

For tt flow (i.e., liquid turbulent, gas turbulent, and $C_\ell = C_g$, $m = n$),

$$\chi^2_{tt} = \left(\frac{W_\ell}{W_g}\right)^{2-m} \left(\frac{\mu_\ell}{\mu_g}\right)^m \left(\frac{\rho_g}{\rho_\ell}\right) \quad , \tag{A.7}$$

and for vt flow (i.e., liquid viscous, gas turbulent, and also assuming n - 1),

$$\chi^2_{vt} = \frac{C_\ell}{C_g} \left(N_{Re_g}\right)^{m-1} \left(\frac{W_\ell}{W_g}\right) \left(\frac{\rho_\ell}{\rho_g}\right)\left(\frac{\rho_g}{\rho_\ell}\right) \quad . \tag{A.8}$$

The values of C_ℓ, C_g m, and n are determined by plotting the friction factor versus the Reynolds number for a number of single-phase fluid flow runs in the desired test section.

The static two-phase pressure-drop results are correlated in terms of the following parameters:

$$\phi^2_\ell = \left(\frac{\Delta P}{\Delta \ell}\right)_{TP} \Big/ \left(\frac{\Delta P}{\Delta \ell}\right)_\ell \tag{A.9}$$

and

$$\phi^2_g = \left(\frac{\Delta P}{\Delta \ell}\right)_{TP} \Big/ \left(\frac{\Delta P}{\Delta \ell}\right)_g \quad , \tag{A.10}$$

where

$\left(\frac{\Delta P}{\Delta \ell}\right)_{TP}$ = two-phase frictional pressure-drop gradient

$\left(\frac{\Delta P}{\Delta \ell}\right)_g$ = single-phase, frictional pressure-drop gradient of the gaseous phase flowing alone in the channel.

$\left(\frac{\Delta P}{\Delta \ell}\right)_\ell$ = single-phase, frictional pressure-drop gradient of the liquid phase flowing alone in the channel.

APPENDIX B
DERIVATION OF THE SLIP RATIO EQUATION

Applying the continuity equations to the gas and liquid phases flowing simultaneously in a channel, we obtain the following equations:

$$W_g = V_g A_g \rho_g \tag{B 1}$$

and

$$W_\ell = V_\ell A_\ell \rho_\ell \tag{B.2}$$

where W_g and W_ℓ are the mass flow rates of the gas and liquid phases, A_g and A_ℓ are the cross-sectional areas that each phase occupies in the channel, and ρ_g and ρ_ℓ are the densities of the gas and liquid phases.

The void volume fraction for the gas and liquid phases may be defined by the following equations:

$$\alpha = A_g/A_T \tag{B.3}$$

and

$$1 - \alpha = A_\ell/A_T \quad , \tag{B.4}$$

where A_T is the total cross-sectional area of the channel.

Substituting (B.3) and (B.4) into (B.1) and (B.2), and dividing (B.1) by (B.2), the following equation is obtained:

$$\frac{W_g}{W_\ell} = \frac{\alpha V_g \rho_g}{(1-\alpha) V_\ell \rho_\ell} \quad . \tag{B.5}$$

The quality of the gas and liquid phase may be defined by the following equations:

$$x = W_g/W_T \tag{B.6}$$

and

$$1 - x = W_\ell/W_T \quad , \tag{B.7}$$

where W_T is the total flow rate of the gas and liquid phases.

Substitution of (B.6) and (B.7) into (B.5) and rearrangement gives the following equation:

$$\frac{V_g}{V_\ell} = \frac{x}{1 - x} \frac{1 - \alpha}{\alpha} \frac{\rho_\ell}{\rho_g} \quad . \tag{B.8}$$

Definition of σ as

$$\sigma = V_g / V_\ell \tag{B.9}$$

and substitution of (B.9) in (B.8) gives the following equation:

$$\sigma = \frac{x}{1 - x} \frac{1 - \alpha}{\alpha} \frac{\rho_\ell}{\rho_g} \quad , \tag{B.10}$$

which is the slip ratio equation corresponding to equation 6.1.

APPENDIX C
SAMPLE CALCULATIONS

A sample calculation based on a typical test run selected from table C.1 is used in the following computation. The data and the results compiled from these calculations are shown at the end of this section in table C.2.

Table C.1. Inlet Flow Conditions for Experimental Program

Liquid flow rate, lb_m/sec	Quality X_1 = 0.00497	X_2 = 0.00833	X_3 = 0.01169	X_4 = 0.01505	X_5 = 0.0184
W_{ℓ_1}	$W_{g_{11}}^*$	$W_{g_{12}}$	$W_{g_{13}}$	$W_{g_{14}}$	$W_{g_{15}}$
0.2	0.001	0.00168	0.00237	0.00306	0.00375
W_{ℓ_2}	$W_{g_{21}}$	$W_{g_{22}}$	$W_{g_{23}}$	$W_{g_{24}}$	$W_{g_{25}}$
0.35	0.00175	0.00294	0.00414	0.00535	0.00656
W_{ℓ_3}	$W_{g_{31}}$	$W_{g_{32}}$	$W_{g_{33}}$	$W_{g_{34}}$	$W_{g_{35}}$
0.50	0.0025	0.0042	0.00592	0.00764	0.00938
W_{ℓ_4}	$W_{g_{41}}$	$W_{g_{42}}$	$W_{g_{43}}$	$W_{g_{44}}$	$W_{g_{45}}$
0.65	0.00325	0.00546	0.0077	0.00994	0.0122
W_{ℓ_5}	$W_{g_{51}}$	$W_{g_{52}}$	$W_{g_{53}}$	$W_{g_{54}}$	$W_{g_{55}}$
0.80	0.004	0.00672	0.00948	0.0122	0.015

*W_g - gas flow rate in lb_m/sec

Selection of Experimental Conditions

Twenty-five experimental runs consisting of five flow rates and five qualities were used in the current investigation. They are designated as Runs 11, 12, ... 21, ... to Run 55, depending on the particular quality and flow rates as shown in table C 1. The following calculation is based on Run 7/15-11, i.e., a liquid flow rate of 0.2 pound per second, a quality of 0.00497, and a gas flow rate of 0.001 pound per second.

Viscosity Determination

Using the equipment illustrated in figure 3.3, the following experimental data were taken:

(a) Water-bath temperature . . . . . 26.2° centigrade

(b) Efflux time for No. 400 viscometer. . . . . 101.5 seconds

(c) Viscometer constant (from table 3.1). . . . 1.110

(d) Density of glycerol mixture assuming 90 percent concentration. . ρ = 1.23 gm/cc (see figure C.1)

(e) Viscosity of the glycerol mixture at 26.2°C.

$$\mu = b\rho t$$
$$= (1.23)(1.110)(101.5)$$
$$= 138.5 \text{ centipoise}$$

(f) Concentration of glycerol mixture

From figure C.2 89.4 percent

Therefore, for a desired viscosity of 150 cp, the temperature of the liquid phase (i.e., glycerol mixture) should be kept at 25.2°C (see figure C.2).

Flow Rate Determination

The difference in the lengths of the liquid columns in the U-tube manometer connected to the orifice plate of the system measured the flow rates of the fluids under consideration. The incremental lengths between the liquid columns were determined in the following manner for a liquid viscosity of 150 cp and a liquid flow rate of 0.2 lb_m/sec.

The Reynolds number in the 0.5215-inch diameter orifice was

$$N_{Re} = \frac{4W}{\pi D\mu} = \frac{(4)(0.2)(3600)(12)}{(\pi)(0.5215)(150)(2.419)}$$
$$= 58.25$$

From figure 3.5,

$K = 0.714$

$W_\ell/K = 0.2/0.714 = 0.28$

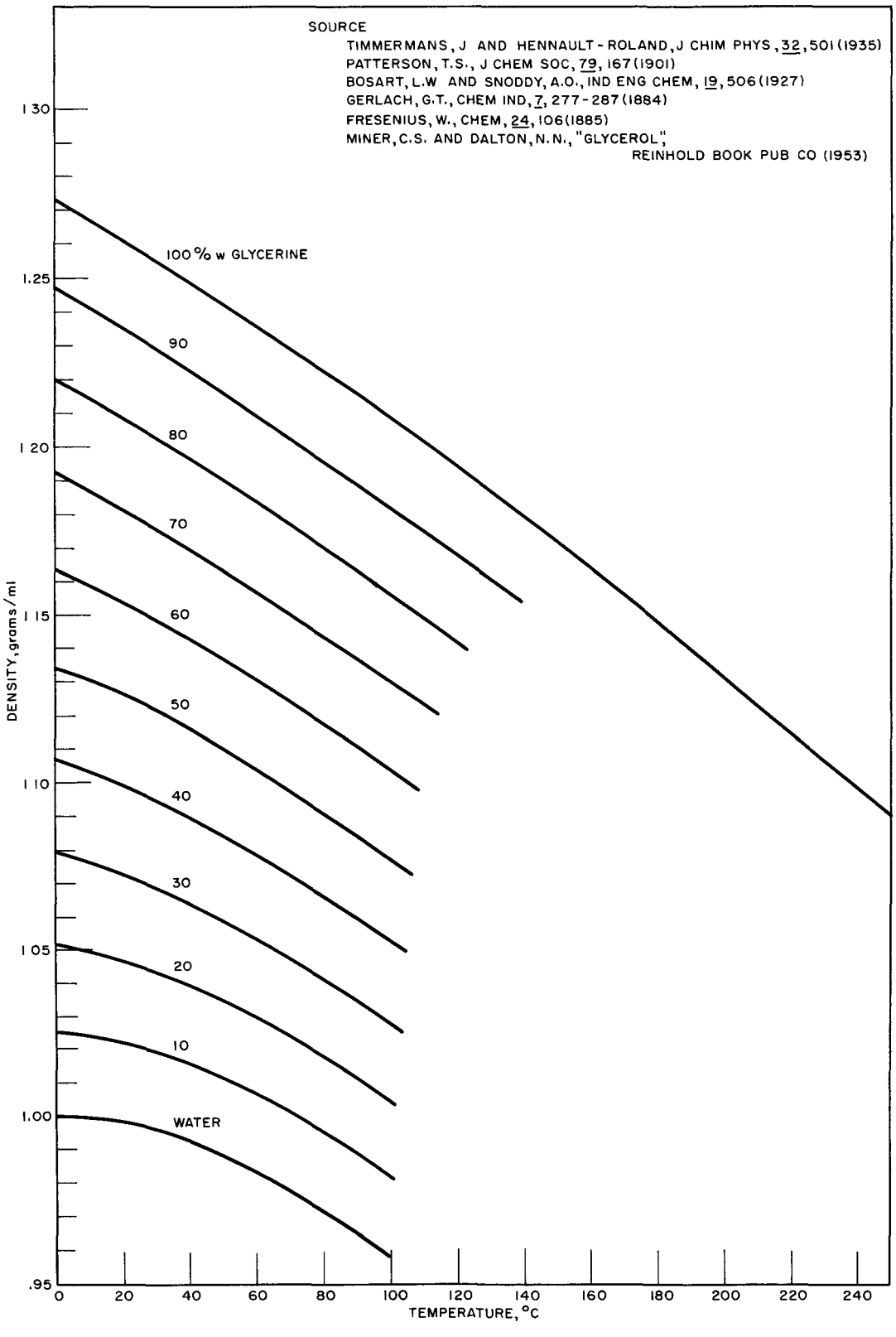

Figure C.1 Densities of Glycerol-water Solutions

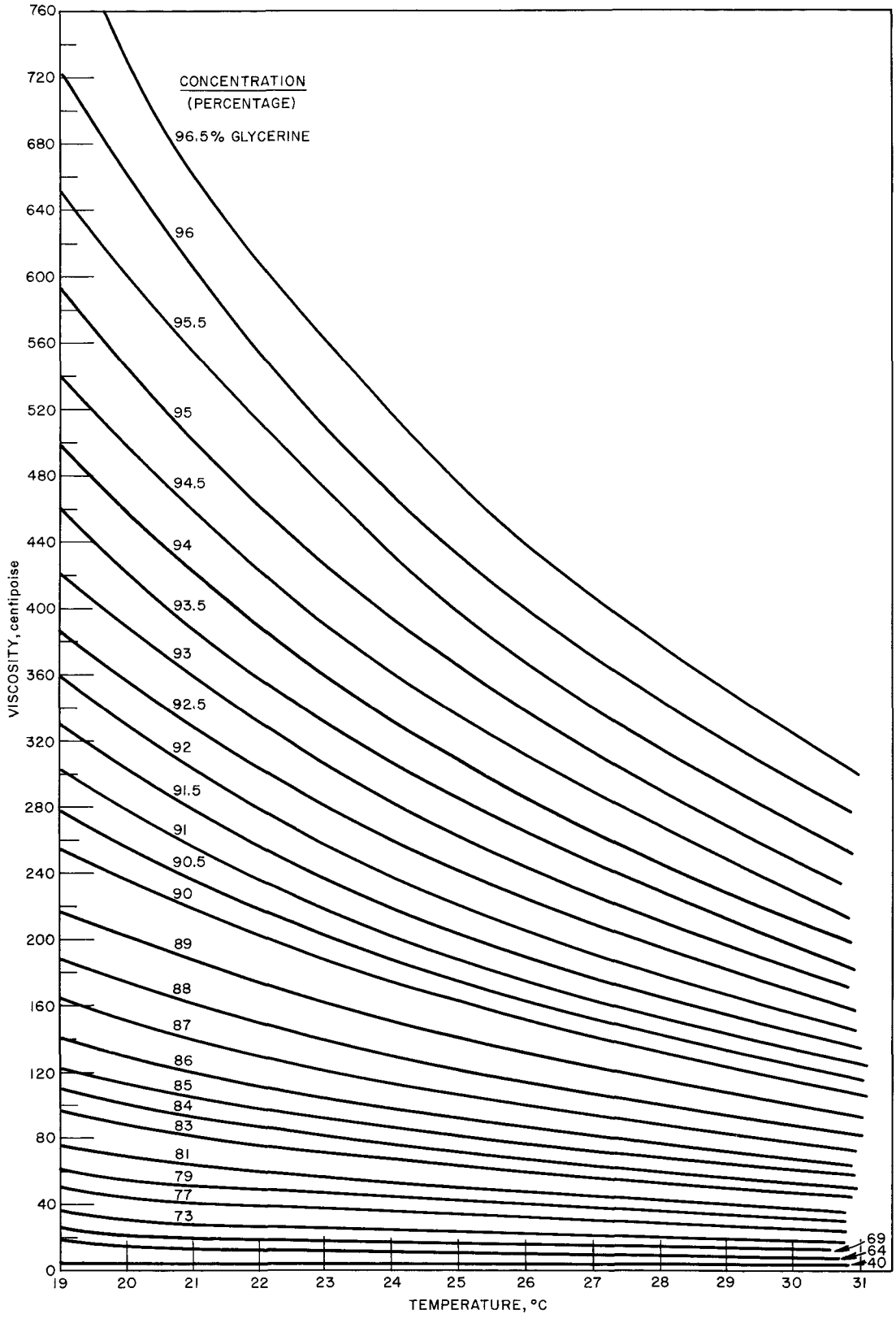

Figure C.2 Viscosities of Glycerol-water Mixtures from Sheely.

From figure C.3, at $\rho = 1.23$, L = 2.85 inches (for the indicating fluid with a specific gravity of 1.72), where L represents the difference of heights of the fluids in the U-tube manometer. The air rate was determined from graphical plot of air flow rate versus "L," which was based on the investigation of Grace and Lapple.[23]

Void Volume Fraction Determination

The void volume fraction was determined by applying equation 2.2 to eleven equally spaced intervals from the traces taken for the full, the empty, and the run traverse. Typical values for Run 7/15-11 at interval six were: I = 680, I_i = 375 and I_e = 760. Therefore, by applying equation 2.2 to these values,

$$\alpha_6 = \frac{\ln(600/375)}{\ln(760/375)} = 0.844 \quad .$$

Applying Simpson's rule to obtain the total void volume fraction for the eleven points,

$$\alpha_T = (\tfrac{1}{3})(\tfrac{1}{10})\,[1(0) + 4(0.00142) + 2(0.0142) + 4(0.32) + 2(0.745) + 4(0.844) + 2(0.844) + 4(0.862) + 2(0.826) + 4(0.405) + 0]$$

$\alpha_T = 0.486$ (see figure 5.22) .

Slip Ratio Determination

The density of the liquid phase was

$$\rho_l = \rho_{H_2O}\, S.G._{Glycerol} = (62.4)(1.23)$$
$$= 76.8 \text{ pounds/ft}^3 \quad .$$

The gas phase was assumed to be at a static pressure equal to that of the liquid phase during the two-phase run. According to the Gas Tables by Keenan and Kaye,[34] the perfect gas law applies to the present case for the range of pressures and temperatures encountered in the experimental investigation. Therefore,

$$\rho_g = \frac{P}{R_0 T} = \frac{(144)(14.81)}{(53.3)(539.4)} = 0.0744 \text{ pound/ft}^3 \quad .$$

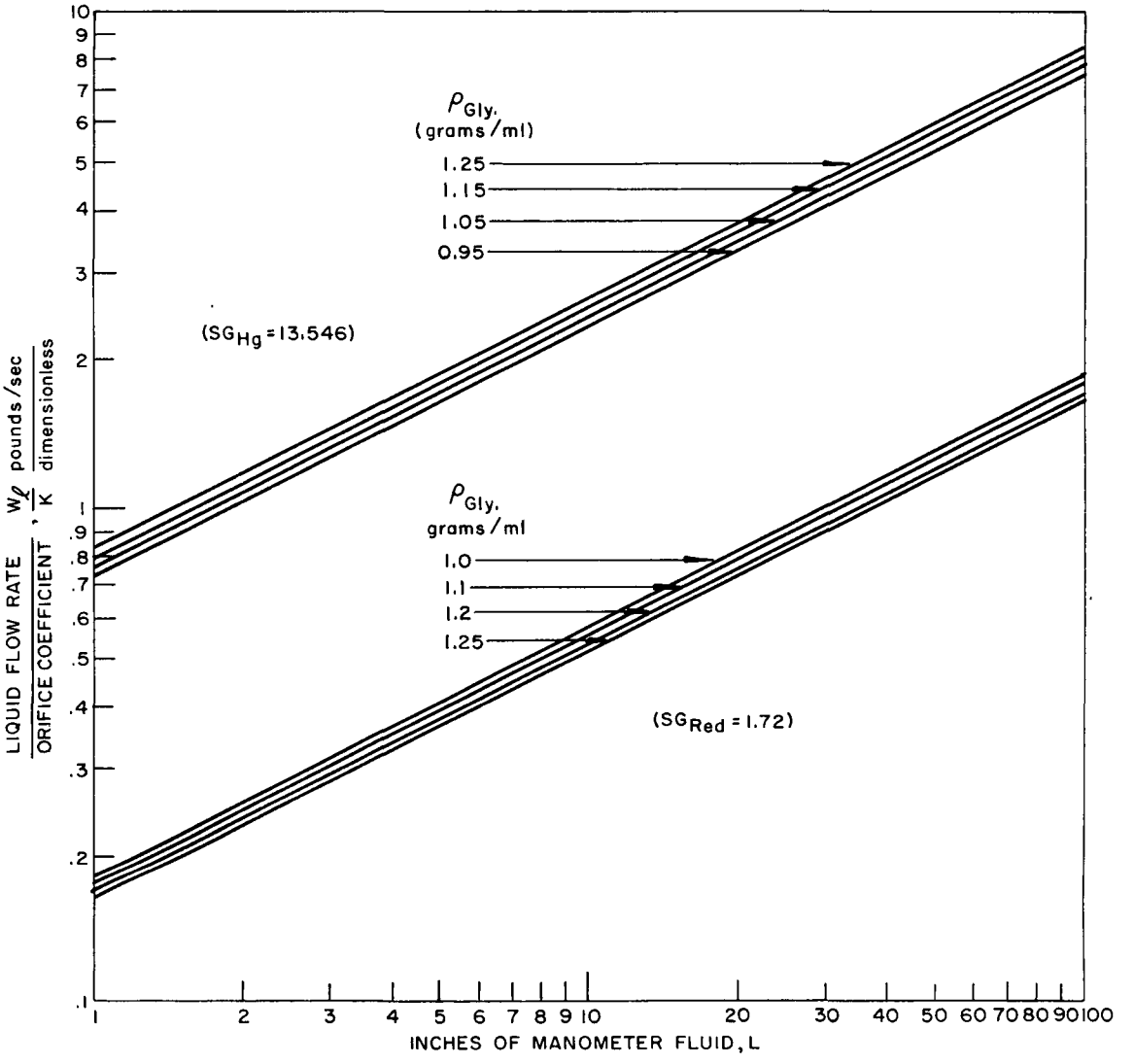

Figure C.3 Ratio of Liquid Flow Rates to Orifice Coefficient for Two Manometer Fluids and Varying Densities of Glycerol-water Solutions.

The quality was determined from the measured gas and liquid flow rates, using equation B.6:

$$x = \frac{0.001}{0.2005 + 0.001} = 0.00497 \quad .$$

The slip ratio was then determined by using equation B.10:

$$\sigma = \frac{0.00497}{(1-0.00497)} \frac{(1-0\ 486)}{0.486} \frac{76.8}{0.0744} = 5.45 \quad .$$

Martinelli Correlation

Void Volume Fraction Correlation

For a liquid viscosity of 150 cp, the liquid is in a laminar state and the gas is in a turbulent state. Therefore, the parameter χ^2_{vt} is determined by the use of equation 7.1:

$$\chi^2_{vt} = \frac{78}{0.269}\left[\frac{(4)(3600)(12)(0.001)}{(5)(0.0449)}\right]^{(0.25-1)} \frac{(0.2205)}{(0.001)} \frac{(150)(2.419)}{(0.0449)} \frac{(0.0744)}{(76.8)}$$

$$= 34{,}400 \quad ,$$

where

$$N_{Re} = 4W/P\mu;$$

and P is the perimeter of a cross-sectional area of the test section.

Pressure Drop Correlation

Using equation A.9 and the experimental data as shown in table C.2,

$$\phi_\ell^2 = \left(\frac{\Delta P}{\Delta \ell}\right)_{TP} \Big/ \left(\frac{\Delta P}{\Delta \ell}\right)_\ell = \frac{0.00737}{0.00584} = 1.262$$

Table C.2. Data.

Run No.	α	W_ℓ*	W_g**	x	σ	χ_{vt}	χ_{tt}	ϕ_ℓ^2
Liquid Viscosity = 500 cp								
7/ 7-11	0.342	0.1955	0.000983	0.005	9.75	103		1.01
12	0.40	0.193	0.00167	0.00858	13.1	64.4		1.10
13	0.415	0.196	0.00235	0.01182	16.9	49.0		1.13
14	0.439	0.1965	0.00305	0.0153	20.1	38.3		1.143
15	0.437	0.203	0.00375	0.0181	24.2	32.8		1.22
7/ 8-21	0.374	0.341	0.00175	0.0051	8.51	82.5		1.03
22	0.398	0.345	0.00294	0.00845	12.75	52.0		1.045
23	0.402	0.355	0.00414	0.01152	17.2	40.4		1.13
24	0.415	0.356	0.00534	0.0148	20.82	31.9		1.145
25	0.425	0.350	0.00657	0.0184	24.9	26.5		1.172
31	0.364	0.497	0.00247	0.00495	8.3	77.5		1.02
32	0.384	0.508	0.00416	0.00813	12.6	48.2		1.05
33	0.394	0.499	0.00592	0.01173	17.52	35.1		1.085
34	0.402	0.502	0.00765	0.015	21.6	28.2		1.23
35	0.423	0.492	0.00938	0.0187	24.7	23.4		1.31
7/ 9-41	0.346	0.65	0.00322	0.00493	8.86	69.6		1.048
42	0.372	0.644	0.00545	0.0084	13.45	43.2		1.10
43	0.408	0.646	0.0077	0.01177	16.25	32.0		1.15
44	0.413	0.654	0.0099	0.01492	20.2	26.0		1.30
45	0.426	0.644	0.0124	0.01925	24.6	21.0		1.38
7/ 9-51	0.342	0.81	0.00398	0.00489	8.7	64.5		1.11
52	0.400	0.79	0.00673	0.00844	13.15	40.6		1.188
53	0.415	0.802	0.00948	0.01165	16.2	30.2		1.293
54	0.439	0.806	0.0123	0.01505	19.05	24.3		1.2
55	0.437	0.793	0.0151	0.0187	22.6	20.2		1.587
Reproducibility Runs								
7/ 9-41-A	0.34	0.65	0.00317	0.00485	8.97	70.9		1.045
7/13-25	0.439	0.352	0.00656	0.01855	24.1	26.22		1.17
44	0.423	0.647	0.00993	0.01532	20.0	25.42		1.3
54	0.409	0.815	0.0121	0.0146	18.85	25.01		
55	0.432	0.798	0.015	0.01845	22.0	20.35		1.587
Liquid Viscosity = 250 cp								
5/25-11	0.435	0.222	0.00099	0.00444	5.96	76.2		1.07
12	0.468	0.216	0.00167	0.00767	9.41	47.0		1.18
13	0.481	0.1922	0.00235	0.01208	13.53	33.7		1.22
14	0.484	0.215	0.00307	0.01407	15.71	28.1		1.365
15	0.498	0.226	0.00375	0.01632	17.22	19.9		1.435
21	0.401	0.354	0.00174	0.00489	7.48	59.5		1.46
22	0.431	0.348	0.00288	0.00821	11.08	37.9		1.52
23	0.464	0.342	0.00411	0.01188	14.12	27.65		1.66
24	0.483	0.344	0.00535	0.0153	16.63	22.1		1.89
25	0.488	0.35	0.0065	0.01823	19.8	18.6		1.96

*W_ℓ = lb_m/sec

**W_g = lb_m/sec

Table C.2. (continued)

Run No.	α	W_ℓ	W_g	x	σ	χ_{vt}	χ_{tt}	ϕ_ℓ^2
Liquid Viscosity = 250 cp (continued)								
5/25-31	0.388	0.511	0.00173	0.00337	5.45	71.5		1.035
32	0.438	0.524	0.00419	0.008	10.52	33.6		1.24
33	0.450	0.49	0.00595	0.0112	14.08	24.8		1.48
34	0.453	0.481	0.00758	0.0155	18.95	18.6		1.61
35	0.495	0.499	0.00922	0.01814	18.75	16.6		1.86
41	0.386	0.641	0.003	0.00466	7.41	50.4		1.181
42	0.404	0.661	0.0059	0.00885	13.1	28.2		1.435
43	0.463	0.651	0.00717	0.0109	12.85	23.4		1.47
44	0.475	0.624	0.0099	0.0156	17.25	17.5		1.76
45	0.492	0.646	0.0122	0.0185	19.1	14.85		1.95
6/ 4-51	0.420	0.761	0.00398	0.00521	7.23	42.6		1.375
52	0.446	0.751	0.00672	0.00888	11.0	27		1.56
53	0.472	0.775	0.00945	0.012	13.5	20.2		1.8
54	0.519	0.761	0.0123	0.0159	14.6	16.22		2.02
55	0.537	0.765	0.015	0.01925	16.4	13.57		2.18
Reproducibility Runs								
7/14-11	0.390	0.1978	0.00099	0.00502	8.09	71.8		1.02
21	0.389	0.354	0.00174	0.00489	7.85	59.3		1.236
34	0.462	0.470	0.00763	0.01595	18.72	18.95		1.582
42	0.407	0.657	0.00544	0.00821	11.82	30.22		1.44
54	0.470	0.820	0.0121	0.01455	15.9	17.1		1.966
55	0.490	0.820	0.015	0.01795	18.05	14.22		2.19
Liquid Viscosity = 150 cp								
6/ 5-11	0.425	0.204	0.00099	0.00483	6.95	55.1		1.3
12	0.473	0.202	0.00168	0.00822	9.55	34.6		1.44
13	0.480	0.200	0.00238	0.01178	13.6	25.4		1.487
14	0.497	0.204	0.00305	0.0147	15.71	20.6		1.56
15	0.542	0.21	0.00375	0.0176	16.0	17.48		1.74
21	0.435	0.354	0.00175	0.00492	6.6	44.1		1.29
22	0.473	0.344	0.00294	0.00848	9.78	27.8		1.4
23	0.495	0.356	0.00414	0.0115	12.2	21.3		1.58
24	0.518	0.357	0.00535	0.0148	14.3	16.7		1.81
25	0.529	0.355	0.00656	0.0182	17.0	14.05		2.18
6/ 8-31	0.461	0.455	0.0025	0.000546	6.59	36.6		1.159
32	0.493	0.472	0.00425	0.00893	9.45	23.55		1.26
33	0.513	0.460	0.00592	0.0127	12.56	17.37		1.31
34	0.527	0.451	0.0077	0.0168	15.65	13.7		1.415
35	0.547	0.461	0.0094	0.02	17.2	11.62		1.456
41	0.468	0.650	0.00326	0.00498	5.8	34.9		1.46
42	0.476	0.656	0.00547	0.00826	9.34	22.2		1.79
43	0.542	0.642	0.00778	0.01195	10.0	15.9		1.735
44	0.536	0.653	0.00997	0.015	13.31	13.2		2.16
45	0.543	0.654	0.0123	0.01845	16.0	10.9		2.43

Table C.2. (continued)

Run No.	α	W_ℓ	W_g	x	σ	χ_{vt}	χ_{tt}	ϕ_ℓ^2
Liquid Viscosity = 150 cp (continued)								
6/ 8-51	0.434	0.798	0.004	0.00498	6.48	33.6		1.274
6/ 9-52	0.480	0.788	0.00678	0.00853	9.31	20.95		1.357
53	0.51	0.798	0.00948	0.01172	11.31	15.8		1.468
54	0.536	0.795	0.0122	0.0151	13.1	12.7		1.554
55	0.56	0.796	0.0151	0.0186	14.6	10.56		1.64
Reproducibility Runs								
7/15-11	0.486	0.2005	0.001	0.00497	5.45	58.6		1.262
15	0.516	0.202	0.00375	0.01825	17.95	17.6		1.64
25	0.512	0.35	0.00653	0.01825	18.05	14.27		1.77
35	0.538	0.499	0.00936	0.01842	16.25	12.58		2.24
45	0.545	0.65	0.0121	0.01828	15.4	11.55		2.52
53	0.528	0.799	0.00947	0.01172	10.5	15.92		2.16
55	0.564	0.807	0.0149	0.01812	13.9	10.78		2.62
Liquid Viscosity = 60 cp								
7/16-31	0.486	0.493	0.0025	0.00504	5.48	24.8		1.632
32	0.543	0.502	0.0042	0.00828	7.2	16.05		2.14
33	0.582	0.508	0.00592	0.01151	8.55	11.95		2.4
34	0.590	0.504	0.0076	0.0148	10.63	9.6		2.82
35	0.595	0.505	0.00938	0.01822	12.85	7.6		3.0
Liquid Viscosity = 20 cp								
7/16-31	0.586	0.489	0.0025	0.00508	3.57	14.55		2.12
7/17-32	0.624	0.497	0.0042	0.00838	5.04	9.35		2.53
33	0.660	0.495	0.00592	0.0118	6.06	6.93		3.87
34	0.689	0.498	0.00764	0.0151	6.8	5.54		4.28
35	0.705	0.495	0.00938	0.0186	7.79	4.62		4.36
Liquid Viscosity = 4.9 cp								
7/20-31	0.709	0.494	0.0025	0.00503	1.93	7.4	6.66	3.38
32	0.715	0.494	0.0042	0.0084	3.13	4.72	4.26	4.62
33	0.724	0.497	0.00593	0.01178	4.2	3.33	3.19	5.35
34	0.735	0.497	0.00764	0.0151	5.11	2.83	2.54	6.32
35	0.750	0.504	0.00938	0.01828	5.72	2.36	2.15	7.75
Liquid Viscosity = 2.8 cp								
7/21-31	0.744	0.504	0.0025	0.00494	1.528	5.85	6.66	3.62
32	0.746	0.494	0.0043	0.00865	2.66	3.7	4.0	4.66
33	0.751	0.493	0.00593	0.01188	3.56	2.71	3.0	5.95
34	0.766	0.497	0.00772	0.0153	4.24	2.15	2.39	7.48
35	0.769	0.498	0.0094	0.01849	5.06	1.825	2.01	8.85
Liquid Viscosity = 1.1 cp (Water)								
7/24-11	0.735	0.204	0.001	0.00488	1.47		6.2	
12	0.768	0.2126	0.00168	0.00782	1.97		4.03	
13	0.777	0.2005	0.00236	0.01161	2.82		2.83	
14	0.777	0.203	0.00306	0.01485	3.58		2.28	
15	0.793	0.2006	0.00375	0.0183	4.01		1.9	

Table C.2. (continued)

Run No.	α	W_ℓ	W_g	x	σ	χ_{vt}	χ_{tt}	ϕ_ℓ^2
Liquid Viscosity = 1.1 cp (Water) (continued)								
7/27-21	0.792	0.348	0.00175	0.00498	1.081		6.08	4.02
22	0.776	0.350	0.00294	0.00833	1.99		3.86	5.86
23	0.780	0.3508	0.0042	0.01182	2.79		2.83	6.3
24	0.763	0.3508	0.00535	0.01501	3.92		2.27	7.34
25	0.790	0.00656	0.00656	0.01878	4.19		1.87	8.9
7/22-31	0.76	0.5033	0.0025	0.00494	1.295		6.2	3.61
32	0.762	0.5033	0.0042	0.008275	2.14		3.8	4.84
33	0.764	0.5033	0.00593	0.01165	3.01		2.83	6.45
34	0.77	0.504	0.00762	0.01488	3.72		2.28	7.22
35	0.778	0.504	0.00938	0.0183	4.35		1.9	8.65
41	0.726	0.667	0.00324	0.00484	1.36		6.14	3.61
42	0.747	0.664	0.00546	0.00818	2.28		3.86	5.2
7/23-43	0.769	0.6493	0.077	0.0117	2.94		2.83	7.16
7/22-44	0.805	0.6493	0.00995	0.0151	3.24		2.27	8.11
45	0.818	0.6493	0.0122	0.01842	3.72		1.9	9.48
7/24-51	0.732	0.8	0.004	0.00497	1.5		6.08	4.28
52	0.759	0.8	0.00672	0.00833	2.18		3.86	6.15
53	0.758	0.8	0.00948	0.01169	3.1		2.83	7.85
54	0.758	0.8	0.0122	0.01505	3.98		2.27	9.55
55	0.769	0.8	0.015	0.0184	4.59		1.9	10.9
Reproducibility Runs								
7/27-25	0.782	0.35	0.00656	0.0184	4.3		1.9	8.4
31	0.762	0.498	0.0025	0.00499	1.29		6.08	3.76
32	0.766	0.498	0.0042	0.00836	2.12		3.79	5.2
35	0.769	0.5	0.00938	0.0184	4.65		1.9	9.0
41	0.737	0.652	0.00325	0.00495	1.465		6.2	3.71
45	0.778	0.655	0.0122	0.0183	4.35		1.9	9.4
55	0.764	0.802	0.015	0.01835	4.7		1.9	11.3
Liquid Viscosity = 0.75 cp (Water)								
7/28-51		0.7978	0.004	0.00499			5.6	4.92
52		0.7978	0.00674	0.00839			3.56	7.1
53		0.7978	0.0095	0.01177			2.61	9.05
54		0.802	0.0122	0.015			2.09	11.0
55		0.802	0.015	0.01835			1.75	12.5

BIBLIOGRAPHY

(1) Levy, S. Theory of Pressure Drop and Heat Transfer for Two-phase, Two-component Annular Flow in Pipes, Ohio State University, Engr. Exp. Station, Bull. No. 149, Proceedings of the Second Midwestern Conference on Fluid Mechanics, 337 (1952).

(2) Richardson, Bobbie L. Some Problems in Horizontal Two-phase, Two-component Flow, ANL-5949 (1959).

(3) Martinelli, R. C., Boelter, L. M. K., Taylor, T. H. M., Thomsen, E. G., and Morrin, E. H., Isothermal Pressure Drop for Two-phase, Two-component Flow in a Horizontal Pipe, Trans. ASME, 66, 139 (1944).

(4) Martinelli, R. C., Putnam, J. A., and Lockhart, R. W., Two-phase, Two-component Flow in the Viscous Region, Trans. Am. Inst. Chem. Engrs., 42, 681 (1946).

(5) Lockhart R. W., and Martinelli, R. C., Proposed Correlation of Data for Isothermal Two-phase, Two-component Flow in Pipes, Chem. Engr. Progress, 45, 39 (1939).

(6) Hoefer, K., Investigation of the Flow Processes in the Rising Main of an Air-lift Pump, VDI Forsch. Heft 138 (1913).

(7) Schmidt, E., Similarity Theory of the Motion of Liquid-gas Mixtures, Verein Deutscher Inginieure, Forschungsheft 365B. 1-3 (1934).

(8) Behringer, P., Velocity Rise of Steam Bubbles in Boiler Tubes, Verein Deutscher Inginieure, Forschungsheft 365B, 4-12 (1934).

(9) Schurig, W., Water Circulation in Steam Boilers and the Motion of Liquid-gas Mixtures in Tubes, Verein Deutscher Inginieure, Forschungscheft 365B, 13-23 (1934).

(10) Cook, W. H., Boiling Density in Vertical Rectangular Multichannel Sections with Natural Circulation, ANL-5621 (1956).

(11) Marchaterre, J. F., Effect of Pressure on Boiling Density in Multiple Rectangular Channels, ANL-5522 (1956).

(12) Galson, A. E., Steam Slip and Burnout in Bulk Boiling Systems, General Electric Atomic Power Equipment Department Tech. Inform. Mem. GEAP - 1076 (June 5, 1957.)

(13) Marchaterre, J. F., and Petrick, M., The Prediction of Steam Volume Fractions in Boiling Systems, Presented at Annual Meeting of the Am. Rocket Soc. in Gatlinburg, Tennessee (June 15, 1959).

(14) Thomsen, E. G., Pressure Drop Accompanying Two-component Flow in a Closed Conduit with Various Liquids and Air, M. S. Thesis, Univ. of California. (1941).

(15) Taylor, T. H. M., Pressure Drop Accompanying Isothermal Two-component, Two-phase Flow in a Horizontal Glass Pipe, M. S. Thesis, Univ. of California, (1942).

(16) Johnson, H. A., and Abou Sabe, A. H. A., Heat Transfer and Pressure Drop for Turbulent Flow of Air-water Mixtures in a Horizontal Pipe, Trans. ASME, 74, 977-987 (1952).

(17) Egen, R. A., Dingee, D. A., and Chastain, J. W., Vapor Formation and Behavior in Boiling Heat Transfer, BMI-1163.

(18) Hooker, H. H., and Popper, G. F., A Gamma-ray Attenuation Method for Void Fraction Determination in Steam-water Mixtures, ANL-5766 (1958).

(19) Petrick, M. P., Two-phase Air-water Flow Phenomena, ANL-5787 (1958).

(20) American Society for Testing Materials, Tentative Method of Test for Kinematic Viscosity, ASTM Designation D445-53T (1953).

(21) Tuve, G. L., and Sprenkle, R. E., Instruments, 6, 201-6 (Nov. 1933).

(22) Sheely, M. L., Determination of Viscosity for Glycerine-water Mixtures, Ind. Eng. Chem., 24, 1060-1064 (1932).

(23) Grace, H. P., and Lapple, C. E., Discharge Coefficients of Small Diameter Orifices and Flow Nozzles, Trans. ASME. (July, 1951).

(24) Baker, O., Design of Pipelines for Simultaneous Flow of Oil and Gas, The Oil and Gas Journal (July 26, 1954).

(25) Bergelin, O. P., and Gazely, C., Jr., Co-current Gas-liquid Flow I. Flow in Horizontal Tubes, Heat Transfer and Fluid Mechanics Institute, Berkeley, California Meeting, (published by ASME), 5-18 (1949).

(26) Gazely, C., Jr., Co-current Gas-liquid Flow. III. Interfacial Shear and Stability, Heat Transfer and Fluid Mechanics Institute, Berkeley, California Meeting, (published by ASME), 29-40 (1949).

(27) Alves, G. E., Co-current Liquid Gas Flow in a Pipe-line Contactor, Chem. Eng. Progress, 50, 449 (1954).

(28) Bernert, R. E., An Analysis of Two-phase Flow: Flow Patterns, Private communication.

(29) Schneider, F. H., White, P. P., and Huntington, R. L., Some Aspects of Simultaneous Horizontal Two-phase Fluid Flow through Pipelines, Presented at Fall Meeting of Petr. Branch, Am. Inst. Mining Met. Engrs. in Dallas, Tex. (Oct 19-21, 1953).

(30) Isbin, H. S., Moen, R. H., and Mosher, D. R., Two-phase Pressure Drops, AECU-2994 (1954).

(31) Masnovi, R., Literature Survey of Two-phase Fluid Flow, WAPD-TH-360 (1958).

(32) Bennett, J. A. R., Two-phase Flow in Gas-liquid Systems, AERE CE/R 2497 (1958).

(33) Vennard, J. K., Elementary Fluid Mechanics, John Wiley and Sons, Inc., New York (January 1954).

(34) Keenan, J. H., Kaye, J., Gas Tables, John Wiley and Sons, Inc., New York (November, 1954).